Polarization And Orbital Angular Momentum Entanglement With Classical And Quantum Sources: Implications And Applications

A THESIS

submitted for the Award of Ph.D. degree of

MOHANLAL SUKHADIA UNIVERSITY

in the

Faculty of Science

by

Chithrabhanu P

Under the Supervision of

Prof. Ravindra P Singh

Professor

Atomic, Molecular, and Optical Physics Division

Physical Research Laboratory

Ahmedabad, India.

DEPARTMENT OF PHYSICS
MOHANLAL SUKHADIA UNIVERSITY
UDAIPUR
Year of submission: 2016

To

My Father,

who always encouraged me to choose the road less travelled.

DECLARATION

I, **Mr. Chithrabhanu P***, S/o Mr. Vasudevan P, resident of A-04, PRL Residences, Navrangpura, Ahmedabad, 380009, hereby declare that the research work incorporated in the present thesis entitled,* **"Polarization And Orbital Angular Momentum Entanglement With Classical And Quantum Sources: Implications And Applications"** *is my own work and is original. This work (in part or in full) has not been submitted to any University for the award of a Degree or a Diploma. I have properly acknowledged the material collected from secondary sources wherever required. I solely own the responsibility for the originality of the entire content.*

Date:

(Chithrabhanu P)

CERTIFICATE

I feel great pleasure in certifying that the thesis entitled, **"Polarization And Orbital Angular Momentum Entanglement With Classical And Quantum Sources: Implications And Applications"** embodies a record of the results of investigations carried out by Mr. Chithrabhanu P under my guidance. He has completed the following requirements as per Ph.D regulations of the University.

(a) Course work as per the university rules.

(b) Residential requirements of the university.

(c) Regularly submitted six monthly progress reports.

(d) Presented his work in the departmental committee.

(e) Published a minimum of one research paper in a referred research journal.

I am satisfied with the analysis, interpretation of results and conclusions drawn. I recommend the submission of the thesis.

Date:

Prof. Ravindra P Singh
(Thesis Supervisor)
Professor, AMOPH,
Physical Research Laboratory,
Ahmedabad - 380 009

Countersigned by

Head of the Department

Acknowledgements

" Happiness is only real, when shared"

– Jon Krakauer, Into the Wild

I am overwhelmed when looking back to the five years of my Ph.D life. No journey is complete without the companions. Acknowledging someone is not merely thanking her/him but sharing the happiness and love. Each and every person is special in their own unique ways and I wish I could name them all.

First and foremost I would like to say that I am so fortunate to have Prof. R P Singh as my supervisor. I really don't have words to express my deep gratitude and respect for him. Whatever I could achieve in these five years is the result of his constant encouragement and guidance. I often feel guilty for not being able to raise to his expectations. You may have seen many cartoons of students blaming his guide at various times of their PhD. I can surely say that I never had to do the same. He was always open to discussion, be it scientific, personal or political. He always appreciates the new ideas and has given me freedom to choose the problems on which I like to work. From the bottom of my heart, I thank him for being there for me.

I am very much thankful to Prof. Goutam Samanta for his constant support and encouragement in my research work. His efforts to popularise subject among common people, and the enthusiasm for science is really motivating. I have learned a lot from him. I would like to express my sincere thanks to Prof. K. P. Subramanian for his kind support during my Ph.D as my doctoral committee member and for teaching a course on statistics. I thank Prof. J Banerji for many fruitful discussion and his charming classes on communication. I thank Prof. A K Singhvi, who had introduced me to PRL and with whom I had the pleasure of working as a Project associate.

I take this opportunity to express my gratitude to PRL for providing the basic infrastructural facilities for carrying out the research work. I thank the director of PRL, dean, academic committee chairman, academic committee members, and registrar for their help and support. I thank Prof. N. M Ashok, Prof. Ashok Singhal, Dr. Namit Mahajan, Dr. B. K. Sahoo, Dr. Dilip Angom, Dr. Ramitendranath Bhattaacharyya, Prof. Nandita Srivastava, Dr. Varun Sheel and Dr. Brajesh Kumar for taking various courses in physics. I thank Dr. Navinder Singh for helpful discussion. I am thankful to Prof. Partha Ghose (SRFTI, Kolkatta), Prof. Anirban Pathak (JIIT, Noida), Dr. Goutam Paul (ISI, Kolkatta), Prof. Surendra Singh

(University of Arkansas) and Dr. Somshubhro Bandyopadhyay (Bose institute, Kolkatta) for their kind help and discussion during my Ph.D.

I had the pleasure of working with my motivating senior Dr. Salla Gangi Reddy, who always geared up my work when I was lagging behind. I thank him for all the help and encouragement that he has given to me. I thank Dr. Aadhi, with whom I used to discuss and whose ideas gave sparks to many of my research work. I thank Ali, Nijil and Jabir who had helped me in experiments, thesis correction and discussion.

I am thankful to my seniors Dr. Ashok Kumar, Dr. Pravin Vaity and Dr. Shashi Prabhakar for their help at the initial stage of my research career. Special thanks to Shashi for teaching many practical aspects of working in a lab. I thank Dr. Vijay for his help in the experiments. I acknowledge Dr. Avesh, Varun and Vinayak, my optics labmates. I thank Khushbu and Raza for their numerous helps. I thank all the summer students and project students for their cooperation.

Midhun and Lekshmy , thanks for being the sweetest next door couple one can ever have. I will always cherish the memories with you guys. Thanks and respect to my 88 old Bansuri guruji, Shri Hemendra Dixit for offering your deep wisdom. Apurv, we had great political and scientific discussion and fights sometimes and I wish to continue those in the future. I can't avoid mentioning our sweet naughty Vavachi, Apurv's daughter and Anju, his wife, for their company. Bhavya, Renjith, Blessen Chettan and Nita along with Midhun and Lekshmy we had a great Malayali group. I acknowledge my best friends right from B.Sc. Manu, Mukhtadir, Ratheesh and Jisha for their wonderful friendship.

My dynamic friends, Manu, Shradha , Ikshu, Anirban and Abhay , I will always cherish the countless memories with them. They have literally made the stay at PRL enjoyable and energetic. Girish, Arun, Saweeta, Gaurav, Tanmoy, Guru, Kuldeep, Sanjay and Alok, we had a lot of fun in trips, dinners and Udaipur days. Shremadi and Abhishek, thanks for the teas and dinners and musical nights during the toughest times of PhD. Thanks to Avdhesh, Venki, Vinni bhayya, Ashimanand, Jaspreeth, Sharad and Damu for enriching the hostel days. Remembering the seniors Shreekant, Bhaswar, Suman, Soumya Bhavik, Amjad and Vishal for the great discussion we had. I express my gratitude to the seniors of the luminescence lab Naveen, Morthekai, Rebiul, and Linto for their helps. I thank Bivin for his "cool" company and Vishnu for the laughters. I am glad that I could have the company of Pradeep, Aman, Ila, Bhavesh and Bharti in the TT rooms and beyond. I would like to acknowledge Niharika, Rupa, Newton, Kiran, Deepti, Pankaj, Gulshan, Satheesh, Varun, Upasana, Chandana, Kuldeep, Rukmini, Navpreeth, Ashish and Naman for their wonderful *company. Though I couldn't interact with many among 2015 Batch students except a few, I remember their awesome performances in the fresher's party.*

I would like to say thanks to all my seniors and 7th floor mates Girish, Arko, Gaurav, Monojit, Gulab, Thanusree, Sudip, Naveen Nabyendu, Gaveshana, Chandan, Lekshmy, Luxmy and Priyanka. Thanks to Akhilesh bhaiya for introducing me to the Bansuri and the world of Hindusthani music, and Zeen didi for her company. I have enjoyed friendship of many visitors of PRL Anindo, Anindita, Sandhya, Biveen and Sean.

I am grateful to all the staff members of PRL library, computer centre, dispensary and administrative staff for their sincere support. It is my duty to acknowledge Google scholar and arXiv for keeping me updated. I am thankful to the cleaning workers of PRL and the canteen cooks, especially Munna bhai and Pappu bhai, for their services.

As Sir Isac Newton said, "If I have seen further, it is by standing on the shoulders of giants". I acknowledge the great minds who lead the path and understanding the subjects of physics, quantum mechanics and optics. I must say I am deeply thankful to great minds like Miles Padgett and GS Agarwal, with whom I had the fortune to discuss the subject.

As Aristotle said, "'Man is by nature a social animal; an individual who is unsocial naturally and not accidentally is either beneath our notice or more than human. Society is something that precedes the individual." Its the interactions with the society that construct any human identity. With all its imperfections, I acknowledge the society for those rigorous interactions which defined me.

Acknowledging the life partner is always a difficult task. My sweetheart and best friend, Swapna, without whom I will be nothing. I can't avoid mentioning my sweet 5 month old son Milan Azad whose photo kept me going in the difficult times of thesis writing. I express my gratitude, respect and love for my mother Sreedevi for her courage and support even in the difficult times of my fathers demise. I thank all my family members for being there for me.

Chithrabhanu P

ABSTRACT

Polarization and orbital angular momentum are two independent discrete degrees of freedom of light. Both of these properties can be extensively used in quantum information and communications. Photons entangled in polarization are widely used for quantum communications. Orbital angular momentum (OAM) of photon is recently getting much attention as it can be used along with polarization and thereby increasing the information carrying capacity of photons. Moreover, entanglement between polarization and OAM have many advantages in many of the quantum protocols. The classical counterpart of this polarization and OAM entanglement, non-separability in vector vortices, is getting a lot attention due to its ability to simulate many quantum protocols.

We study the classical and quantum aspects of polarization and OAM entanglement. In classical system we study the non-separability of OAM and polarization with the Bell's inequality measurement and study its properties under scattering. In the quantum system, where we have entangled pair of photons, we conceptualise new measurement systems for OAM entanglement and introduce novel three particle hyper-entangled state which we apply for many interesting quantum protocols.

We generate the non-separable state of polarization and orbital angular momentum (OAM) using a laser beam. The generated state undergoes a cyclic polarization evolution which introduces a Pancharatnam geometric phase to the polarization state and in turn a relative phase in the non-separable state. We experimentally study the violation of Bell - CHSH inequality for different Pancharatnam phases introduced by various cyclic polarization evolutions with linear and circular states as measurement bases. While measuring in linear bases, the Bell-CHSH parameter oscillates with Pancharatnam phase. One can get rid of this dependence by introducing a relative phase in one of the projecting state. However, for measurement in circular bases, the Pancharatnam phase does not affect the Bell-CHSH violation.

We experimentally show that the non-separability of polarization and orbital angular momentum present in a light beam remains preserved under scattering through a random medium like rotating ground glass. We verify this by measuring the degree of polarization and observing the intensity distribution of the beam when projected to different polarization states, before as well as after the scattering. We extend our study to the non-maximally non-separable states also.

In quantum systems, we address the possibility of using even/odd states of orbital angular momentum (OAM) of photons for the quatum information tasks. Single photon qubit states and two photon entangled states in even/odd basis of OAM are considered. We present a method for the tomography and general projective measurement in even/odd basis. With the general projective measurement, we show the Bell violation and quantum quantum cryptography with Bell's inequality as a safeguard against breach of security. We also describe hyper and hybrid entanglement of even/odd OAM states with polarization and apply this for the implementation of superdense coding.

We also present a scheme to generate three particle hyper-entanglement utilizing polarization and orbital angular momentum (OAM) of a photon. We show that the generated state can be used to teleport a two-qubit state described by the polarization and the OAM. Apart from teleportation, the proposed quantum system has been used to describe a new efficient quantum key distribution (QKD) protocol. We give a sketch of the experimental arrangement to realize the proposed teleportation and the QKD.

Keywords : Orbital angular momentum, Polarization, Entanglement, Bell's inequality, Teleportation, Non-separability, Hyper-entanglement, Hybrid-entanglement.

Contents

List of Tables

List of Figures

Chapter 1

Introduction

Entanglement is one of the most interesting and exciting phenomena in the quantum theory right from its inception in 1935. In their historical paper, Albert Einstein, Boris Podolsky and Nathan Rosan (EPR) considered a joint non-separable quantum mechanical system and proved that the quantum mechanical wave function is an incomplete description since it violates local realism [1]. This discussion followed by the famous EPR paper, is of the highest importance in the philosophical development of quantum mechanics [2, 3]. However, this debate gave rise to the birth of a vast field of quantum information and quantum communication [4]. These non-separable states or entangled states were experimentally generated in several systems which form a resource for quantum information processing. The basic fact that the quantum information cannot be cloned [5], made them useful for generating keys of data encryption. Entanglement arises due to the non-separability of the state of two particles. In this thesis, we consider entanglement in optical systems. Polarization (or spin angular momentum) and orbital angular momentum (OAM) are the two properties of light that we study in the context of entanglement. Classical beams, can have non-separability and exhibits entanglement-like features which are coined as non-quantum or classical entanglement. With OAM and polarization entanglement, we propose new efficient protocols for quantum communication and cryptography. In this chapter, I will give a brief introduction to entanglement and quantum information and their implementation in optical systems.

1.1 EPR Paradox, Hidden Variable Theory and Bell's Inequality

Here we give a brief introduction to the philosophical development of entanglement which led to the quantum revolution in information processing and communication. EPR poses a question on quantum mechanics which is evident in the title of the paper "Can quantum mechanical description of physical reality be considered completely ?". They gave the condition for completeness that *every element of physical reality must have a counter part in the physical theory*. They explain the term physical reality as follows

" If, without in any way disturbing the system, we can predict with certainty (i. e. probability equal to unity) the value of physical quantity, then there exists an element of physical reality corresponding to the physical quantity."

From the non-commutative nature of two observable such as momentum and position it is shown that the precise knowledge of one precludes such a knowledge. In other words any attempt to precisely measure one of the quantity will alter the system in such a way that the knowledge about the other quantity is destroyed. This could be explained in two ways. Either,

1 quantum mechanical description of reality given by wave function is not complete

or,

2 when the operators corresponding to two physical quantities do not commute the two quantities cannot have simultaneous reality.

They have considered a composite non-separable system, which we now call as entangled system, where they have proved that with different projections on one system one can change the wave function of the second. In other words it is possible to assign different wave functions to the same reality. Furthermore, they have shown that with such a system, one can measure the values of two quantities which are non-commuting. Thus they have negated the second possibility as the two quantities have simultaneous reality. With negation of the second argument EPR concluded that quantum mechanical description of reality given by wave function is not complete.

Thus many believed that there exist some variables, that are hidden, which affect the measurement results [3]. These hidden variables along with the state vector will determine precisely the result of individual measurements. This theory was ruled out by John S Bell in 1965 by his famous inequality which cannot be violated using local hidden variable theory[6, 7].

Consider an ensemble of pair of correlated particles each of them entering to different measurement devices I_a and Π_b, where a and b are the adjustable parameters. The particles are in singlet spin state, generally known as EPR state. The measurement results are dichotomous variables $A(a)$ and $B(b)$ which can take values either $+1$ or -1. According to local hidden variable theory the statistical correlation between $A(a)$ and $B(b)$ is due to some variable λ with a probability distribution $\rho(\lambda)$. The results of the measurement are deterministic functions of the adjustable parameter and the hidden variable as $A(a, \lambda)$ and $B(b, \lambda)$. The locality condition restricts $A(a, \lambda)$ from having any dependence on b and $B(b, \lambda)$ on a. Also, the probability distribution of λ ($\rho(\lambda)$) which is defined during the emission of the correlated particles is independent of the adjustable parameters a and b. We have

$$\int_\Gamma \rho(\lambda) d\lambda = 1 \tag{1.1}$$

The correlation is defined as

$$P(a, b) = \int_\Gamma \rho(\lambda) A(a, \lambda) B(b, \lambda) d\lambda \tag{1.2}$$

Where Γ is the total λ space. For the singlet state we have $P(a, a) = -1$ which leads to

$$A(a, \lambda) = -B(a, \lambda) \tag{1.3}$$

$$\begin{aligned} P(a, b) - P(a, c) &= \int \rho(\lambda) \left[A(a, \lambda)B(b, \lambda) - A(a, \lambda)B(c, \lambda)\right] d\lambda \\ &= \int \rho(\lambda) \left[B(b, \lambda) - B(c, \lambda)\right] A(a, \lambda) d\lambda \end{aligned} \tag{1.4}$$

Using $[B(b, \lambda)]^2 = 1$ we get

$$P(a, b) - P(a, c) = \int \rho(\lambda) \left[1 - B(b, \lambda)B(c, \lambda)\right] B(b, \lambda)A(a, \lambda) d\lambda \tag{1.5}$$

Taking modulus

$$\begin{aligned} |P(a, b) - P(a, c)| =& \left| \int \rho(\lambda) \left[1 - B(b, \lambda)B(c, \lambda)\right] B(b, \lambda)A(a, \lambda) d\lambda \right| \\ \leq& \int \rho(\lambda) \left[1 - B(b, \lambda)B(c, \lambda)\right] |B(b, \lambda)A(a, \lambda)| d\lambda \\ =& \int \rho(\lambda) \left[1 - B(b, \lambda)B(c, \lambda)\right] d\lambda \\ =& 1 - \int \rho(\lambda) B(b, \lambda)B(c, \lambda) d\lambda = 1 + P(b, c) \end{aligned} \tag{1.6}$$

We have used Eq. 1.2 and Eq. 1.3 for the final simplification. Hence the inequality is given as

$$|P(a,b) - P(a,c)| \leq 1 + P(b,c) \tag{1.7}$$

For the singlet state, this inequality is getting violated and thus Bell ruled out the possibilities for the existence of local hidden variables. Thus, entanglement and non-locality are considered to be an inherent quantum nature. Later on, Clauser, Horne, Shimony and Holt (CHSH) formulated a variant of Bell's inequality which is experimentally more realizable [8].

1.2 Quantum Information and Entanglement

Quantum information had its origin in the fundamental questions on the quantum nature of a system and now it is an emerging field in physics with great technological applications.

1.2.1 What is Quantum Information ?

Before moving to this question, we need to address the question "what is information?". We live in an era where information is omnipresent. It is so common that we are often unable to define it. Many people will think of information as a phone call or a written transcript that describe about something. Information can be any sequential arrangement of alphabets which can be conveyed with a set of rules that defines a language. Thus a video or a picture one sees in a television are also information. Historically, the development of battery and understanding of static electricity in the late 18^{th} century led to the development of electrical communication. In 1837, Samual Morese demonstrated electrical telegraph in which the alphabets are represented by sequences of dots and dashes. The length of the sequence was designed considering the redundancy of the letters. Frequently occurring letters were assigned to shorter sequences there by decreasing the total length of the coded information. These codes are called "Morse codes". By the end of 19^{th} century, telegraph could connect all the continents.

The wireless revolution of the communication was initiated by Maxwell's studies on electromagnetic waves. In the late 19^{th} century, Jagadish Bose and Guglielmo Marconi independently developed radio which used electromagnetic waves to transmit the information. The digitalization of information was followed by Claude Shannon's phenomenal paper "*Mathematical theory of communication*" in 1948 [9]. The invention of electronics revolutionized the information technology. Here the information is coded in bits. A bit is a variable that can take only two values: 0 or 1. Almost all present day communication and computation systems use the information as series of bits. In a vector space a bit represents only two points.

A quantum bit, shortly qubit, is a fundamental unit of quantum information. From the fundamentals of quantum mechanics, we know that particles can be in complex superposition of states. This opens up a huge space for the information storage and possibility for faster computing. Like bits, qubits have two orthogonal states say $|0\rangle$ and $|1\rangle$. However, the state of the particle is a linear complex superposition of these orthogonal states. Thus it can span a two dimensional complex vector space $|0\rangle, |1\rangle$. All the possible pure states can be geometrically represented on a sphere called Bloch sphere.

$$|\psi\rangle = \alpha|0\rangle + \beta|1\rangle \tag{1.8}$$

α and β are complex numbers. For the normalization

$$|\alpha|^2 + |\beta|^2 = 1 \tag{1.9}$$

$|\alpha|^2$ - Probability that system is in $|0\rangle$; $|\beta|^2$ - Probability that system is in $|1\rangle$
Thus a qubit can exist in any of the continuum of states between $|0\rangle$ and $|1\rangle$ until it is observed. When a measurement is done, it will fall to one of its (operator's) eigenstates. Now, $\{|0\rangle, |1\rangle\}$ forms an orthonormal vector space so that any vector can be expressed in terms of the two independent base vectors as a linear combination. Example of qubit states are photon polarization states, electron spin states, two level energy states etc.

1.2.1.1 Bloch Sphere

Bloch sphere provides a useful means of visualizing the state of a single qubit. Expressing the state given in Eq. 1.8 in polar form as $\alpha = r_\alpha e^{i\phi_\alpha}$ and $\beta = r_\beta e^{i\phi_\beta}$ the state becomes

$$|\psi\rangle = r_\alpha e^{i\phi_\alpha}|0\rangle + r_\beta e^{i\phi_\beta}|1\rangle \tag{1.10}$$

where $r_\alpha, r_\beta, \phi_\alpha$ and ϕ_β are real parameters.

Since the measurable quantities are the probabilities $|\alpha|^2$ and $|\beta|^2$, multiplying with a factor $e^{i\gamma}$ has no observable consequences on the state ($|e^{i\gamma}\alpha|^2 = |\alpha|^2$). Thus we can multiply $e^{-i\phi_\alpha}$ to Eq. (1.10)

$$|\psi'\rangle = r_\alpha|0\rangle + r_\beta e^{i(\phi_\beta - \phi_\alpha)}|1\rangle \tag{1.11}$$

$$|\psi'\rangle = r_\alpha|0\rangle + r_\beta e^{i\phi}|1\rangle \tag{1.12}$$

where $\phi = \phi_\beta - \phi_\alpha$. We can write Eq. 1.12 as

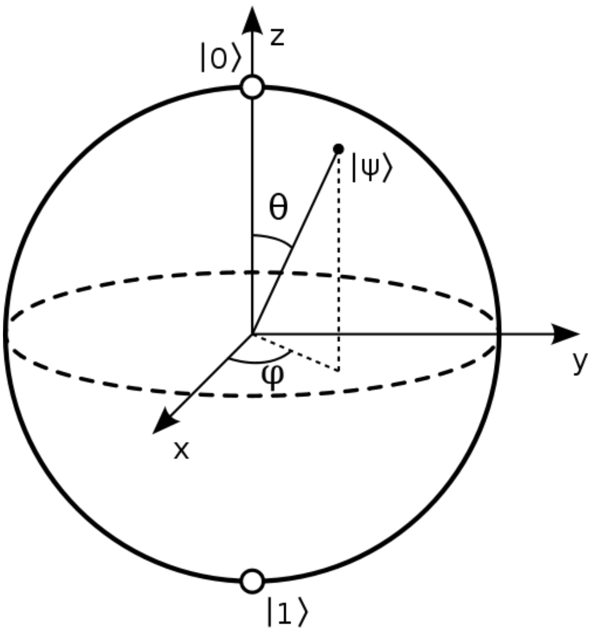

Figure 1.1: Geometrical representation of qubits on Bloch sphere

$$|\psi'\rangle = r_\alpha|0\rangle + (x + iy)|1\rangle \tag{1.13}$$

The normalization condition $\langle\psi'|\psi'\rangle = 1$ gives

$$r_\alpha^2 + x^2 + y^2 = 1 \tag{1.14}$$

Eq. 1.14 is an equation of sphere in real 3D space with Cartesian coordinates (x, y, r_α). We replace r_α with z.

$$|\psi'\rangle = z|0\rangle + (x + iy)|1\rangle \tag{1.15}$$

In spherical polar coordinates,

$$|\psi'\rangle = r\cos(\theta)|0\rangle + (r\sin(\theta)\cos(\phi) + ir\sin(\theta)\sin(\phi))|1\rangle \tag{1.16}$$

where $r = \sqrt{x^2 + y^2 + z^2} = 1$. Thus

$$|\psi'\rangle = \cos(\theta)|0\rangle + \sin(\theta)(\cos(\phi) + i\sin(\phi))|1\rangle, \tag{1.17}$$

$$|\psi'\rangle = \cos(\theta)|0\rangle + \sin(\theta)e^{i\phi}|1\rangle. \tag{1.18}$$

We rewrite Eq. (1.18) as

$$|\psi\rangle = \cos(\theta')|0\rangle + e^{i\theta}\sin(\theta')|1\rangle. \tag{1.19}$$

When $\theta' = 0$; $|\psi\rangle = |0\rangle$ and when $\theta' = \pi/2$; $|\psi\rangle = e^{i\phi}|1\rangle \equiv |1\rangle$ by neglecting the global phase. This suggests that $0 \leq \theta' \leq \pi/2$ may generate all points on the Bloch sphere.

Consider a state $|\psi'\rangle$ corresponding to the opposite point of $|\psi\rangle$ with coordinates $(1, \pi - \theta', \pi + \phi)$. [Note:- when $(x, y, z) \rightarrow (-x, -y, -z)$; $(r, \theta, \phi) \rightarrow (1, \pi - \theta, \pi + \phi)$]

$$\begin{aligned} |\psi'\rangle &= cos(\pi - \theta')|0\rangle + e^{i(\phi+\pi)} sin(\pi - \theta')|1\rangle, \\ &= -\cos(\theta')|0\rangle + e^{i\phi} e^{i\pi} \sin(\theta')|1\rangle, \\ &= -\cos(\theta')|0\rangle - e^{i\phi} \sin(\theta')|1\rangle, \\ &= -|\psi\rangle. \end{aligned} \tag{1.20}$$

So it is only necessary to consider the upper hemisphere $0 \leq \theta' \leq \pi/2$, as opposite points differ only by a phase factor of -1 and so are equivalent in the Bloch sphere representation.

Thus we map points on the upper hemisphere onto points on a sphere defining $\theta = 2\theta' \rightarrow \theta' = \theta/2$, with

$$|\psi\rangle = \cos(\theta/2)|0\rangle + e^{i\phi} \sin(\theta/2)|1\rangle \tag{1.21}$$

where $0 \leq \theta \leq \pi$ and $0 \leq \phi \leq 2\pi$ are the coordinates of points on the Bloch sphere.

1.2.2 Multiple Qubits and Qudits

If we have two classical bits, we can have four states as 00, 01, 10, 11. Similarly, with two qubits we can form $|00\rangle$, $|01\rangle$, $|10\rangle$, $|11\rangle$. The pair of qubits can also exist in superposition state as

$$|\psi\rangle = \alpha_{00}|00\rangle + \alpha_{01}|01\rangle + \alpha_{10}|10\rangle + \alpha_{11}|11\rangle \tag{1.22}$$

with normalization condition

$$\sum_{i,j} \alpha_{ij}^2 = 1 \tag{1.23}$$

If we have "n" number of qubits, we need 2^n coefficients to describe the system completely.

A qudit is a d-dimensional quantum state which can be expressed as

$$|\psi_d\rangle = \sum_{i=0}^{d-1} c_i |i\rangle \tag{1.24}$$

with $\sum_{i=0}^{d-1} |c_i|^2 = 1$.

1.2.3 Measurement Bases for a Qubit

Since it is a quantum state we can measure it in different bases. However, the measurement operators have eigenvalues ± 1 only. Thus each measurement will have only two possible outcomes. We list some common measurement bases:

- Computational basis $\{|0\rangle, |1\rangle\}$: In this basis, measurement on a general qubit $\alpha|0\rangle+\beta|1\rangle$ will give result +1 with probability $|\alpha|^2$ and -1 with probability $|\beta|^2$.

- Diagonal basis $\{|+\rangle, |-\rangle\}$ where

$$|\pm\rangle = \frac{1}{\sqrt{2}}\left(|0\rangle \pm |1\rangle\right) \tag{1.25}$$

A general qubit when measured in diagonal basis will give result ±1 with probability $|\alpha \pm \beta|^2/2$.

- Circular basis $\{|\circlearrowright\rangle, |\circlearrowleft\rangle\}$: Here

$$\begin{aligned} |\circlearrowright\rangle =& \frac{1}{\sqrt{2}}\left(|0\rangle + i|1\rangle\right) \\ |\circlearrowleft\rangle =& \frac{1}{\sqrt{2}}\left(|0\rangle - i|1\rangle\right) \end{aligned} \tag{1.26}$$

The measurement in circular basis will give result ±1 with probability $|\alpha \pm i\beta|^2/2$. Note that to get the complete state of the qubit, or in other words to obtain the Bloch vector, we need to do measurements in these bases.

- General linear basis $\{|\theta\rangle, |\theta^{\perp}\rangle\}$

$$\begin{aligned} |\theta\rangle =& cos(\theta)|0\rangle + sin(\theta)|1\rangle \\ |\theta^{\perp}\rangle =& sin(\theta)|0\rangle - cos(\theta)|1\rangle \end{aligned} \tag{1.27}$$

These states define a complete equatorial circle. This is very important measurement since it used to check the Bell's inequality.

- General circular basis $\{|\phi\rangle, |\phi^{\perp}\rangle\}$

$$\begin{aligned} |\phi\rangle =& \frac{1}{\sqrt{2}}\left(|0\rangle + e^{i\phi}|1\rangle\right) \\ |\phi^{\perp}\rangle =& \frac{1}{\sqrt{2}}\left(|0\rangle - e^{i\phi}|1\rangle\right) \end{aligned} \tag{1.28}$$

- General qubit basis $\{|\psi(\theta,\phi)\rangle, |\psi^{\perp}(\theta,\phi)\rangle\}$: These are general qubit basis. We can arrive at the other basis by fixing specific values from θ and ϕ. In terms of the computational basis we can define them as

$$\begin{aligned} |\psi(\theta,\phi)\rangle =& cos(\theta)|0\rangle + e^{i\phi}sin(\theta)|1\rangle \\ |\psi\rangle^{\perp}(\theta,\phi\rangle =& sin(\theta)|0\rangle - e^{i\phi}\cos(\theta)|1\rangle \end{aligned} \tag{1.29}$$

1.2.4 Quantum Register

Collection of N qubits is called a quantum register of size N. Let $N = 2$

$$|\psi\rangle = C_{00}|00\rangle + C_{01}|01\rangle + C_{10}|10\rangle + C_{11}|11\rangle \tag{1.30}$$

$|ij\rangle$ implies that qubit 1 is in state i and qubit 2 is in state j.

N-qubit register is described by a 2^N dimensional wave function with amplitudes $C_{ijk..}$. The quantum information is stored in these amplitudes which are complex numbers with modulus between 0 and 1.

The amount of information grows exponentially with register size, but information is hidden and large number of it is lost when measurements are made. We only manipulate qubits and let them interact coherently without making measurements, then all the information are preserved. This is the basis of huge quantum parallelism that makes quantum computation efficient.

1.2.5 Entangled Qubits and Bell States

If two systems are entangled, the total state cannot be written as product states of two individual systems.

$$\Psi_{12} \neq \psi_1 \otimes \psi_2 \tag{1.31}$$

In two dimensions, two particles, each of them carrying a qubit, can be entangled as

$$|\Psi\rangle = \frac{1}{\sqrt{2}} \left(\alpha|0\rangle|0\rangle + \beta|1\rangle|1\rangle\right). \tag{1.32}$$

Here one cannot write Ψ as the product of two individual qubits unless $\alpha, \beta \neq 0$. Maximally entangled states of two qubits are called Bell states, which are defined as

$$|\Psi^{\pm}\rangle = \frac{1}{\sqrt{2}} \left(|0\rangle|1\rangle \pm |1\rangle|0\rangle\right) \tag{1.33}$$

$$|\Phi^{\pm}\rangle = \frac{1}{\sqrt{2}} \left(|0\rangle|0\rangle \pm |1\rangle|1\rangle\right). \tag{1.34}$$

Quantum entanglement provides new protocols for quantum information eg. quantum cryptography [10], quantum teleportation [11] and superdense coding [12].

1.2.6 Quantum Gates

Like logic gates in electronics, quantum gates are basic units of a quantum circuit. Here are some basic quantum gates.

- NOT gate $\{X\}$:- This is similar to the computational logic gate NOT. It converts

$$X\left(\alpha|0\rangle + \beta|1\rangle\right) \longrightarrow \alpha|1\rangle + \beta|0\rangle \tag{1.35}$$

- Hadamard gate $\{H\}$

$$H\left(\alpha|0\rangle + \beta|1\rangle\right) \longrightarrow \alpha\frac{|0\rangle + |1\rangle}{\sqrt{2}} + \beta\frac{|0\rangle - |1\rangle}{\sqrt{2}} \tag{1.36}$$

- Z gate

$$Z\left(\alpha|0\rangle + \beta|1\rangle\right) \longrightarrow \alpha|0\rangle - \beta|1\rangle \tag{1.37}$$

- C_{NOT} gate :- Controlled NOT gate or C_{NOT} gate is a two qubit gate. It flips the second qubit (target) only if the first qubit (control) is $|1\rangle$. When the control qubit is in state $|0\rangle$ the C_{NOT} gate leaves the target qubit unaltered. It is similar to XOR $|A, B\rangle \rightarrow |A, B \oplus A\rangle$

- Controlled unitary gate:- This two qubit gate does a unitary transformation on the second qubit only when the control qubit is in state $|1\rangle$.

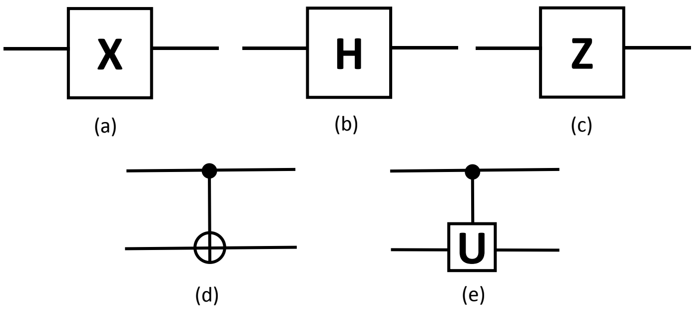

Figure 1.2: Representation of quantum gates a) NOT gate b) Hadamard gate c) Pauli Z gate d) Controlled NOT gate e) Controlled unitary gate

1.3 Entanglement Based Quantum Protocols

Entanglement serves as a basic resource for many quantum information protocols. Some of the popular protocols are discussed below.

1.3.1 Superdense Coding

Superdense coding [12] is a transfer of classical information through a quantum channel. Information is classical since they code bits in quantum entangled states. Consider a Bell state where one particle is with Alice and another with Bob. Alice encodes two bits of information by applying one of four unitary transformations which will transform the combined state from one Bell state to another. Then Alice sends her particle to Bob and he does a Bell state analysis to decode the message. It is advantageous over classical communication using bits, since here by action on one qubit, we can code two classical bits.

1.3.2 Teleportation

Quantum teleportation [11] is a non classical transfer of an unknown quantum state using entanglement and classical communication. This can be seen as the distribution of quantum information through quantum and classical channels.

- *Alice* and *Bob* initially share a pair of entangled particles (say particle 2 & particle 3).
- *Alice* receives the particle with an unknown state (say particle 1) .
- *Alice* does a joint Bell operator measurement on the particle with unknown state and her entangled particle. Particles 1 & 2 gets destroyed due to the measurement.
- *Alice* sends the outcome of her measurement to *Bob* through a classical channel.
- *Bob* does a unitary transformation on his particle (particle 3) with respect to *Alice*'s measurement results to recover the quantum state of the particle 1.

Initially, the unknown state and the entangled pair are given by

$$|\phi_1\rangle = \alpha|0\rangle + \beta|1\rangle \ ; \ |\Psi^-_{23}\rangle = \frac{1}{\sqrt{2}}\left(|01\rangle - |10\rangle\right) \tag{1.38}$$

Total wave function

$$|\Psi_{123}\rangle = \frac{1}{\sqrt{2}}\left(\alpha|0\rangle_1 + \beta|1\rangle_1\right) \otimes \left(|01\rangle_{23} - |10\rangle_{23}\right) \tag{1.39}$$

It can be written as

$$\begin{aligned} |\Psi_{123}\rangle = \ & \tfrac{1}{\sqrt{2}}(\alpha|00\rangle_{12}|1\rangle_3 - \alpha|01\rangle_{12}|0\rangle_3 + \\ & \beta|10\rangle_{12}|1\rangle_3 - \beta|11\rangle_{12}|0\rangle_3) \end{aligned} \tag{1.40}$$

Outcome	Unitary operator
Ψ^-	$\hat{\sigma_0}$
Ψ^+	$\hat{\sigma_3}$
Φ^-	$\hat{\sigma_1}$
Φ^+	$\hat{\sigma_3}\ \hat{\sigma_1}$

Table 1.1: Alice's measurement outcomes and corresponding unitary transformations that Bob does to complete the teleportation

From the Bell states (Eq. 1.33 & Eq. 1.34), we can have

$$|00\rangle = \frac{|\Phi^+\rangle+|\Phi^-\rangle}{\sqrt{2}}\ ;\ |11\rangle = \frac{|\Phi^+\rangle-|\Phi^-\rangle}{\sqrt{2}} \tag{1.41}$$

$$|01\rangle = \frac{|\Psi^+\rangle+|\Psi^-\rangle}{\sqrt{2}}\ ;\ |10\rangle = \frac{|\Psi^+\rangle-|\Psi^-\rangle}{\sqrt{2}} \tag{1.42}$$

Substituting in Eq. 1.40 and rearranging the terms

$$\begin{aligned} |\Psi_{123}\rangle = \frac{1}{2}\{&|\Psi^-_{12}\rangle(-\alpha|0\rangle_3 - \beta|1\rangle_3)+ \\ &|\Psi^+_{12}\rangle(-\alpha|0\rangle_3 + \beta|1\rangle_3)+ \\ &|\Phi^-_{12}\rangle(\alpha|1\rangle_3 + \beta|0\rangle_3)\ + \\ &|\Phi^+_{12}\rangle(\alpha|1\rangle_3 - \beta|0\rangle_3)\} \end{aligned} \tag{1.43}$$

Depending on Bell measurement by Alice, Bob applies the unitary operation on his entangled particle to recover the quantum state of the particle 1. The unitary transformations for different measurement outcomes are given in table 1.1.

1.3.3 Quantum Cryptography

As entanglement provides perfectly correlated or anti correlated photons, we can use them to distribute a secret key between two parties, say Alice and Bob [10]. In this scheme Alice and Bob shares an entangled pair of particles. Both of them measure their entangled photon in different projection angles. They choose one of the three (or four) predefined angles randomly. After sufficient measurements they disclose the angles used in each measurement. When angles are matched, they used the data to generate the key. With mismatched angle data they calculate the Bell parameter. Thus the Bell's inequality provides the security and the non-local correlation provides the key.

1.4 Photons for Quantum Information

Photons are natural choice for any quantum information or communication protocols because of the ease of handling. They are often called as “flying qubits” and are an irreplaceable part of communication. Development of efficient single photon detectors made the photonic quantum information easier [13]. Single photon sources were developed in the past decades using controlled excitation of atomic vapor, solid state color centres or quantum dots. Parametric down conversion of photons were shown to generate entangled photons which can essentially be used for any quantum communication. Almost all quantum information protocols were initially demonstrated using photons. One can use many degrees of freedom of photon such as polarization, orbital angular momentum, path, position, momentum, time or frequency for carrying the information. We study two discrete degrees of freedom polarization and orbital angular momentum of photons.

1.4.1 Polarization

Polarization of light field is being studied since the birth of the theory of electromagnetic fields by James Clerk Maxwell. Polarization is associated with the spin angular momentum of photons which was experimentally proved independently by C V Raman [14] and Beth[15]. Thus it is considered to be an intrinsic property of light. The basic two dimensional polarization state is equivalent to a qubit state. Hence it is a good choice for communication protocols.

2D Polarization State

Any plane wave propagating in $\hat{\mathbf{z}}$ direction has its components in $\hat{\mathbf{x}}$ and $\hat{\mathbf{y}}$ directions.

$$\vec{\mathbf{E}} = \vec{E_0} e^{ikz-\omega t} \tag{1.44}$$

Now $\vec{E_0}$ is a two dimensional vector which does not evolve with time. This defines the amplitude and direction of the electric field at a given instant of time.

$$\begin{aligned} \vec{E_0} =& E_x\hat{\mathbf{x}} + E_y\hat{\mathbf{y}} \\ =& E_0\left(\alpha\hat{\mathbf{x}} + \beta\hat{\mathbf{y}}\right) \end{aligned} \tag{1.45}$$

where $\alpha = E_x/\sqrt{E_x^2 + E_y^2}$ and $\beta = E_y/\sqrt{E_x^2 + E_y^2}$. By discarding the common amplitude term we get a normalized wave function which defines the polarization state of light. We can use the ket notation for the vectors. So a polarization state is defined as

$$|\psi\rangle = \alpha|H\rangle + \beta|V\rangle \tag{1.46}$$

$|H\rangle$ and $|V\rangle$ represent horizontal and vertical polarization respectively. Note that the state is normalized as $|\alpha|^2 + |\beta|^2 = 1$.

Measurements and Operations

All the single qubit operations can be done using wave plates. A NOT gate is a half wave plate with fast axis orientation $\theta = 45°$. The half wave plate oriented at $\theta = 22.5°$ acts as a Hadamard gate. Any transformation of the polarization qubit on its Bloch sphere can be done with combinations of quarter wave plates and half wave plates. Also, any projections onto linear bases can be done with a polarizer or using combination of a half wave plate and a polarizing beam splitter (PBS). For projections onto circular bases, we need to use a quarter wave plate and a PBS.

The ease of transformation and measurement make the polarization qubit as the best choice for quantum information. However, two qubit states don't have straight forward implementations. C_{NOT} gate operations are not that trivial and many experimental realizations are probabilistic.

Polarization Entanglement

Polarization entangled photons are one of the earliest realization of quantum entanglement. Initially it was realized with the emission from atomic cascade system and latter on with parametric down conversion of light in a non-linear crystal. Now bright entangled photons can be generated using type 2 second order non-linear crystal, cascaded type I crystals or type 0 periodically poled crystals. One can easily transform one Bell state to another by the action of wave plates. They were used to perform quantum protocols such as teleportation [16], super dense coding [17] and quantum cryptography [18]. However, a complete deterministic Bell state analysis for polarization entangled pairs is is yet to be implemented effectively.

1.4.2 Orbital Angular Momentum

Light beams such as Laguerre Gaussian (LG) modes with a phase singularity are known to possess an orbital angular momentum (OAM) [19]. These beams are also called optical vortices. OAM is associated with the helical phase of the light beam and is given as $\pm m\hbar$.

Here m is the order of the vortex which is defined as the number of helical windings in one wavelength. The electric field of an optical vortex is given as

$$E = r^{|m|} e^{im\phi} e^{-r^2/\omega^2} \tag{1.47}$$

where $\phi = tan^{-1}(y/x)$ is the azimuthal angle and ω is the beam width. Poynting vector of electromagnetic field, which is always parallel to the surface normal of the phase fronts, has an azimuthal component that results in the orbital angular momentum along the beam axis. This OAM can be transferred to colloidal particles in an optical trap [20]. Thus it can be used as an "optical spanner" in fields like biophysics [21, 22] and micromechanics [23]. Optical vortices has interesting properties and has many applications in data storage, imaging, metrology and free space communication [24–30]. OAM states can be generated using diffraction holograms [31–33], mode converters [34] or spiral phase plates [35].

OAM has infinite dimensions in which information can be encoded, and this can be used as a new degree of freedom for quantum information [36, 37]. The OAM state of a photon spans an infinite dimensional Hilbet space $\{.., |-m\rangle, .., |-1\rangle, |0\rangle, |+1\rangle, .., |+m\rangle, ..\}$. In general, OAM and spin cannot be considered independently. However, in the paraxial approximation spin (polarization) and OAM can be measured and manipulated separately. Thus, one can essentially use OAM along with polarization. OAM states find exciting applications in quantum information protocols [38–40].

OAM Entanglement

Orbital angular momentum is a conserved quantity in non-linear processes like second harmonic generation [41, 42] and sum frequency generation [43, 44], but it was experimentally shown that the classical beam generated by spontaneous parametric down conversion will not conserve the OAM [45]. However it was later shown that spin, orbital and total angular momentums are conserved in SPDC as the angular momentum of the pump is shared between the down conversion medium and the down converted photons [46–48]. In 2002 Mair et. al. experimentally demonstrated the quantum correlations between OAM states of twin photons generated by SPDC [49]. They have used a Gaussian beam with zero OAM as pump beam for SPDC. The OAM of the signal and idler photons produced by SPDC should add up to zero for the OAM conservation. Thus, either of the photon can take any value of OAM or be in state $|m\rangle$ where m can take any integer value from $-\infty$ to $+\infty$ with a condition that its twin pair should have equal OAM value with opposite sign to be in state $|-m\rangle$. The state can be written as

$$|\Psi\rangle_{12} = c_0|0\rangle_1|0\rangle_2 + \sum_{m=1}^{\infty} c_m(|m\rangle_1|-m\rangle_2 + |-m\rangle_1|m\rangle_2) \tag{1.48}$$

where c_0, c_m are the complex amplitudes. In such cases, OAM states with opposite sign, for example $|1\rangle_{1/2}$ and $|-1\rangle_{2/1}$, will have perfect correlation while that of same sign (except the $|0\rangle_1, |0\rangle_2$) will have perfect anti correlation. The measurement of OAM states were done by a computer generated hologram and a single mode fibre. This OAM entanglement opened a great possibility for quantum correlations in higher dimensions. Higher dimensional entanglement was demonstrated using OAM of photon [50–55]. This has huge application in quantum cryptography [56] and quantum teleportation [57].

1.4.3 Photons Entangled in Polarization and OAM

As we discussed in previous subsection, OAM and polarization can be treated as independent degrees of freedom (DOFs) and two photons can be entangled in both. This is called hyper-entanglement. Note that in this case there is no correlation between polarization and OAM. A hyper entangled photon pair can be expressed as

$$|\Psi^p\rangle_{12} \otimes |\psi^o\rangle_{12} = \frac{1}{2}\left(|HH\rangle_{12} + |VV\rangle_{12}\right) \otimes \left(|l, -l\rangle_{12} + |-l, l\rangle_{12}\right) \tag{1.49}$$

These states can be generated by cascaded SPDC [58]. These states have received great deal of attention as they are applied in efficient dense coding [59, 60], teleportation of states in multiple DOF of a single photon [57] , remote state preparation [61], joining of quantum states [62] and quantum error correction [63].

Now we consider the correlations between polarization and OAM of photons. In the larger Hilbert space of polarization and OAM, it is possible to have non separable states of them. The non-separability can be between the two DOFs of single particle or between DOF1 of first and DOF2 of the second. These states are called hybrid entangled states [64, 65]. Single photon hybrid entangled states are used in the hyperentanglement assisted polarization Bell state analysis [66]. A single photon hybrid entangled states are given as

$$|\psi\rangle = \frac{1}{\sqrt{2}}\left(|Hl\rangle + |V-l\rangle\right). \tag{1.50}$$

In case of biphoton hybrid-entanglement, the polarization state will correspond to first photon and OAM state will correspond to the second. Such states are often used to demonstrate many quantum properties such as complementarity and non-local steering [67, 68]. These states also violate the Bell's inequality [69] Hybrid entangled photons have lot of applications such as implementation of quantum algorithms [70] quantum cryptography [71] etc.

1.5 Non-separable States and Entanglement

Right from its initial formulation, entanglement was considered as a unique quantum feature with no classical counterpart. It appears to be true for the non-local multiparty entanglement. However, this non-locality is not a necessary condition for the violation of Bell's inequality. Any non-separable states can violate Bell's inequality. Non-separability is not unique to the quantum world. One can have non-separable wave functions in classical electromagnetic fields too. And one can have classical analogy of quantum entanglement using laser beams. This is due to the fact that we can construct a Hilbert space for discrete degrees of freedoms of light such as polarization and OAM.

Radially and azimuthally polarized beams are examples of such non-separable states [72]. In such beams the polarization is correlated with the spatial mode of the beam. For example, radially polarized beams are represented in Hermite Gaussian as

$$\vec{\mathbf{E}} = HG_{01}\hat{\mathbf{x}} + HG_{10}\hat{\mathbf{y}}. \tag{1.51}$$

HG Modes are given as

$$HG_{mn} = \xi_0 H_m(ax)H_n(by)e(-(x^2+y^2)/\omega_z^2) \tag{1.52}$$

where H_n and H_m are hermite polynomial of order n and m, ξ_0 is the complex amplitude, a and b are complex numbers and ω_z is the radius at which the field amplitudes falls to $1/e$ of their axial values, at the plane z along the beam. Here selecting any particular polarization will change the spatial structure of the beam which is analogous to the steering of quantum entanglement.

In 1998, R Spreeuw formulated the "classical" Hilbert space of polarization and spatial modes [73] . He called the polarization and spatial mode states as cebits, which are analogous to qubits. Here, polarization and the spatial modes of a beam can be considered as a bipartite system. States $\{|H\rangle, |V\rangle\}$ forms a polarization Hilbert space $\mathcal{H}^p$ and the spatial mode states $\{|a\rangle, |b\rangle\}$ forms Hilbert space of the spatial mode $\mathcal{H}^s$. Thus in the combined Hilbert space $\mathcal{H}^p \otimes \mathcal{H}^s$ we can have non-separable bipartite states which are mathematically equivalent to entangled states. The state is given as

$$|\psi\rangle^{p,s} = \frac{1}{\sqrt{2I_0}}\left(|H\rangle|a\rangle + |V\rangle|b\rangle\right) \tag{1.53}$$

Many use symbol $|..)$ for the cebit states. However, we are sticking to the traditional ket notation. Also the normalization of I_0 is omitted in the further discussions for a compact representation. This state is similar to the hybrid entangled state given in Eq. 1.50.

There were many important works which studied the classical non-separability in the context of entanglement [74–82]. Many people call these states as nonquantum entanglement or classical entanglement. However there were some serious criticism for the use of the word entanglement for these classical states [83]. We prefer to call it as non-separability.

Various classical non-separable states are shown to violate Bell like inequalities [84–88]. They have been used to demonstrate classical analogue of many quantum protocols such as teleportation [89], state transfer [90], quantum walks [91] and quantum algorithms [92, 93]. The non-seperable states have also found applications in coherence studies [94], metrology [95], communication [96, 97] and kinematic sensors and ultra sensitive measurements [98, 99].

Now the question is that how does the classical non-separability differ from quantum entanglement. Answer lies in the non-locality and no-cloning nature of quantum systems. With classical wave field one cannot achieve non-local steering of a state. Thus the non-local correlations must be considered distinctively quantum in nature. The classical non-separability cannot replace the quantum entanglement. No cloning nature of quantum state cannot be applied to any classical wave fields.

1.6 Objective of the thesis

Polarization and orbital angular momentum are two independent and discrete degrees of freedom of light. Both DOFs can be extensively used in quantum information and communications. Photons entangled in polarization are widely used for quantum communications. OAM of photon is recently getting much attention as it can be used along with polarization. Also entanglement between polarization and OAM have many advantages in many of the quantum protocols. The classical counterpart of this polarization and OAM entanglement, non-separability in vector vortices, is getting a lot attention due to its ability to simulate many quantum protocols.

We wish to study the non-separability of polarization and OAM of a laser beam with Bell's parameter as a measure under cyclic polarization evolution. This has implications in the experimental generation of these states for the applications as well as the generation and measurement of entangled photons which follows the same mathematics. As an application of classical non-separable state, we can use it for generating arbitrary 2 dimensional OAM states on the OAM Poincaré sphere. The Poincaré sphere for OAM states proposed earlier [100] is applicable for the OAM quantum number ± 1 only. So it is necessary to describe a general OAM Poincaré sphere which can represent 2D OAM states in the $\{|l\rangle, |-l\rangle\}$ Hilbert space. Non-separable states are used in free space communication and hence studying its properties under scattering is of great importance. Also reviving the non-separable states from a completely scattered field can have applications in public broadcasting.

Most of the quantum protocols using OAM uses the $\{|l\rangle, |-l\rangle\}$ subspace of the infinite dimensional OAM Hilbert space. This restriction causes huge loss of photons and reduces the efficiency of the protocol. We address the possibility of using the even and odd states of OAM for quantum information protocols along with polarization. We try to develop new protocols using even/odd states of OAM and polarization statesm for teleportation, quantum cryptography and super dense coding.

1.7 Overview of the thesis

Chapter 1 gives a general overview of entanglement in the context of quantum information. We briefly describe optical ralization of quantum information along with the discussion of quantum entanglement-like classical non-separability. In chapter 2, we study the non-separable state of polarization and OAM generated using a simple interferometer. We study violation of Bell-like inequality for such a state. We show the effect of Pancharatnam phase induced cyclic polarization evolution on the non-separability and the Bell's measure. We conceptualize a general OAM Poincaré sphere with the use of non-separable sates.

In chapter 3, we study the scattering of non-separable states of OAM and polarization. We study the revival of non-separable state after it gets completely scattered off by a rotating ground glass. We also demonstrate the generation and scattering of non-maximally non-separable states.

Chapter 4 discusses the possibility of using even/odd states of OAM as a basic qubit which has great advantages over the present OAM schemes. We describe the single photon states and entangled states of even-odd OAM qubit and define the operators for its measurement. Using these operators we give experimental schematics for tomography and Bell's inequality. We discuss hyper entanglement and hybrid entanglement of even-odd qubits with polarization as another DOF. We give the setup for spin orbit Bell state analysis and apply it for super dense coding.

In chapter 5, we propose a three particle hyper entangled state, which can teleport two simultaneous qubits and can also be used for an efficient key distribution protocols. We discuss the single photon hybrid gates and Bell projections with experimental schematics. Finally we conclude in chapter 6.

Chapter 2

Evaluation of Non-separability through Bell's Inequality: Effect of Pancharatnam Phase

Non-separability in classical light fields has been studied recently in the context of quantum information and entanglement[73–77]. This arises due to the vector nature of electromagnetic fields. The intrinsic angular momentum, or spin, of light is related to its polarization. Polarization is defines the direction of the electric field vector at a given point. In general, the laser beams produced in a cavity have uniform polarization. But one can generate beams with non-uniform polarizations in which case the polarization will vary according to the position. Polarization singular beams and vector vortices are some examples [101]. The state of these beams are mathematically non-separable in polarization and its spatial mode. This non-separability is analogous to intra-system entanglement involving different degrees of freedom of a light beam. In the conventional entanglement, two particles are entangled in a particular degree of freedom. But as explained in the first chapter, hybrid-entanglement is the entanglement between two degrees of freedom (DOF) of a single particle. The state of the particle is expressed in combined Hilbert space of two degrees of freedom and the operators in DOF-1 and DOF-2 are commuting. However, the term "classical entanglement" has received some serious criticism recently [83]. They argue that the distinctive nature of entanglement is the non-locality which is absent in the classical non-separable states. Quoting them "Ascribing a new meaning to a term that has been in wide use in quantum physics for more than 80 years can only lead to confusion. But more deeply, these new situations lack the key feature nonlocality that led to the concept of entanglement in the first place". We follow the terminology "non-separability" instead of classical entanglement although both are mathematically equivalent. One can construct classical equivalent of many exotic quantum states using polarization and spatial modes of light. These non separable states are used to mimic many quantum protocols [102–104]. Apart from the basic interest of demonstrating quantum protocols using classical light beams, they also find applications in various fields such as polarization metrology, ultra sensitive angular measurements and optical communication.[94–96, 99].

Bell's inequality is one of the most important tool for verifying the presence of entanglement and the maximum value of the Bell parameter (B_{MAX}) can be considered as a measure of entanglement. In single particle non-separable states (hybrid entanglement), Bell inequality is shown to violate and that is accounted for the contextuality of the state, the measurement result in one DOF depends on the measurement in other. The non-separability can exist in between continuous or discrete variables, for which the classical light beams are shown to violate the corresponding form of the Bell's inequality [85, 86, 105, 106].

We consider non-separable state of OAM and polarization which has spatially non-uniform polarization as that of the vector vortex beams. If we measure OAM and polarization, individually, we will get completely mixed state. So for measure any properties of the state we must perform joint measurements involving both DOFs. Since the OAM and polarization are coupled to each other, projection on different polarization state yield different states of OAM. Thus for checking the Bell's inequality violation, we need to measure the state by projecting on different polarization and OAM states.

When light fields undergo a cyclic polarization evolution, they acquire a geometric phase which is known as Pancharatnam phase [107]. The phase acquired by the light depends on the path taken by the polarization state upon its evolution on the Poincaré sphere. The geometric phase is generalized to any quantum system under cyclic evolution by a time dependent Hamiltonian and called as the Berry phase[108]. Entangled states, when generated experimentally, may possess a relative phase due to the phase delays in the generating process. One can nullify this relative phase by introducing a geometric phase in one of the subsystem. In such cases, we need to see the Bell violation, as a measure of entanglement, to optimize the state corresponding to different relative phases. There were many studies regarding the geometric and topological phase with classical non-separable states and entangled states [109, 110]. The effect of Berry phase in entangled systems and their violation of Bell's inequality were studied for spin-$\frac{1}{2}$ particles [111, 112]. The measurement in two degrees of freedom of a non-separable state, be it classical or quantum, is very important for various protocols. Any relative phase will change the measurement outcome which will affect the efficiency of the protocol. Thus, optimizing the measurements in two degrees of freedom, when the state acquires a relative phase is very important for efficient implementation of such protocols.

We generate a classical non-separable Bell-like state of polarization and orbital angular momentum (OAM) of light using a polarizing Sagnac interferometer. We demonstrate the presence of non-separability by violating Bell's inequality for the generated state. Next, we study the effect of Pancharatnam phase introduced by the polarization subsystem, through its cyclic evolution on the Poincaré sphere, on the violation of Bell's inequality. The maximum violation B_{MAX} varies sinusoidally according to the Pancharatnam phase when maximized over the set of linear bases. We experimentally show that the Bell parameter can reach its maximum value of $2\sqrt{2}$ irrespective of the Pancharatnam phase if we introduce a corresponding relative phase in the projecting basis. We also investigate the effect of Pancharatnam phase on the spatially varying polarization structure of these non-separable beams. The results give insight to the measurement optimization of Bell CHSH inequality for a non-separable state under different relative phases.

The geometrical representation of 2D OAM state, a Poincaré sphere equivalent for OAM, was described[100, 113] by taking Hermite-Gaussian modes as the basis vectors. But this will hold only for the OAM state in thge Hilbert space $|1\rangle, |-1\rangle$. We conceptualise a general OAM Poincaré sphere for $|l\rangle, |-l\rangle$ basis from the non-separable state of OAM and polarization. The mixed state of OAM in the $\{l, -l\}$ subspace is visualized as a non-separable state for which the partial trace in the other DOF, say polarization, will cause the mixedness in OAM. We also demonstrate the experimental generation of all the points on the surface of the OAM Poincaré sphere using a non-separable state.

2.1 Violation of Bells Inequality for Non-separable states

2.1.1 Non-seperable State and Projective Measurements

We start with a maximally non-separable Bell-like state of polarization and OAM that can be written as

$$|\psi\rangle = \frac{1}{\sqrt{2}}\left(|H\rangle|l\rangle + |V\rangle|-l\rangle\right) \tag{2.1}$$

where $|H\rangle, |V\rangle$ and $|l\rangle, |-l\rangle$ are basis vectors for 2D complex vector spaces of polarization and OAM respectively. The combined state is a vector in 4 dimensional product Hilbert space. We need to project this state to polarization and OAM states for combined measurement. We define the set of linear bases corresponding to polarization and OAM as

$$\begin{aligned} |\theta\rangle &= \cos(\theta)|H\rangle + \sin(\theta)|V\rangle; |\theta_{\perp}\rangle = -\sin(\theta)|H\rangle + \cos(\theta)|V\rangle; \\ |\chi\rangle &= \sin(\chi)|l\rangle + \cos(\chi)|-l\rangle; |\chi_{\perp}\rangle = -\cos(\chi)|l\rangle + \sin(\chi)|-l\rangle; \end{aligned} \tag{2.2}$$

This set of bases defines a circle in the Poincaré sphere of polarization and OAM. We define Poincaré sphere of OAM by taking $|l\rangle$ and $|-l\rangle$ as basis vectors $(0,1)^T$ and $(1,0)^T$ respectively. The orthogonal states $|\theta\rangle$ and $|\theta^{\perp}\rangle$ are two opposite points of the circle on the Poincaré sphere. Similarly $|\chi\rangle$ and $|\chi^{\perp}\rangle$ are the two opposite points of the circle pn the OAM Poincaré sphere. The linear states of polarization and OAM are represented on the respective Poincaré sphere as shown in Fig. 2.1.

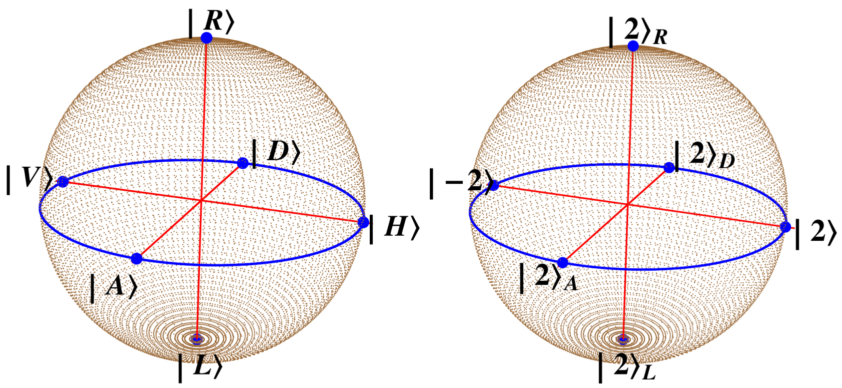

Figure 2.1: Linear bases of polarization (left) and OAM(right) states. H, V, D, A, R and L represents the horizontal, verticlal, diagonal, antidiagonal, right circular and left circular polarization. $|2\rangle$ and $|-2\rangle$ are OAM states corresponding to the topological charge +2 and -2 respectively. Also $|2\rangle_D = \frac{1}{\sqrt{2}}(|2\rangle + |-2\rangle)$, $|2\rangle_A = \frac{1}{\sqrt{2}}(|2\rangle - |-2\rangle)$, $|2\rangle_R = \frac{1}{\sqrt{2}}(|2\rangle + i|-2\rangle)$ and $|2\rangle_L = \frac{1}{\sqrt{2}}(|2\rangle - i|-2\rangle)$ analogous to polarization.

When we project the state given in Eq.2.1, to a general linear polarization state , we get

$$|\psi_l\rangle = \langle\theta|\psi\rangle = cos(\theta)|l\rangle + sin(\theta)|-l\rangle. \tag{2.3}$$

Thus one can control the OAM state using polarization projection. The polarization projection can be done using a half wave plate, a quarter wave plate and a horizontal polarizer. θ should be the twice of the angle of the fast axis orientation of the half wave plate. To complete the measurement we need to project this state $|\psi_l\rangle$ to a general linear OAM state $|\chi\rangle$ as

$$\langle\chi|\psi_l\rangle = \langle\chi|\langle\theta|\psi\rangle = cos(\chi)sin(\theta) + sin(\chi)cos(\theta) = cos(\chi - \theta) \tag{2.4}$$

The OAM projections are done by diffraction holograms using spatial light modulators. Defining probability of the state $|\psi\rangle$ being in the state $|\theta\rangle|\chi\rangle$ is given as

$$c(\theta, \chi) = |\langle\chi|\langle\theta|\psi\rangle|^2 = cos^2(\chi - \theta) \tag{2.5}$$

Similarly one can define circles in the respective Poincaé spheres which are perpendicular to the plane of the linear bases circle. It intersects the linear bases circle at diagonal and anti-diagonal states of polarization and OAM as shown in the Fig. 2.2.

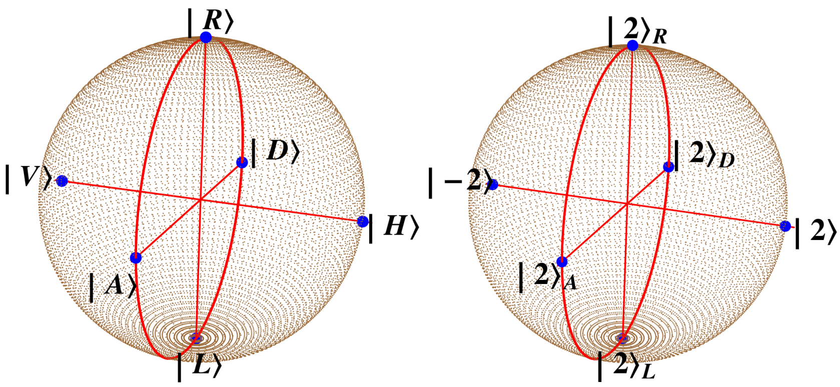

Figure 2.2: Circular bases for polarization (left) and OAM(right) states.

The general states in this set of basis for polarization and OAM are given as

$$|\theta\rangle = e^{-i\theta}|H\rangle + e^{i\theta}|V\rangle;\ |\chi\rangle = e^{-i\chi}|l\rangle + e^{i\chi}|-l\rangle. \tag{2.6}$$

Now the joint detection probability for the projection of the state $|\psi\rangle$ to state $|\theta\rangle|\chi\rangle$ is given as

$$|\langle\theta|\chi|\psi\rangle|^2 = \cos^2(\theta - \chi) \tag{2.7}$$

This is the essential measurement for checking the Bell's inequality for the state.

2.1.2 Experimental Generation of Non-separable State and Implementation of Projective Measurements

We have used a diode pumped solid state green laser (Verdi 10) of wavelength 532nm with vertical polarization for our study. The laser beam passes through a half wave plate oriented at -22.5^o with the horizontal that changes the polarization from vertical to diagonal. Then it passes through a polarizing Sagnac interferometer [114] containing a spiral phase plate

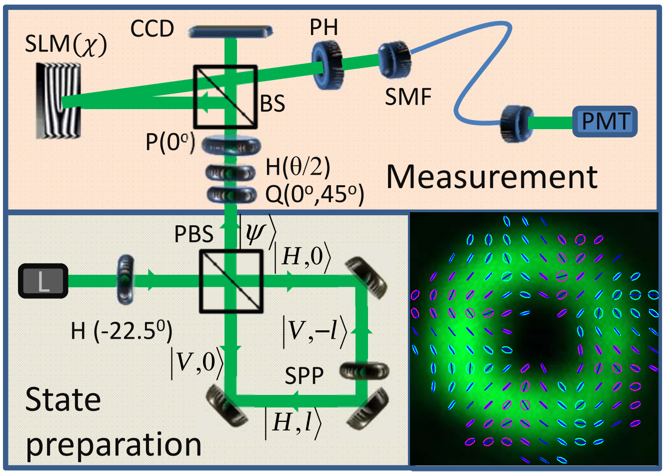

Figure 2.3: Experimental setup for the state preparation, measurement and spatial polarization profile of the non-separable beam. L - laser, H - half wave plate, PBS - polarizing beam splitter, SPP - spiral phase plate, Q - quarter wave plate, BS - beam splitter, SLM - spatial light modulator, CCD - charge coupled device (camera), P - polarizer, PH - pin hole, SMF - single mode fiber, PMT - photo multiplier tube.

(SPP) to generate a light beam with non-separable polarization and OAM. Two orthogonally polarized (H and V) counter propagating Gaussian beams are converted into optical vortices of orders l (for H) and $-l$ (for V) by the SPP designed for order $|l| = 2$. These orthogonally polarized and oppositely charged vortices superpose at the same PBS to form the non-separable state. The experimental set up for the generation and measurement of the non-separable state is given in Fig. 2.3.

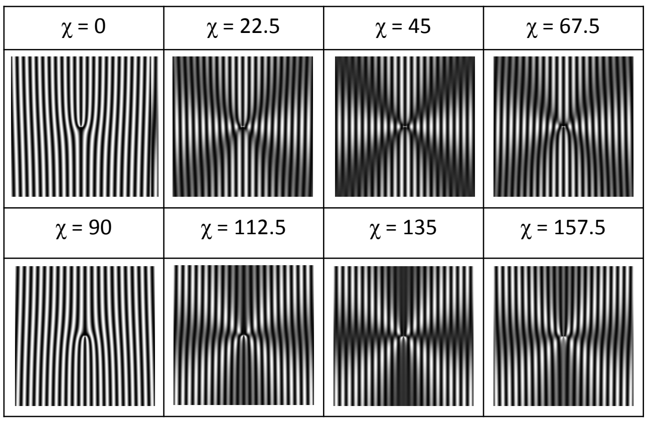

Figure 2.4: Holograms for different values of χ for the measurements of OAM states in linear bases

The measurement in polarization is done by a quarter wave plate (at 0° or 45° for linear and circular projections respectively), half wave plate (at $\frac{\theta}{2}$) and a polariser oriented at 0°. For OAM measurements we use a spatial light modulator (SLM) along with a single mode fibre and a photo multiplier tube for the detection. The holograms for the SLM are made in such a way that they converts the particular OAM state $|\chi\rangle$ into Gaussian. The conversion happens in a projective manner. If the OAM state is $|\chi'\rangle$, then the hologram converts $|\langle\chi|\chi'\rangle|^2$ of the total power into the Gaussian. The remaining intensity will form an outer ring to the Gaussian pattern. The Gaussian part can be easily separated from the rest by using a single mode fibre (SMF). The Holograms for the projection in liner OAM bases for different value of χ are given in Fig. 2.4. The circular projection of OAM at $\chi = 0$, correspond to the $\chi = 45°$ hologram shown in Fig. 2.4. For other values of χ the same hologram is used with a rotation $\frac{\chi}{2}$.

To study the spatially varying polarization structure and its evolution with the introduced geometric phase, we have carried out the Stokes polarimetric imaging of the beam. For this we have imaged the beam after the polarizer (P) using a CCD camera for projections to three sets of orthogonal polarization states. Spatially varying Stokes parameters are calculated from the images corresponding to different polarization projections. The spatial polarization profile is also given in Fig. 2.3.

2.1.3 Violation of Bell's Inequality

Measurements on a light beam with non-separable state of polarization and OAM give raise to contextual results. The measurements are similar to two photon correlation experiments in entangled photon pairs. Instead of measuring one quantity, say polarization, of two spatially separated photons, here we are performing a measurement in two independent degrees of freedom, namely polarization and OAM, of the same beam. The measurement in polarization affects the measurement outcome in OAM. We measure the power coupled to the single mode fibre after the polarization projection and OAM projections. We vary the value θ by changing HWP orientation for different values of OAM projection angle χ. The the projective measurement results for the state given in Eq. 2.5, are given in Fig. 2.5. The theoretical curves which follow the Eq. 2.5 are also given for comparison.

The Bell-CHSH inequality is defined as

$$B(\theta, \theta', \chi, \chi') = |E(\theta, \chi) - E(\theta, \chi') + E(\theta', \chi) + E(\theta', \chi')| \leq 2 \tag{2.8}$$

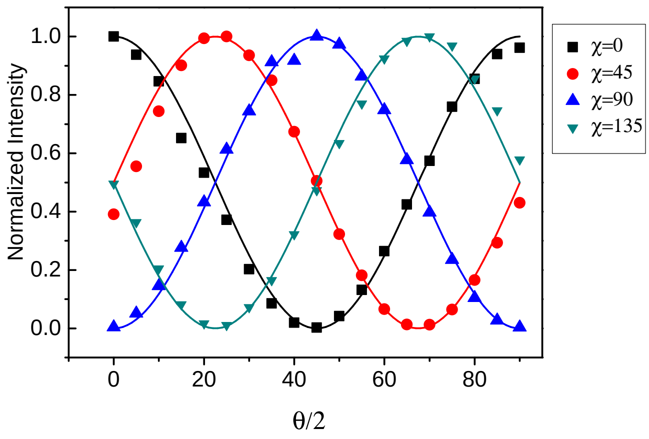

Figure 2.5: Joint polarization-OAM measurement results for a non-seperable state. The half wave plate angle $\theta/2$ is varried for different holograms defined by χ. The theoretical curves follows the Eq. 2.5.

where

$$E(\theta,\chi) = \frac{C(\theta,\chi) + C(\theta_\perp,\chi_\perp) - C(\theta_\perp,\chi) - C(\theta,\chi_\perp)}{C(\theta,\chi) + C(\theta_\perp,\chi_\perp) + C(\theta_\perp,\chi) + C(\theta,\chi_\perp)}.$$

$C(\theta,\chi)$ is the probability amplitude of a state for being in $|\theta\rangle|\chi\rangle$.

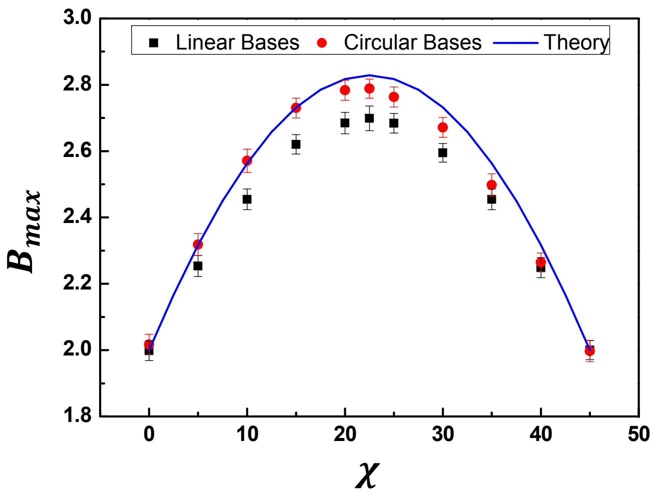

Figure 2.6: Bell-CHSH parameter for different measurement angles (χ).

To find the optimum angles corresponding to the maximum violation of Bell-CHSH inequality, we vary the projecting angle from 0° to 45° fixing $\chi' = \chi + 45°, \theta = 0°$ and $\theta' = 45°$. For the generated non-separable state, we have carried out the measurements in linear (black squares) and circular bases (red circles) and the results are given in Fig. 2.6. For comparing the experimental results, the corresponding theoretical curve is also given.. With ($\theta = 0°, \theta' = 45°, \chi = 22.5°, \chi' = 67.5°$) we experimentally obtain $B_{MAX} = 2.69 \pm 0.036$ corresponding to $\phi = 0°$ when measurement is carried out in linear bases. Measurement in circular bases with the angles mentioned yields a value of $B_{MAX} = 2.79 \pm 0.029$. These are close to the theoretical maximum value of $2\sqrt{2}$. The violation of Bell-CHSH inequality indicates the presence of non-separability between polarization and OAM in the light beam. This accounts for the contextuality in measuring these two properties of light. The imperfections in projecting to the linear bases of OAM while using SLM and single mode fiber result in the lesser violation of Bell CHSH inequality. When projecting the input OAM state (after the polarization projections) by the holograms given in Fig. 2.4, the centre of the Gaussian mode at the fiber coupler slightly gets shifted for different projections which affects the coupling to the single mode fiber. In the case of projections to circular bases, the centres of the projected Gaussian mode are comparatively stable due to the circular symmetry of different holograms.

2.2 Pancharatnam Phase in Non-separable States of Light

We consider a cyclic evolution of polarization for the state given in Eq. 2.1. This cyclic polarization evolution is done using Simon-Mukunda (SM) gadget [115, 116], a combination of two quarter wave plates (Q) and a half wave plate (H). We have used the gadget in Q-H-Q order. The setup and the corresponding polarization evolution are given in Fig. 2.7. A quarter wave plate with fast axis oriented at 45° with the horizontal convert the horizontal and vertical polarizations into right and left circular polarizations respectively. Now a half wave plate, irrespective of its fast axis orientation, will convert right circular polarization to left circular polarization and vice-versa. The second quarter wave plate at 45° will convert the circular polarization to the initial linear polarization state. However, the evolution on the Poincaré sphere takes different path according to the fast axis orientation angle (ϕ') of the half wave plate. Here, the two orthogonal polarization states evolve as $|H\rangle \rightarrow e^{2i\phi'}|H\rangle$ and $|V\rangle \rightarrow -e^{-2i\phi'}|V\rangle$. If considered separately it is a global phase and has no effect in the measurement of polarization or OAM. However, here in the case of non-separable state, the orthogonal polarizations will introduce phase of opposite signs which effectively will introduce a relative phase. The state after the polarization evolution is becomes

$$|\psi'\rangle = \frac{1}{\sqrt{2}} \left(e^{2i\phi'}|H\rangle| - l\rangle - e^{-2i\phi'}|V\rangle| - l\rangle \right) \tag{2.9}$$

$$|\psi'\rangle = \frac{1}{\sqrt{2}}\Big(|H\rangle|+l\rangle + e^{-i\phi}|V\rangle|-l\rangle\Big) \tag{2.10}$$

where $\phi = \pi + 4\phi'$. Global phase of $e^{2i\phi'}$ is omitted since it does not change polarization or OAM measurement outcomes.

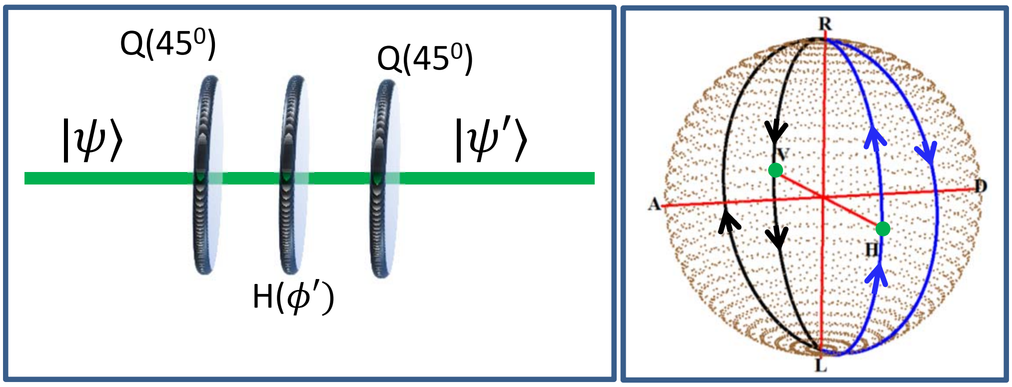

Figure 2.7: Setup for the polarization evolution and its representation on the Poincaré sphere.

2.2.1 Effect of Pancharatnam Phase in the Violation of Bell's Inequality

The measurement on state given in Eq. 2.10 will yield different outcome. The joint measurement probability becomes

$$C(\theta, \chi, \phi) = \cos^2(\theta)\sin^2(\chi) + \sin(2\theta)\sin(2\chi)\cos(\phi) + \cos^2(\chi)\sin^2(\theta) \tag{2.11}$$

which is a function of ϕ also. Thus the B_{MAX} will also be a function of ϕ along with θ, θ', χ and χ'. Changing ϕ will affect the angles corresponding to B_{MAX} as well as its value. For B_{MAX} with $\theta = 0°, \theta' = 90°$, χ and χ' are varied as

$$\chi = \frac{1}{2}\text{arct}^{-1}(\cos\,\phi);\;\; \chi' = \frac{\pi}{2} - \chi. \tag{2.12}$$

The B_{MAX} varies periodically with the relative phase ϕ. Theoretical curves for the variation of the measurement angle χ and B_{MAX} with ϕ are given in Fig.2.8

We have changed the relative phase ϕ using the SM gadget and obtained B_{MAX} using conditions given in Eq. 2.12. Experimental curve for the B_{MAX} with the phase ϕ is given in Fig.2.9. At $\phi = 90$ the value of B_{MAX} drops to zero, and there is no violation of Bell inequality.

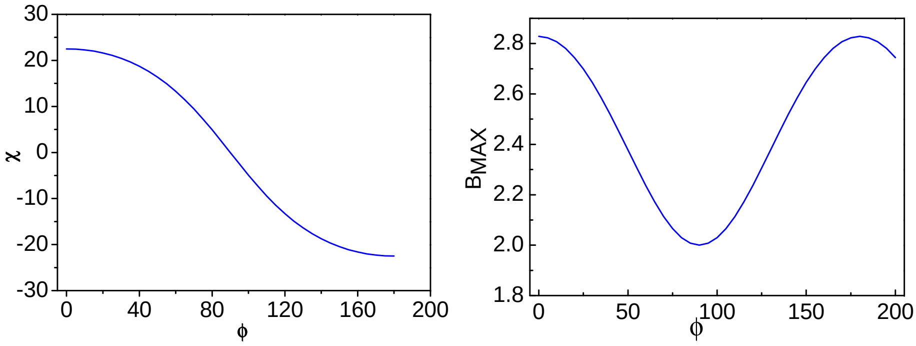

Figure 2.8: Theoretical curves for the variation of χ and B_{MAX} as a function of ϕ.

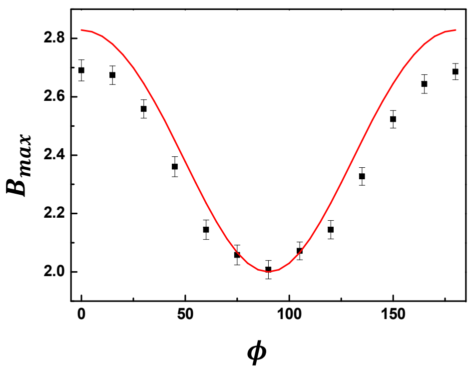

Figure 2.9: Variation of B_{MAX} with the relative phase when maximized over the linear bases

2.2.2 Optimized Measurement and Phase Independent B_{MAX} in Linear and Circular bases

However, the state given in Eq. 2.10 is always maximally non-separable/ entangled as the other entanglement measures like concurrence or von Neumann entropy are independent of ϕ. To get back the maximum Bell violation, one need to use different bases for the maximization of the Bell parameter. We redefine the OAM projecting state as

$$|\chi'\rangle = \cos(\chi)|l\rangle + e^{-i\phi}\sin(\chi)|-l\rangle \tag{2.13}$$

that gives

$$C(\theta, \chi') \propto |\langle\theta|\langle\chi'|\psi'\rangle|^2 = \cos^2(\theta - \chi) \tag{2.14}$$

One can obtain the same by introducing a relative phase in polarization state $|\theta\rangle$ too. Now the Bell-CHSH parameter B_{MAX} is independent of the relative phase ϕ. The different OAM measurement bases for different ϕ are given in Fig. 2.10.

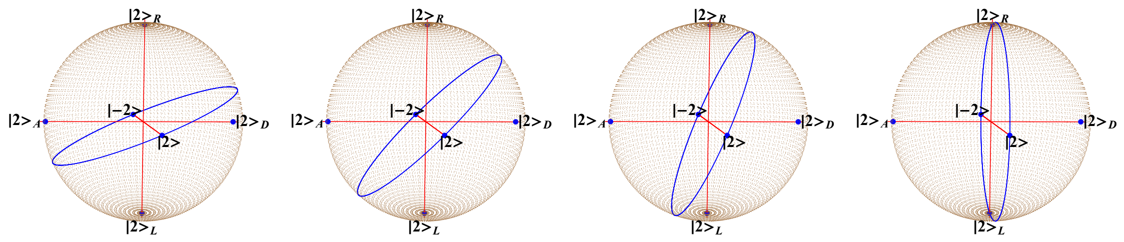

Figure 2.10: Choice of measurment bases for OAM in order to obtain maximum violation for Bell-CHSH parameter for $\phi = 22.5°, 45°, 67.5°$ and $90°$

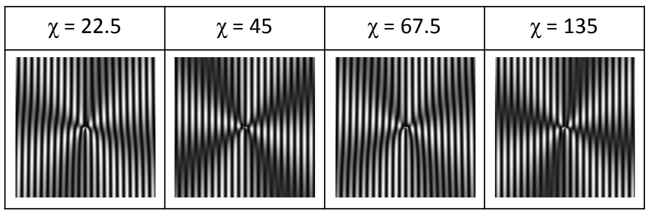

Figure 2.11: Holograms for optimizing the measurements of OAM states in linear bases with relative phase $\phi = 45°$ as given in Eq.2.13 and $\chi = 22.5, 45, 67.5, 135$

Next we check the Bell-CHSH parameter by projecting the state $|\psi'\rangle$ in circular basis of polarization and OAM. The states are given as

$$|\theta\rangle = e^{-i\theta}|H\rangle + e^{i\theta}|V\rangle; \; |\chi\rangle = e^{i\chi}|l\rangle + e^{-i\chi}|-l\rangle. \tag{2.15}$$

These measurement bases are given as red circles in Fig.2.2. Measuring the state $|\psi\rangle$ will result the same outcome as given in Eq. 2.5. Now the joint detection probability for the projection of the state $|\psi'\rangle$ to state $|\theta\rangle|\chi\rangle$ is given as

$$|\langle\theta|\chi|\psi'\rangle|^2 = \cos^2(\theta - \chi - \frac{\phi}{2}) \tag{2.16}$$

Thus with $\theta = 0°, \theta' = 45°, \chi = 22.5° + \frac{\phi}{2}$ and $\chi' = 67.5° + \frac{\phi}{2}$ we can obtain the Bell-CHSH parameter as $2\sqrt{2}$.

We have carried out the Bell parameter measurement with the introduction of relative phase in $|\chi\rangle$ to transform it to $|\chi'\rangle$ as given in Eq. 2.14. The holograms for optimizing the measurements of OAM states in linear bases with relative phase $\phi = 45°$ are given in Fig. 2.11. We also measure in circular basis for which projecting states are described by Eq. 2.6. With the change in measurement angles as mentioned above Bell - CHSH parameter is found to be constant with the relative phase ϕ. The results are given in Fig. 2.12. Here we don't have to change the measurement basis, as we have done in the linear case, to maximize B. So, when

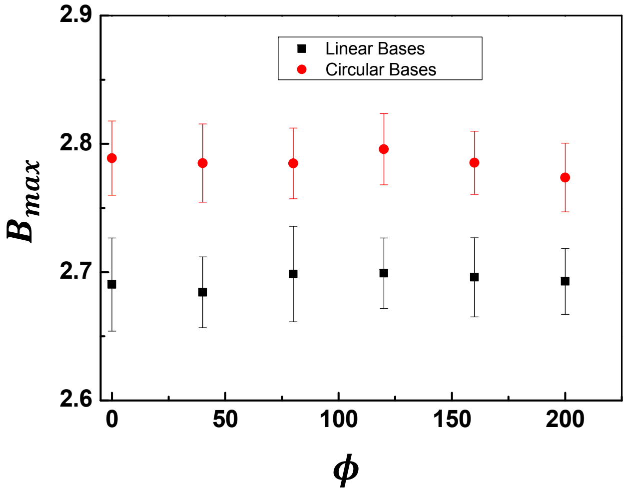

Figure 2.12: Measured values of phase independent B_{MAX} by introducing phase compensation in linear bases (black squares) and changing χ in circular bases (red circles)

projecting in circular basis, one can easily compensate the effect of Pancharatnam phase in the Bell-CHSH inequality measurement.

2.2.3 Stokes Imaging of Non-separable State with Pancharatnam Phase

We have analyzed the spatially varying polarization structure with the cyclic polarization evolution. The results are given in Fig. 2.13. The magenta and cyan circles show right and left circular polarizations. Two black lines are drawn corresponding to the diagonal polarization. It is found that the total polarization structure rotates with the relative phase introduced. We also give the images corresponding to different polarization projections for different ϕ. One can see that the images corresponding to diagonal and anti-diagonal projections are rotated with the relative phase ϕ. However, it doesn't affect the mode structure corresponding to horizontal or vertical projection. For the projection in any other linear state, the mode rotates with the relative phase. Thus a hologram that is supposed to convert the diagonal OAM state $\frac{1}{\sqrt{2}}(|l\rangle + |-l\rangle)$ to Gaussian, will not effectively convert the state $\frac{1}{\sqrt{2}}(|l\rangle + e^{i\phi}|-l\rangle)$. By introducing a phase in the OAM projecting bases as given in Eq. 2.14, which gives a rotation for the hologram corresponding to the projection onto χ other than $0°$& $90°$, one can compensate this effect and achieve the maximum violation of Bell CHSH inequality as given in Fig. 2.12. The optimized holograms are given in Fig. 2.11 for $\phi = 45°$.

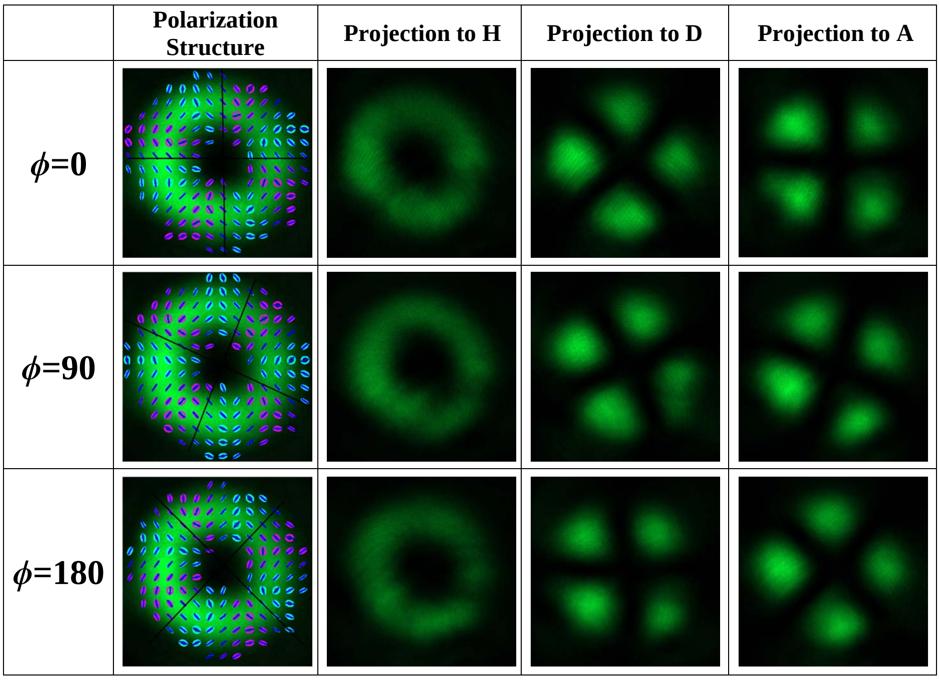

Figure 2.13: Polarization structure and the intensity profile corresponding to different polarization projections for different relative phase ϕ

2.3 A General OAM Poincaré Sphere from Non-separable States of Light

In an information theoretical point of view, it is favorable to consider a 2-D subspace of the infinite dimensional OAM space for simple construction of qubits [117]. Thus, a general superposition of $\{l, -l\}$ OAM states are similar to the polarization states. The geometrical representation of polarization, which spans a 2-D complex vector space, as points on the Poincaré sphere is known for many years. It is constructed using the real and measurable Stokes parameters that are derived from the complex Jones vectors [118]. A similar construction has been made for light beams carrying orbital angular momentum by considering it as a complex superposition of Hermite Gaussian (HG) spatial modes[100, 113]. This construction is valid only for a Laguerre Gaussian (LG) beam of azimuthal index $|l| = 1$. In spite of this many quantum information experiments are demonstrated with superposition state in $\{l, -l\}$ Hilbert space for higher value of $|l|$ [119]. In those cases the Hermite sphere will not act as an OAM Poincarés sphere. Here, we construct a Poincaré sphere for 2-D OAM states of arbitrary $\{l, -l\}$ Hilbert space. We generate all the points on this Poincaré experimentally using a non separable light beam of polarization and OAM. The mixed states of OAM are thus visualized and represented as points inside the Poincaré sphere.

2.3.1 Hermite Gaussian Sphere as OAM Poincaré Sphere

Orbital angular momentum Poincaré sphere is constructed based on the transformations between Laguerre-Gaussian (LG) and Hermite-Gausian modes of a laser beam [100]. A general LG mode of zero radial index and azimuthal index of "l" represents an optical vortex of order "l" and can be expressed in terms of HG modes as

$$LG_0^l = \frac{1}{2^l}\sum_{s=0}^{l}\binom{l}{s} i^s HG_{l-s,s} \tag{2.17}$$

where $\binom{l}{s}$ is the binomial coefficient. For $l = 1$,

$$LG_0^1 = \frac{1}{2}(HG_{0,1} + iHG_{1,0});\ LG_0^{-1} = \frac{1}{2}(HG_{0,1} - iHG_{1,0}). \tag{2.18}$$

This is in the similar to the relation between circularly and linearly polarized light. All the polarization states can be represented on the Poincaré sphere geometrically with horizontal and vertical polarizations as basis vectors. Similar Poincaré sphere has been constructed for OAM too with HG_{01} and HG_{10} modes as basis vectors. The Stokes vectors for these states are defined as

$$\begin{aligned} o_1 &= \frac{I_{HG_{10}^{0^o}} - I_{HG_{10}^{90^o}}}{I_{HG_{10}^{0^o}} + I_{HG_{10}^{90^o}}} \\ o_2 &= \frac{I_{HG_{10}^{45^o}} - I_{HG_{10}^{135^o}}}{I_{HG_{10}^{45^o}} + I_{HG_{10}^{135^o}}} \\ o_3 &= \frac{I_{LG_0^1} - I_{LG_0^{-1}}}{I_{LG_0^1} + I_{LG_0^{-1}}} \end{aligned} \tag{2.19}$$

where $I_{HG_{mn}^{\alpha}}$, is the intensity of the Hermite Gaussian mode HG_{mn} at an angle α. The unit sphere constructed by these Stokes parameters is considered to be an OAM Poincaré sphere. Surface of the sphere represents the pure OAM superposition states. HG_{01} and HG_{10} states form [X,-X] axes of the Poincaré sphere and LG_0^1, LG_0^{-1} are represented at the poles. On this Poincaré sphere one can represent all the superposition states of HG_{01} and HG_{10} modes.

Nevertheless, one cannot use this HG basis Poincaré sphere for OAM when $l > 1$. For $l = 2$, the expression for the LG mode is given by (Eq.2.17)

$$LG_0^2 = \frac{1}{4}(HG_{0,2} + 2iHG_{1,1} - HG_{2,0}). \tag{2.20}$$

This transformation includes the extra term of $2iHG_{1,1}$ and hence cannot be used to construct a Poincaré sphere with HG_{02} and HG_{20} modes as basis vectors. In general, one cannot represent all the pure OAM states on the Poincaré sphere. For representing all the OAM states and their superposition, we generalize the previous Poincaré sphere by replacing the HG basis vectors with $LG_0^{\pm l}$ modes.

2.3.2 An Alternate OAM Poinceré Sphere

We have considered a 2-D subspace of OAM for constructing this sphere. The Stokes parameters can be rewritten as

$$
\begin{aligned}
o_1 &= \frac{I_{LG_0^l} - I_{LG_0^{-l}}}{I_{LG_0^l} + I_{LG_0^{-l}}} \\
o_2 &= \frac{I_{LG_0^{l_D}} - I_{LG_0^{l_A}}}{I_{LG_0^{l_D}} + I_{LG_0^{l_A}}} \\
o_3 &= \frac{I_{LG_0^{l_R}} - I_{LG_0^{l_L}}}{I_{LG_0^{l_R}} + I_{LG_0^{l_L}}}
\end{aligned}
\tag{2.21}
$$

where

$$
LG_0^{l_{D/A}} = LG_0^l \pm LG_0^{-l};\; LG_0^{l_{R/L}} = LG_0^l \pm iLG_0^{-l}. \tag{2.22}
$$

The two OAM modes form the [X,-X] axes and their complex superposition can be represented at the poles. With this, one can realize all possible pure states of OAM geometrically on the surface of Poincaré sphere. We have shown the previous and present Poincaré spheres in Fig. 2.14.

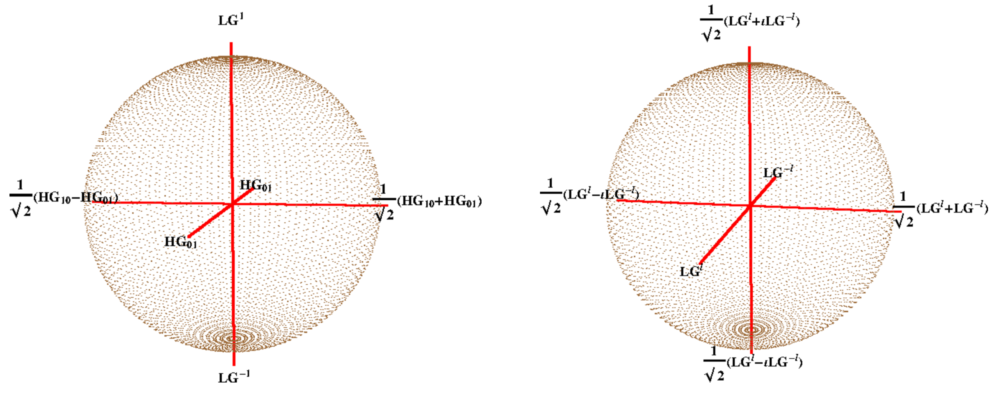

Figure 2.14: OAM Poincaré sphere with HG modes as basis vectors (left) and the present Poincaré sphere with LG modes as basis vectors in $\{l, -l\}$ subspace (right).

2.3.3 Generation of all points on the Surface of OAM Poincaré sphere

A non-separable state of polarization and OAM can be written as

$$|\psi\rangle = \frac{1}{\sqrt{2}}\left(|H\rangle|l\rangle + |V\rangle|-l\rangle\right) \tag{2.23}$$

where $|H\rangle, |V\rangle$ and $|l\rangle, |-l\rangle$ are basis vectors of two dimensional complex vector spaces of

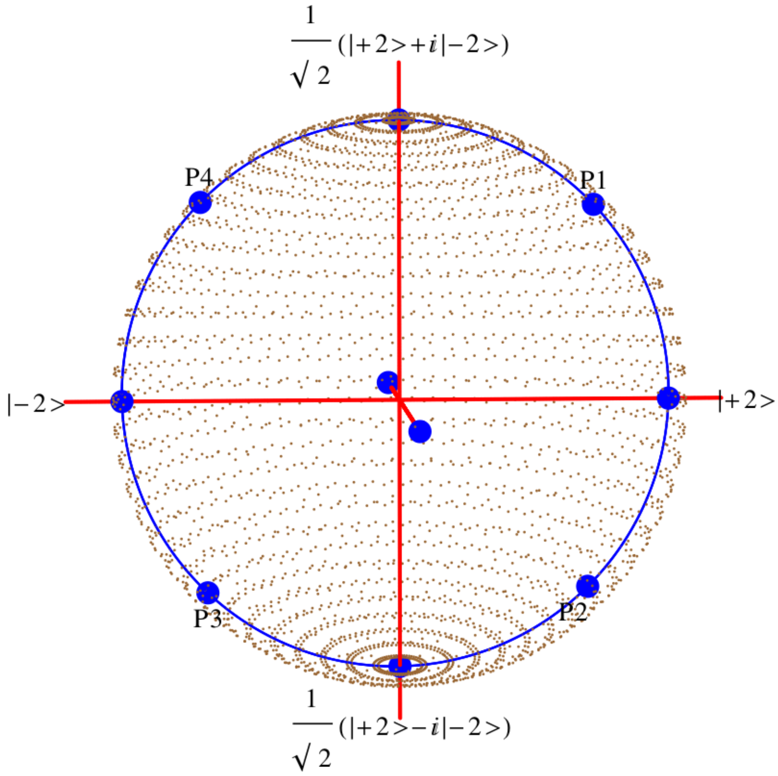

Figure 2.15: Generated points represented on the Poincaré sphere.

polarization and OAM respectively. The intensity distribution of this non-separable beam is similar to an optical vortex of order l.

Allow this beam pass through a Simon Mukunda gadget arranged in Q-H-Q manner. We use the similar configuration as in the section 2.2.1 where the orthogonal polarizations acquire Pancharatnam phase of opposite signs. The state becomes as given in Eq. 2.10

$$|\psi'\rangle = \frac{1}{\sqrt{2}}\left(|H\rangle|l\rangle + e^{-i\phi}|V\rangle|-l\rangle\right) \tag{2.24}$$

where $\phi = \pi + 4\phi'$. Now project this state to a linear polarization state using a half wave plate at angle $\frac{\theta}{2}$ and a polarizing beam splitter which transmit only the horizontal polarization . The state will be

$$|\psi_o\rangle = \cos(\theta)|l\rangle + e^{-i\phi}\sin(\theta)|-l\rangle \tag{2.25}$$

State	$\vert 2\rangle$	$\frac{1}{\sqrt{2}}(\vert 2\rangle + \vert -2\rangle)$	$\frac{1}{\sqrt{2}}(\vert 2\rangle - \vert -2\rangle)$	$\frac{1}{\sqrt{2}}(\vert 2\rangle + i\vert -2\rangle)$	$\frac{1}{\sqrt{2}}(\vert 2\rangle - i\vert -2\rangle)$
Stokes Vector	$\{1\ 0\ 0\}$	$\{0\ 1\ 0\}$	$\{0\ -1\ 0\}$	$\{0\ 0\ 1\}$	$\{0\ 0\ -1\}$
Theoretical	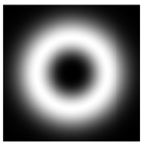	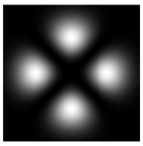	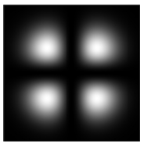	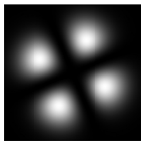	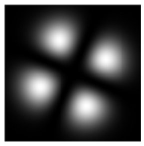
Experimental	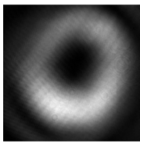	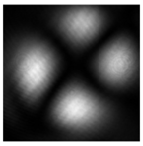	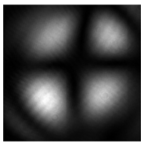	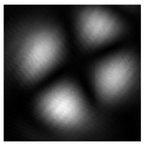	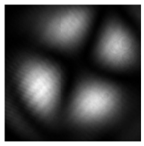
State	$\vert -2\rangle$	$\cos(\frac{\pi}{8})\vert 2\rangle + i\sin(\frac{\pi}{8})\vert -2\rangle$	$\cos\left(\frac{\pi}{8}\right)\vert 2\rangle - i\sin(\frac{\pi}{8})\vert -2\rangle$	$\sin\left(\frac{\pi}{8}\right)\vert 2\rangle + i\cos(\frac{\pi}{8})\vert -2\rangle$	$\sin\left(\frac{\pi}{8}\right)\vert 2\rangle - i\cos(\frac{\pi}{8})\vert -2\rangle$
Stokes Vector	$\{-1\ 0\ 0\}$	$P_1:\{\frac{1}{\sqrt{2}}\ 0\ \frac{1}{\sqrt{2}}\}$	$P_2:\{\frac{1}{\sqrt{2}}\ 0\ -\frac{1}{\sqrt{2}}\}$	$P_4:\{-\frac{1}{\sqrt{2}}\ 0\ \frac{1}{\sqrt{2}}\}$	$P_3:\{-\frac{1}{\sqrt{2}}\ 0\ -\frac{1}{\sqrt{2}}\}$
Theoretical	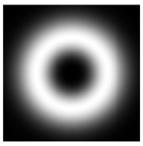	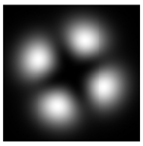	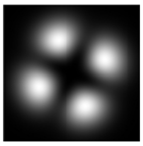	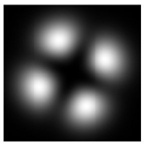	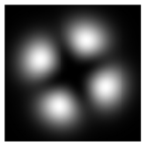
Experimental	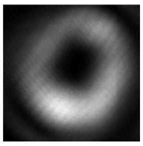	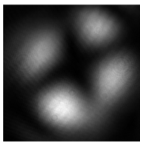	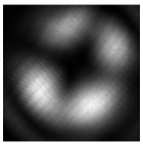	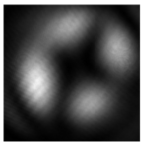	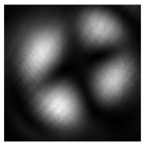

Figure 2.16: Generated states and its intensity distributions.

By varying θ and ϕ we can generate all points on the Poincaré sphere. To demonstrate the same we generate 10 points lying on a great circle of the OAM Poincaré sphere. The points are shown in Fig. 2.15. The intensity distribution of the generated states are given in Fig.2.16

2.3.4 Points inside the sphere, centre and mixed states of OAM

The points inside the Poinceré shpere, by construction, constitutes the mixed states of polarization whose degree of polarization is $s_1^2 + s_2^2 + s_3^2 < 1$. The centre corresponds to completely mixed/unpolarized light state. All natural sources of light give this mixed state of polarization which has a 2-D basis. OAM has infinite dimensional basis and to the best of our knowledge, no natural source gives the mixed state of OAM in 2-D OAM space. To obtain this, we need to couple the OAM of a light beam to the other degree of freedom such as *polarization* that prevents their superposition. For example, the hybrid entangled state of OAM and polarization gives the mixed state in 2-D OAM state. Now, one can represent all the hybrid entangled states of OAM and another degree of freedom inside the OAM Poinacré sphere. The centre gives the maximally entangled states while the others give non-maximally entangled states with decreased amount of mixedness. The degree of entanglement increases from 0 to 1 if we move from the surface to the centre where as the purity of the OAM states decreases from 1 to 0. The purity of the OAM states and the degree of entanglement can be measured from radial distance.

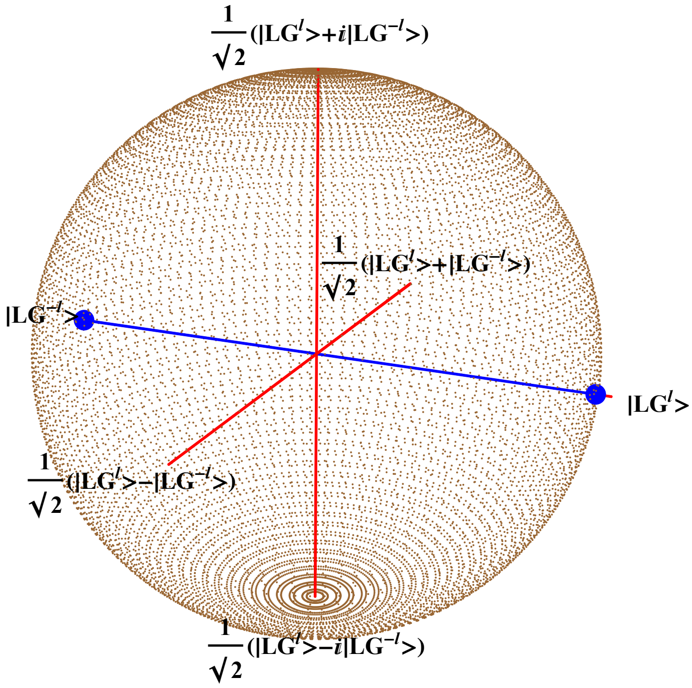

Figure 2.17: All the OAM state defined by Eq.2.27 are given in blue.

Consider the state given

$$|\psi\rangle = \cos(\xi)|Hl\rangle + \sin(\xi)|V - l\rangle \tag{2.26}$$

Its density matrix is given as $\rho = |\psi\rangle\langle\psi|$. Taking a partial trace over polarization we get

$$\rho_o = Tr_p\{|\psi\rangle\langle\psi|\} = \cos^2(\xi)|l\rangle\langle l| + \sin^2(\xi)| - l\rangle\langle -l| \tag{2.27}$$

Degree of purity is defined as

$$D = \frac{\sqrt{o_1^2 + o_2^2 + o_3^2}}{s_o} \tag{2.28}$$

From the density matrix, we can have

$$D^2 = 2\left(Tr\{\rho_o^2\} - \frac{1}{2}\right) = 2\left(\cos^4(\xi) + \sin^4(\xi) - \frac{1}{2}\right) \tag{2.29}$$

Thus when $\xi = \pi/4$ the state given in Eq. 2.26 will be maximally non separable which correspond to zero degree of purity. In the OAM subspace, the state is maximally mixed and can be represented as the centre of the OAM Poincaré sphere. When $\xi = 2n\pi, (2n+1)\pi/2$, $D = 1$ and state is represented on the surface of OAM Poincaré sphere. The state given in Eq. 2.27 can be obtained from the same set up used to generate the non-separable state Fig.2.3. In this case the half wave plate before the beam splitter has to be aligned at an angle $\frac{\xi}{2} - \frac{\pi}{4}$.

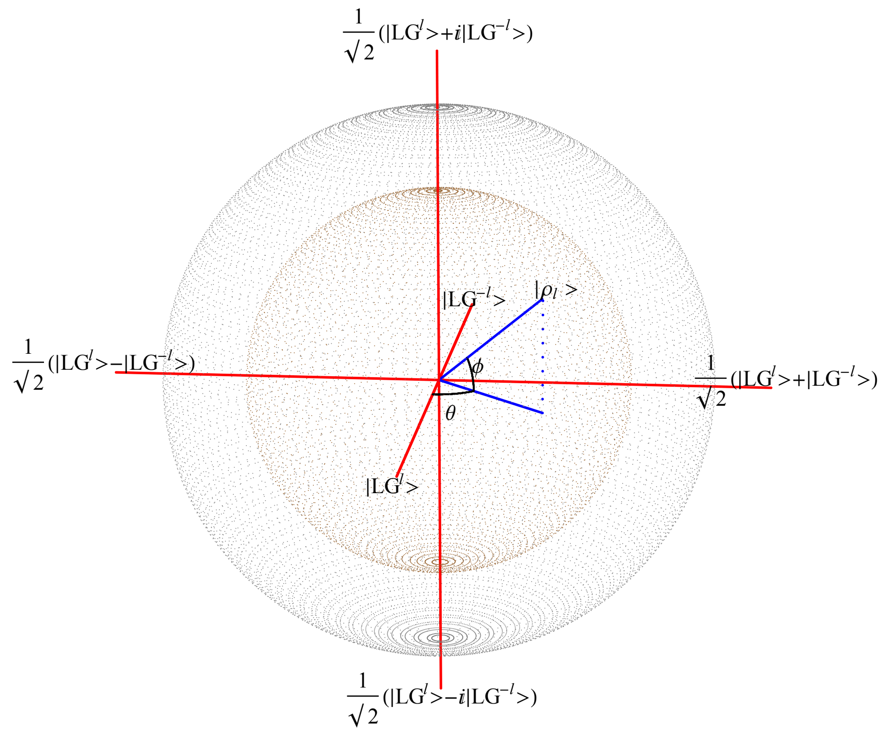

Figure 2.18: OAM states with degree of purity = 0.7 is represented as a sphere inside the Poincaré sphere with radius r=0.7.

However, The state defined in Eq. 2.27 doesn't represent a general mixed state. By varying ξ one can generate points lying on the X-axis, including the centre, only. These points are given in Fig.2.17.

A general state can be defined as

$$|\psi_g\rangle = \cos(\xi)|H\Psi_l\rangle + \sin(\xi)|V\Psi_l^{\perp}\rangle \tag{2.30}$$

where

$$\begin{aligned}\Psi_l &= \cos(\theta)|+l\rangle + e^{-i\phi}\sin(\theta)|-l\rangle \\ \Psi_l^{\perp} &= \sin(\theta)|+l\rangle - e^{-i\phi}\cos(\theta)|-l\rangle\end{aligned} \tag{2.31}$$

The general OAM state is obtained by taking a partial trace of the density matrix corresponding to the state given in Eq. 2.30

$$\rho_o = Tr_p\{|\psi_g\rangle\langle\psi_g|\} = \cos^2(\xi)|\psi_l\rangle\langle\psi_l| + \sin^2(\xi)|\psi_l^{\perp}\rangle\langle\psi_l^{\perp}| \tag{2.32}$$

For a particular value of D , which define the radial distance, θ and ϕ can be varied to form a sphere inside the unit OAM Poincaré sphere. Fig.2.18 represents all the points with $D = 0.7$.

2.4 Conclusion

We have generated non-separable state of polarization and OAM using a polarizing Sagnac interferometer. We have studied the effect of Pancharatnam geometric phase in a non-separable state of polarization and OAM. The non-separability is confirmed by the violation of Bell-CHSH inequality. The geometric phase introduced in the polarization subsystem induces a relative phase in the Bell like state of OAM and polarization. The maximum value of the Bell parameter, B_{MAX}, maximized over the measurement angles, varies sinusoidally according to the relative phase. We obtain a constant B_{MAX} for different geometric phase by introducing a relative phase in the projected OAM state. We also show that the Bell CHSH inequality measurement in circular bases can remove the phase dependence of the B_{MAX} by shifting the measurement angle. We have analyzed the polarization structure of the non-separable state for different Pancharatnam phases that gives a rotation to it. This physically explain the effect of Pancharatnam phase in the joint measurement of polarization and OAM.

We have described an OAM Poincaré sphere which can represent all OAM superposition states in $\{l, -l\}$ subspace even for $|l| \geq 1$. We also have presented an experimental method for the generation of all such states using a non-separable state of OAM and polarization. We have also described the representation of OAM mixed states as non-separable states inside the Poincaré sphere.

Chapter 3

Scattering of Non-separable States of Light

In the previous chapter we have studied the properties of non-separable states of polarization and orbital angular momentum (OAM) along with its violation of Bell-CHSH inequality. These non-separable stats have application in optical communications and its interesting to study the nature of them under scattering. As the non-separable states can be coded with more information, its desirable to revive the state after scattering for decoding the information. In this chapter, we study the effect of scattering on a non-separable state of light.

Scattering of structured light beams such as optical vortices has been studied for their coherence properties and applications [120–124]. It has been shown that one can generate ring shaped beams from the scattering of coherent optical vortices [125]. Here, we generate light beams with non-separable OAM and polarization and verify the preservation of non-separability under scattering through a rotating ground glass (RGG). These non-separable beams can be generated using q-plates [126, 127] or interferometers [85, 114] . In our set up, we use a modified polarizing Sagnac interferometer [114] containing a spiral phase plate (SPP) to generate these non-separable beams. The generated beams scatter through a RGG and the scattered light is collected by a plano-convex lens to measure their polarization and intensity distributions at the focus. We measure the degree of polarization of the beam, as a measure of non-separability [128–130], before and after scattering which should be 0 for a maximally non-separable state and 1 for a completely separable state. We also project the scattered as well as coherent light to different polarizations and record their corresponding intensity distributions which confirm the non-separability. Using the same experimental setup, we vary the degree of non-separability by controlling the intensities in the two arms of the interferometer. These recovered partially coherent non-separable states can be used to generate any arbitrary superposition of partially coherent OAM states.

3.1 Preservation of Non-separability Under Scattering

We generate beams with non-separable polarization and OAM states and experimentally verify the preservation of non-separability under scattering. Preservation is confirmed by measuring degree of polarization and contextual imaging.

In subsection 3.1.1 we give a theoretical introduction to the OAM-polarization non-separable state and describe the methods we use to witness the non-separability. Experimental setup to generate the described states is given in subsection 3.1.2. The results and discussion are given in subsection 3.1.3. For simplicity, we use the Dirac notation to describe the states even though we are using classical light beams.

3.1.1 Theoretical Background

A maximally entangled/non-separable state of polarization and OAM can be written as

$$|\psi\rangle = \frac{1}{\sqrt{2}} \left(|H\rangle| + l\rangle + |V\rangle| - l\rangle\right) \tag{3.1}$$

where $|H\rangle, |V\rangle$ and $|+l\rangle, |-l\rangle$ are basis vectors of 2D complex vector spaces of polarization and OAM subspace respectively. This state is formed simply by superposing two orthogonally polarized optical vortices of equal intensities and with equal and opposite charges. The density matrix for the non-separable state $|\psi\rangle$ is given by $\rho_{ns} = |\psi\rangle\langle\psi|$. One can obtain the reduced density matrix corresponding to the polarization by taking a partial trace over OAM states on this density matrix,

$$\rho_p = Tr_l\{\rho_{ns}\} = \sum_{i=H,V} \langle i|\psi\rangle\langle\psi|i\rangle \ = \frac{I_p}{2}$$

here, I_P is a 2×2 identity matrix. For a given density matrix ρ one can define linear entropy (S_L) [131]

$$S_L = \frac{d}{d-1}(1 - Tr(\rho^2)). \tag{3.2}$$

S_L characterizes the amount of mixedness for a given density matrix. It is known that for an entangled/non-separable state, the subsystems will be in a mixed state. Stronger the non-separability, larger the amount of mixedness present in the subsystems. Thus by measuring

S_L of the subsystem, one can measure the degree of entanglement or the non-separability. For the maximally non-separable state given in Eq. 3.1, one can find the linear entropy of polarization,

$$S_L = 2(1 - Tr(\rho_p^2)) = 1. \tag{3.3}$$

This corresponds to a completely mixed polarization state in contrast to a completely polarized state with $S_L = 0$. We know, the state of polarization represented by a Poincare sphere can be completely described by

$$\rho_p = \frac{1}{2}\sum_{i=0}^{3} \sigma_i . s_i \tag{3.4}$$

where σ_i's and s_i's are the Pauli matrices and normalized Stokes parameters respectively. The trace of square of this density matrix is given by

$$Tr\{\rho_p^2\} = \frac{1}{2}\left(1 + s_1^2 + s_2^2 + s_3^2\right) = \frac{1}{2}(1 + DOP^2) \tag{3.5}$$

where DOP is the degree of polarization which is measured as the magnitude of the Stokes vector $\sqrt{s_1^2 + s_2^2 + s_3^2}$. Using Eq. 3.3 and Eq. 3.5 one can relate DOP to linear entropy as

$$S_L = 1 - DOP^2. \tag{3.6}$$

Thus for a maximally non-separable state of polarization and OAM, for which $S_L = 1$, the degree of polarization should be zero. One can easily determine the degree of polarization experimentally by measuring the Stokes parameters [118].

Another characteristic of the non-separable state is contexuality. For a separable state, measurement on one degree of freedom doesn't affect the measurement outcome of the other. However, in the case of a non-separable state, measurement outcome in one degree of freedom will depend on the context of measurement in the other. In our experiment the OAM state of the beam varies according to the projections to different polarization states due to their non-separability. Consider a general polarization state defined as

$$|\xi\rangle = \cos(\theta)|H\rangle + e^{i\phi}\sin(\theta)|V\rangle \tag{3.7}$$

where θ and ϕ are the Euler angles corresponding to the state $|\xi\rangle$ on the Poincaré sphere. Projecting $|\psi\rangle$ given in Eq. 3.1 to $|\xi\rangle$, we obtain the OAM state as

$$|\psi_o\rangle_{\theta,\phi} = \langle\xi|\psi\rangle = \cos(\theta)|l\rangle + e^{-i\phi}\sin(\theta)| - l\rangle. \tag{3.8}$$

This is a pure OAM superposition state. The transverse profile of the beam will correspond to superposition of two equal and oppositely charged vortices with different relative amplitudes and phase. So according to θ and ϕ defined by polarization projection, the intensity profile of the beam will vary. For demonstration we take $(\theta, \phi) = (0, 0), (90, 0), (45, 0), (-45, 0), (45, 90)$ and $(-45, 90)$ which correspond to $|H\rangle, |V\rangle, |D\rangle = |H\rangle + |V\rangle, |A\rangle = |H\rangle - |V\rangle, |R\rangle = |H\rangle + i|V\rangle$ and $|L\rangle = |H\rangle - i|V\rangle$ polarization states.

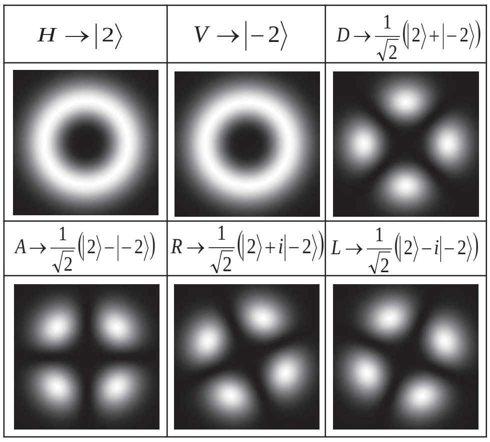

Figure 3.1: Theoretical images for the transverse intensity profile of a non-separable state described by Eq. 3.1 with $|l| = 2$ for projections to different polarization states. H-Horizontal, V- vertical, D-diagonal, A-anit-diagonal, R-rightcircular, L-leftcircular

Figure 3.1 shows the theoretical intensity distributions corresponding to different polarization projections for $|l| = 2$. The projection on H (V) polarization gives a vortex of order $2(-2)$. The projections of the state on diagonal (D), anti-diagonal (A), left circular (L) and right circular (R) gives superposition of two vortices that contain $2l$ (in our case $|l| = 2$) number of lobes with different orientations. The number of lobes confirms the order or the azimuthal index of the vortex and the change in their orientation confirms the presence of non-separability in a light beam.

3.1.2 Experiment

The experimental set up used to generate the non-separable state and to study its properties is shown in Fig. 3.2. We have used a diode pumped solid state green laser (Verdi 10) with vertical polarization for our study. The laser beam passes through a half wave plate, whose fast axis is oriented at -22.5^o with the horizontal that changes beam polarization from vertical to diagonal. Then it passes through a polarizing Sagnac interferometer containing a spiral phase plate (SPP) to generate a light beam which is non-separable in polarization and OAM.

Two orthogonally polarized (H and V) counter propagating Gaussian beams are converted

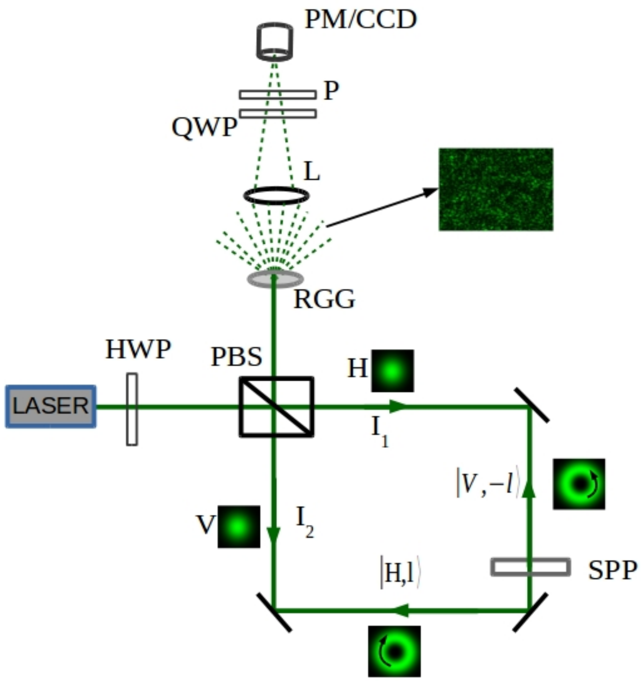

Figure 3.2: Experimental setup for the generation and scattering of non-separable state of polarization and OAM. HWP- half wave plate, QWP- quarter wave plate, P- polarizer, *L*- lens with focal length 15 cm, CCD- charge coupled device (camera), PM-power meter, PBS- polarizing beam splitter

into optical vortices of orders l (for H) and $-l$ (for V) by the SPP designed for order $|l| = 2$. These orthogonally polarized and oppositely charged vortices superpose at the same PBS to form the described non-separable state. This non-separable state is generated only in the presence of SPP otherwise two orthogonally polarized Gaussian beams will superpose resulting in a diagonally polarized light beam. The doughnut shaped non-separable beam forms a random speckle distribution after scattering through the ground glass. A part of the scattered light collected with a lens of focal length 15 cm placed at a distance of 22 cm from the ground glass plate. The ground glass plate is rotating at $\approx$ 930 revolutions per minute to average out the speckles. We have measured the Stokes parameters using a quarter wave plate and a polarizer. The power measurements for determining Stokes parameters were done with an optical power meter (Thorlab) of sensitivity 1 nW. We have recorded the intensity distributions corresponding to the different polarization projections with an Evolution VF color cooled camera (pixel size 4.65μm) kept at the focus of the lens.

State	Before scattering			After scattering		
	Stokes Vectors		DOP	Stokes Vectors		DOP
Separable state (without SPP)	s_1	0.044	0.957	s_1	0.056	0.924
	s_2	0.956		s_2	0.922	
	s_3	-0.02		s_3	-0.026	
Non-separable state(with SPP)	s_1	-0.03	0.001	s_1	0.01	0.001
	s_2	-0.01		s_2	-0.02	
	s_3	0.02		s_3	-0.02	

Table 3.1: Stokes vectors and the degree of polarization corresponding to separable and non-separable states of light before and after scattering.

3.1.3 Results and Discussion

We have measured the Stokes parameters (s_0, s_1, s_2, s_3) of coherent and scattered light beams for both separable (without SPP) and non-separable states (with SPP). We compare the degree of polarization of beams before and after scattering and the results are given in table 3.1. From the table, it is clear that the separable light beam is completely polarized (diagonal) while the non-separable state is completely unpolarized. The deviations in degree of polarization may be due to uncertainties in the orientation of the wave plates and small misalignment of the interferometer. However, our experimental findings are very close to theoretical predictions.

We also generate non-maximally entangled states simply by controlling intensities in the two arms of the interferometer. This can be easily done by rotating the fast axis of the HWP. Then the state will be

$$|\psi\rangle = \frac{1}{\sqrt{I_1 + I_2}} \left(\sqrt{I_1} |H\rangle| + 2\rangle + \sqrt{I_2} |V\rangle| - 2\rangle \right) \tag{3.9}$$

By varying I_1 from 0 to I and correspondingly I_2 from I to 0, we have generated different states given in Eq. 3.9. Note that the total intensity, $I_1 + I_2 = I$ is always constant. For the state described in Eq. 3.9, we can check the mixedness of the subsystem (here polarization) by calculating S_L which also indicates the degree of non-separability. It reduces to a simple analytic expression,

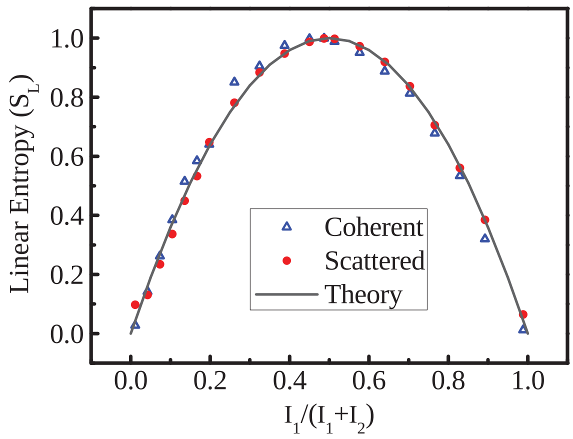

Figure 3.3: Linear entropy *vs.* normalized intensity $\frac{I_1}{I_1+I_2}$ plot for coherent and scattered non-separable states of light along with theoretical curve given by Eq. 3.10.

$$S_L = \frac{4I_1I_2}{(I_1+I_2)^2}. \tag{3.10}$$

Line curve in Fig. 3.3 shows the variation of linear entropy S_L of polarization with the normalized intensity in one arm of the interferometer as given in Eq. 3.10. The linear entropy becomes zero when for $I_1 = 0$ or $I_2 = 0$, for which the state become $|H\rangle|l\rangle$ and $|V\rangle|-l\rangle$ respectively. When two intensities are same ($I_1 = I_2$), the state becomes completely non-separable for which $S_L = 1$.

We measure the Stokes parameters and calculate the degree of polarization and linear entropy experimentally corresponding to each value of I_1 for coherent and scattered light beams. The results are shown in Fig. 3.3. One can clearly see that the S_L *vs.* normalized intensity curve for both the coherent and scattered light are matching well and in good agreement with the theoretical curve. The results of polarization measurements given in table 3.1 and Fig. 3.3 which confirm the preservation of non-separability in polarization and OAM under scattering by the RGG.

Figure 3.4 shows the intensity distributions for a coherent and a scattered light beam with non-separable state projected to the different polarizations. Our results show the similar behavior for both coherent and scattered light beams and are in good agreement with the theoretical images shown in Fig. 3.1 that confirm the preservation of non-separability.

We also observe that the amount of scattered light collected by the lens is irrelevant regarding the non-separable properties. In fact, one can use multiple number of lenses and collimate again to form several copies of a partially coherent non-separable beam. This

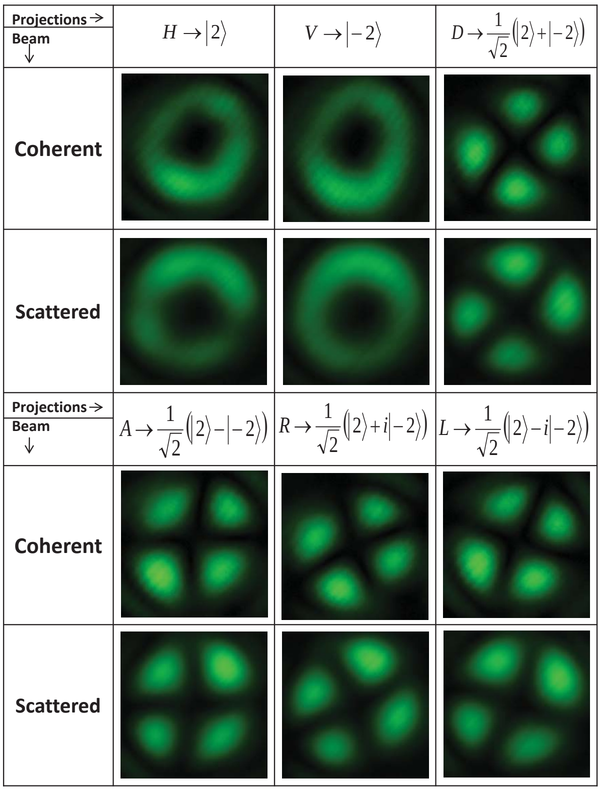

Figure 3.4: Experimental images of coherent and scattered non-separable states of light with $l = 2$ for different polarization projections. OAM states corresponding to each intensity distribution are also given.

property can be used in public communication systems.

3.2 Polarization Controlled Generation of Partially Coherent OAM States

There are a number of studies dealing with partially coherent vortex beams for the identification of charge [132], propagation [133] and spatial correlation studies [134]. Thus, generation of an arbitrary super position of partially coherent OAM beams is of high importance. We have already shown in the previous section that, one can revive the non-separable beam after the scattering by collection it using a lens. This can be used to generate arbitrary partially coherent OAM states too. One can project the regenerated partially coherent non-separable states for different polarization giving different OAM states. One can see the states in Fig. 3.4 as the scattered beam represent the partially coherent ones. The temporal coherence can be decreased of increased by increasing or decreasing the speed of the RGG. The spatial coherence can be increased by introducing a lens before the scattering plate and focusing to a tighter spot.

3.3 Conclusion

We have produced a light beam with non-separable polarization and orbital angular momentum states using a simple interferometer and experimentally verified the preservation of non-separability under scattering through a rotating ground glass. The polarization measurements and the images of the beam projected to different polarizations show the presence of non-separability for coherent and scattered light. We have also demonstrated the generation of non-maximally non-separable states of light and studied their behaviour under scattering by measuring the degree of polarization. This recovered partially coherent non-separable states can be used to generate arbitrary superposition states of OAM by polarization selection. Our results can have application in public broadcasting systems.

Chapter 4

Quantum Information With Even and Odd Orbital Angular Momentum States of Light

In the previous chapters we have studied the properties of OAM-polarization non-separability for classical laser beams. In this chapter we describe the quantum states of OAM and its applications. We use OAM and polarization entanglement for implementing different quantum protocols. Here we give a brief introduction for quantum protocols with OAM and polarization states and give a rationale behind the intention of using even/odd states of OAM.

Quantum information protocols mainly rely on the fact that particle can be in a complex superposition of states. Polarization state of photons is used extensively to implement many quantum protocols. The polarization of a photon spans in a two dimensional Hilbert space. So the polarization state of a photon is considered as a qubit. Also, one can generate photons entangled in polarization using spontaneous parametric down conversion (SPDC) of a laser beam. All four maximally entangled states, Bell states, can be achieved in the polarization degree of freedom (DOF).

Orbital angular momentum (OAM) is another degree of freedom of photon that can be used in quantum protocols along with polarization so that the information carried per photon can be increased [36]. OAM entanglement can also be achieved by SPDC and many quantum protocols were demonstrated using the same [49–56]. The basis states of OAM span an infinite dimensional Hilbert space. This higher dimensionality is really useful for the denser coding of information in single photons [135]. One can achieve OAM entanglement in higher dimensions which can be used for many quantum protocols. However, we often need to use two dimensional OAM states for the ease of measurements. Also for many protocols using hybrid-entanglement, entanglement between polarization and OAM of photons, we need the 2 dimensional OAM sub-space[64, 65].

Experimentally the restriction of OAM states to 2D is done by post selection using diffractive holograms and a single mode fibre [49]. This results in the loss of photons which reduces efficiency of the protocol. We investigate the possibility of using a 2D OAM space without any photon loss. This is possible since any infinite set of integers can be grouped into two natural categories: even and odd. In the case of OAM, this becomes possible because of an effective even/odd OAM sorter, an optical set up designed to separate even and odd states of OAM. However, the even/odd states of OAM have not been extensively explored for quantum information tasks. For that, we need to develop projective measurement in even/odd basis. We propose simple interferometric method for the projective measurements.

We demonstrate the tomography of the even/odd states with projective measurement in Pauli's operator bases. We also describe hyper-entanglement and hybrid-entanglement with polarization as another DOF and propose interferometric set up for the spin orbit Bell state analysis (SOBA). Measurements for checking the Bell's inequality in even/odd OAM entanglement is discussed for the first time. This can be applied in entanglement based cryptographic protocol. It is theoretically impossible to distinguish all Bell states using local operations and classical communications (LOCC) [136]. However, with hyper-entanglement and SOBA, one can distinguish all the Bell states of polarization using LOCC. Using the same, we describe efficient super dense coding.

4.1 From Infinite Dimensional OAM Space to Two Dimensional Even/odd OAM Space

The general infinite dimensional OAM space is spanned by the OAM values from $-\infty, .. -1, 0, +1, ... +\infty$. A general state in this infinite dimensional basis can be written as

$$|\psi\rangle = \sum_{m=-\infty}^{+\infty} c_m |m\rangle \tag{4.1}$$

with $\sum_{m=-\infty}^{+\infty} |c_m|^2 = 1$. However, many quantum experiments were realized using the OAM qubits in the reduced Hilbert space $\{m, -m\}$. In such cases OAM encoding or measurements were performed using diffraction through holograms and the mode filtering. Basically here one neglects the photons generated with OAM $l \neq m, -m$ which result in photon loss. Moreover, the efficiency of mode filtering is also a limiting factor for quantum experiments with OAM. Thus to make an equivalent qubit state, Eq. 4.1 can be re written as

$$|\psi\rangle = \sum_k \left(c_{2k}|2k\rangle + c_{2k+1}|2k+1\rangle\right). \tag{4.2}$$

We define the appropriate operators in order to perform the measurements in the even/odd basis. The general projection operator is

$$P(\theta,\phi) = \sum_k \Big(\cos(\theta)|2k\rangle + e^{i\phi}\sin(\theta)|2k+1\rangle\Big)\Big(\cos(\theta)\langle 2k| + e^{-i\phi}\sin(\theta)\langle 2k+1|\Big). \tag{4.3}$$

With these projective measurements we can consider the whole OAM state as a qubit state and use for quantum protocols.

In the case of OAM entanglement, when we work with $\{m, -m\}$ basis, photons corresponding to other modes are lost in the measurement. For example, when we pump a non-linear crystal for SPDC using a Gaussian beam, the signal and idler photons are entangled in OAM. The two photon state is given as

$$|\Psi\rangle_{12} = c_0|0\rangle|0\rangle + \sum_{m=1}^{+\infty} c_m\left(|m\rangle|-m\rangle + |-m\rangle|m\rangle\right) \tag{4.4}$$

with $\sum_{m=0}^{+\infty}|c_m|^2 = 1$ In many of the OAM entanglement experiments, this state is projected in $\{+1,-1\}$ basis for treating it as a two qubit entangled state. In such cases, the probability of getting photons entangled in $\{+1,-1\}$ OAM states is $|c_1|^2 \ll 1$. Thus most of the down converted photons remain unused.

For even/odd OAM entanglement, we consider the parametric down conversion of an optical vortex of order 1 and having vertical polarization in a type I second order non-linear crystal. The state corresponding to the pair of photons produced by SPDC of this beam is given by

$$|\Psi\rangle_{12} = \sum_{m=-\infty}^{+\infty} c_m|m\rangle_1|1-m\rangle_2 \otimes |H\rangle_1|H\rangle_2 \tag{4.5}$$

By grouping all even and odd OAM states, one can rewrite the expression for the OAM state in Eq. 4.5 as

$$\sum_{m=-\infty}^{+\infty} c_m(|m\rangle_1|1-m\rangle_2) = \sum_{k=-\infty}^{+\infty} c_{2k}(|2k\rangle_1|1-2k\rangle_2) + \sum_{k=-\infty}^{+\infty} c_{1-2k}(|1-2k\rangle_1|2k\rangle_2).$$

Thus

$$|\Psi\rangle_{12} = \left(\sum_{k=-\infty}^{+\infty} c_{2k}(|2k\rangle_1|1-2k\rangle_2) + \sum_{k=-\infty}^{+\infty} c_{1-2k}(|1-2k\rangle_1|2k\rangle_2)\right) \otimes |H\rangle_1|H\rangle_2 \tag{4.6}$$

From the conservation of OAM, we have

$$\sum_{k=-\infty}^{+\infty} (c_{2k})^2 = \sum_{k=-\infty}^{+\infty} (c_{1-2k})^2 = \frac{1}{2} \sum_{m=-\infty}^{+\infty} (c_m)^2 = \frac{1}{2}. \tag{4.7}$$

Thus one can arrive at an operational expression for even/odd OAM entanglement as

$$|\Psi\rangle_{12} = \frac{1}{\sqrt{2}} (|E\rangle_1 |O\rangle_2 + |O\rangle_1 |E\rangle_2) \otimes |H\rangle_1 |H\rangle_2. \tag{4.8}$$

Here $|E\rangle$ and $|O\rangle$ correspond to the even/odd states on detection. Thus, we get a two qubit entanglement in OAM without loosing any photons.

4.2 State tomography for OAM states in even/odd basis

Similar to polarization, we need to find the Stokes vector for the super position state given in Eq. 4.2 by projective operators which are

$$\begin{aligned}
P_0 &= \sum_k (|2k\rangle\langle 2k| + |2k+1\rangle\langle 2k+1|) \\
P_1 &= \sum_k (|2k\rangle\langle 2k| - |2k+1\rangle\langle 2k+1|) \\
P_2 &= \sum_k (|2k\rangle\langle 2k+1| + |2k+1\rangle\langle 2k|) \\
P_3 &= \sum_k i(|2k\rangle\langle 2k+1| - |2k+1\rangle\langle 2k|)
\end{aligned} \tag{4.9}$$

Now, we define the Stokes parameters as

$$\begin{aligned}
s_0 &= \langle\psi|P_0|\psi\rangle \equiv \sum_k \left(c_{2k}c_{2k}^* + c_{2k+1}c_{2k+1}^*\right) \\
s_1 &= \langle\psi|P_1|\psi\rangle \equiv \sum_k \left(c_{2k}c_{2k}^* - c_{2k+1}c_{2k+1}^*\right) \\
s_2 &= \langle\psi|P_2|\psi\rangle \equiv \sum_k \left(c_{2k}^*c_{2k+1} + c_{2k}c_{2k+1}^*\right) \\
s_3 &= \langle\psi|P_3|\psi\rangle \equiv i\sum_k \left(c_{2k}^*c_{2k+1} - c_{2k}c_{2k+1}^*\right)
\end{aligned} \tag{4.10}$$

4.2.1 Measurements in Linear Even/odd Basis for s_0 and s_1

We consider an OAM sorter for the measurement of s_0 and s_1. The setup is given in Fig. 4.1 Consider a general even/odd OAM superposition state given in Eq. 4.2. Applying beam splitter operation, the state evolves through two arms of the interferometer with a $\frac{\pi}{2}$ phase. In the

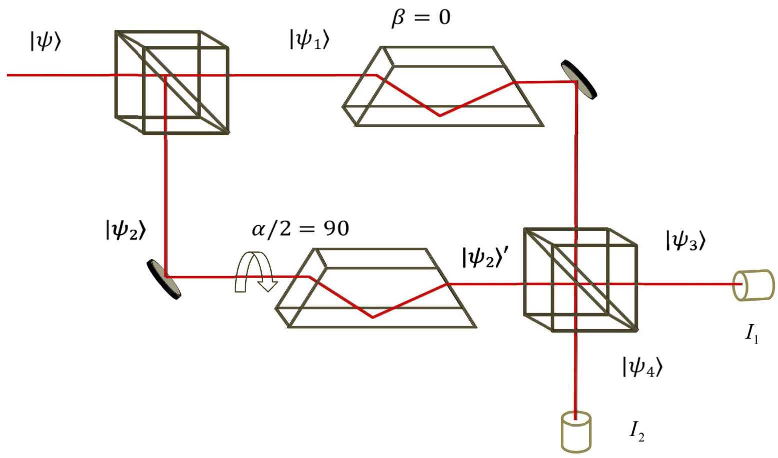

Figure 4.1: Even/odd OAM sorter

reflected arm, a dove prism is inserted which is rotated by an angle $\frac{\alpha}{2}$. The dove prism angle can be calibrated using an Hermite Gaussian beam HG_{01} passing through it, as the rotation of the dove prism will result in rotation of the two lobes. Dove prism introduces an OAM dependent phase $\exp(im\alpha)$, where m correspond to OAM state $|m\rangle$. When $\alpha = \pi$, the even states will acquire a phase of $\exp(i2k\pi)$ which leaves the state unchanged. However, odd states acquire a phase of $\exp(i(2k+1)\pi)$ which brings a negative sign to all odd states. Thus the state $|\psi_2\rangle = \frac{i}{\sqrt{2}}\sum_k (c_{2k}|2k\rangle + c_{2k+1}|2k+1\rangle)$ transforms to $|\psi_2\rangle' = \frac{i}{\sqrt{2}}\sum_k (c_{2k}|2k\rangle - c_{2k+1}|2k+1\rangle)$. The state $|\psi_1\rangle = \frac{1}{\sqrt{2}}\sum_k (c_{2k}|2k\rangle + c_{2k+1}|2k+1\rangle)$ of the other arm remains unchanged since the dove prism angle is $0°$. These states combines at the second beam splitter. The phase due to reflections on both the beams are same and therefore neglected in the calculation. One port of the second beam splitter gives

$$|\psi_3\rangle = \frac{i}{2}\sum_k (c_{2k}|2k\rangle - c_{2k+1}|2k+1\rangle) + \frac{i}{2}\sum_k (c_{2k}|2k\rangle + c_{2k+1}|2k+1\rangle) = i\sum_k c_{2k}|2k\rangle \tag{4.11}$$

Thus the detection (refer Fig. 4.1) yields

$$I_1 = \sum_k |c_{2k}|^2 \tag{4.12}$$

Similarly the other port gives

$$\begin{aligned} |\psi_4\rangle &= \frac{1}{2}\sum_k (-c_{2k}|2k\rangle + c_{2k+1}|2k+1\rangle) + \frac{1}{2}\sum_k (c_{2k}|2k\rangle + c_{2k+1}|2k+1\rangle) \\ &= \sum_k c_{2k+1}|2k+1\rangle \end{aligned} \tag{4.13}$$

which gives $I_2 = \sum_k |c_{2k+1}|^2$ on detection (refer Fig. 4.1) . Thus we can calculate the stokes parameters $s_0 = I_1 + I_2$ and $s_1 = I_1 - I_2$ from this setup.

4.2.2 Measurements in Diagonal Basis for the Estimation of s_2

For measuring s_2, a modified Mach-Zhender interferometer is introduced which contains a spiral phase plate in one arm and the first beam splitter is replaced by an OAM sorter. The setup is given in Fig. 4.2. As described earlier, a general OAM state $\sum_k (c_{2k}|2k\rangle + c_{2k+1}|2k+1\rangle)$ is split into $i\sum_k c_{2k}|2k\rangle$ and $\sum_k c_{2k+1}|2k+1\rangle$ in both ports. A spiral phase plate (SPP) of order $m = \pm 1$ is introduced in one arm of the interferometer. This will act as a ladder operator in $\{..|-m\rangle..,|-1\rangle,|0\rangle,|1\rangle,..,|m\rangle\}$ basis. However in the even/odd basis, SPP with $m = \pm 1$ works as NOT gate. So the state $\sum_k c_{2k+1}|2k+1\rangle$ will convert to $\sum_k c_{2k+1}|2k\rangle$. This is combined with state $i\sum_k c_{2k}|2k\rangle$ on another 50:50 beam splitter. One port of the beam splitter yields the state

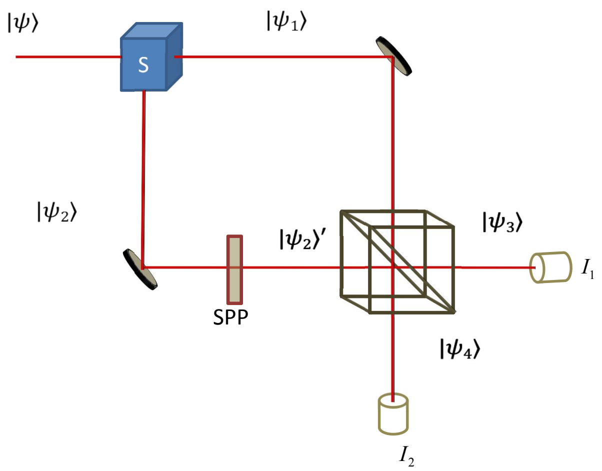

Figure 4.2: Setup for measuring stoke's parameter s_2

$$|\psi_3\rangle = \frac{1}{\sqrt{2}} \sum_k (c_{2k+1} - c_{2k})\, |2k\rangle \tag{4.14}$$

On detection (refer Fig. 4.2) it gives

$$
\begin{aligned}
I_1 &= \left|\frac{1}{\sqrt{2}}\sum_k (c_{2k+1} - c_{2k})\,|2k\rangle\right|^2 \\
&= \frac{1}{2}\left(\sum_l (c^*_{2l+1} - c^*_{2l})\,\langle 2l|\right)\cdot\left(\sum_k (c_{2k+1} - c_{2k})\,|2k\rangle\right) \\
&= \frac{1}{2}\sum_{k,l} (c^*_{2l+1} - c^*_{2l})\,(c_{2k+1} - c_{2k})\,\langle 2l|2k\rangle \\
&= \frac{1}{2}\sum_k (c^*_{2k+1} - c^*_{2k})\,(c_{2k+1} - c_{2k})
\end{aligned}
$$

$$
I_1 = \frac{1}{2}\sum_k (c^*_{2k+1}c_{2k+1} - c^*_{2k}c_{2k+1} - c_{2k}c^*_{2k+1} + c^*_{2k}c_{2k}) \tag{4.15}
$$

Similarly the other port of the BS (refer Fig. 4.2) gives

$$
|\psi_4\rangle = \frac{i}{\sqrt{2}}\sum_k (c_{2k+1} + c_{2k})\,|2k\rangle \tag{4.16}
$$

which gives

$$
I_2 = \frac{1}{2}\sum_k (c^*_{2k+1}c_{2k+1} + c^*_{2k}c_{2k+1} + c_{2k}c^*_{2k+1} + c^*_{2k}c_{2k}) \tag{4.17}
$$

Thus we obtain Stokes parameter s_2 by simply subtracting the intensities as

$$
I_2 - I_1 = \sum_k (c_{2k}c^*_{2k+1} + c^*_{2k}c_{2k+1}) = s_2. \tag{4.18}
$$

4.2.3 Measurement in Circular Basis for the Estimation of s_3

For the measurement of s_3, an extra phase delay of $\exp(i\pi/2)$ is inserted after the spiral phase plate as shown in Fig. 4.3. Thus the states combining at the BS are $ic_2|E\rangle$ and $ic_1|E\rangle$. In this case one port of the BS (refer Fig. 4.3) gives

$$
|\psi_3| = \frac{1}{\sqrt{2}}\sum_k (ic_{2k+1} - c_{2k})\,|2k\rangle \tag{4.19}
$$

so that

$$
I_1 = \frac{1}{2}\sum_k (c^*_{2k+1}c_{2k+1} - ic^*_{2k}c_{2k+1} + ic_{2k}c^*_{2k+1} + c^*_{2k}c_{2k}) \tag{4.20}
$$

The other port of the BS (refer Fig. 4.3) gives

$$
|\psi_4\rangle = \frac{1}{\sqrt{2}}\sum_k (ic_{2k} - c_{2k+1})\,|2k\rangle \tag{4.21}
$$

which gives

$$
I_2 = \frac{1}{2}\sum_k (c^*_{2k+1}c_{2k+1} + ic^*_{2k}c_{2k+1} - ic_{2k}c^*_{2k+1} + c^*_{2k}c_{2k}) \tag{4.22}
$$

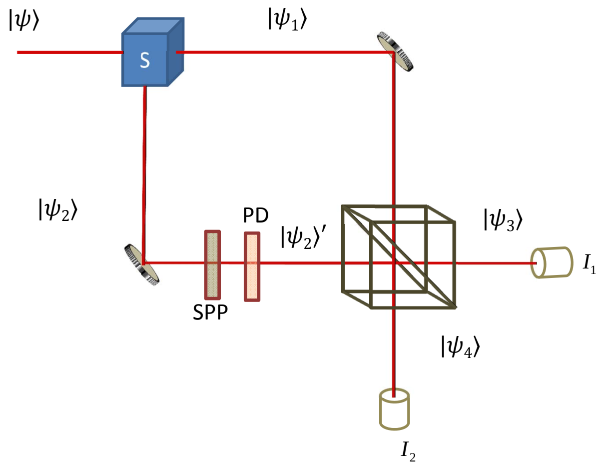

Figure 4.3: Setup for measuring stoke's parameter s_3. PD - phase delay

To obtain s_3 the intensities are subtracted as

$$I_2 - I_1 = i\sum_k (c_{2k}c^*_{2k+1} - c^*_{2k}c_{2k+1}) = s_3. \tag{4.23}$$

Thus, once can do the complete state tomography in even/odd OAM states.

4.2.4 General Linear Basis Projection

A general linear projection is essential for the measurement of Bell's inequality and quantum cryptography. The general linear projections are given as

$$\begin{aligned} P_\theta = \sum_k (&\cos^2(\theta)|2k\rangle\langle 2k| + \sin(\theta)\cos(\theta)|2k\rangle\langle 2k+1| + \\ &\sin(\theta)\cos(\theta)|2k+1\rangle\langle 2k| + \sin^2(\theta)|2k+1\rangle\langle 2k+1|) \end{aligned} \tag{4.24}$$

$$\begin{aligned} P_{\theta^\perp} = \sum_k (&\cos^2(\theta)|2k\rangle\langle 2k| - \sin(\theta)\cos(\theta)|2k\rangle\langle 2k+1| - \\ &\sin(\theta)\cos(\theta)|2k+1\rangle\langle 2k| + \sin^2(\theta)|2k+1\rangle\langle 2k+1|) \end{aligned} \tag{4.25}$$

These operators acting on $|\psi\rangle$ will give

$$C(\theta) = \langle\psi|P_\theta|\psi\rangle = \sum_k |(\cos(\theta)c_{2k} + \sin(\theta)c_{2k+1})|^2 \tag{4.26}$$

$$C(\theta^\perp) = \langle\psi|P_{\theta^\perp}|\psi\rangle = \sum_k |(\sin(\theta)c_{2k} - \cos(\theta)c_{2k+1})|^2 \tag{4.27}$$

Consider the setup given in Fig. 4.2. In the case of measurement of s_2 we used a 50:50 beam splitter. Now consider a beam splitter with transmission coefficient $\cos(\theta)$ and reflection coefficient $\sin(\theta)$ instead of 50:50 beam splitter. Thus the states after the beam splitter becomes,

$$\psi_4 = \sum_k (\cos(\theta)c_{2k} + \sin(\theta)c_{2k+1})|2k\rangle \tag{4.28}$$

$$\psi_5 = i\sum_k (\sin(\theta)c_{2k} - \cos(\theta)c_{2k+1}|2k\rangle \tag{4.29}$$

On detection, we get

$$I_1 = \sum_k |(\cos(\theta)c_{2k} + \sin(\theta)c_{2k+1})|^2 \tag{4.30}$$

$$I_2 = \sum_k |(\sin(\theta)c_{2k} - \cos(\theta)c_{2k+1})|^2 \tag{4.31}$$

Thus we achieve the general linear projections on a given state.

Alternatively, one can also implement the same measurement with polarization as an additional degree of freedom. We consider the initial photons with OAM state ψ_1 as horizontally polarized. In both arms of the interferometer, a half wave plates at angle $\theta/2$ is introduced which will convert the horizontal polarization to any other linear polarization along $\hat{\theta}$. The beam splitter is replaced by a polarizing beam splitter. It will transmit horizontal polarization and reflect vertical polarization. Thus by changing the HWP's angle $(\theta/2)$ we can tune the transmission and reflection function as $\sin(\theta)$ and $\cos(\theta)$. The polarization assisted projection is easy to implement. However, when we consider OAM and polarization together for quantum protocols, for example hyper-entanglement, this cannot be used since the polarization operations affect the entanglement.

4.3 Polarizing Sagnac Interferometer for Even/odd OAM Sorting

Here, for even/odd OAM sorting, we give an alternative measurement technique using polarization as an additional degree of freedom. We use polarizing Sagnac ineterferometer containing a dove prism at an angle $\pi/4$. Since we use a common path interferometer, the OAM sorter is more stable and robust against small misalignments. The experimental setup is given in Fig.4.4. We start with an OAM state with horizontal polarization.

$$|\psi\rangle|H\rangle = \sum_k (c_{2k}|2k\rangle + c_{2k+1}|2k+1\rangle)\,|H\rangle \tag{4.32}$$

This state passes through a half wave plate oriented at $\pi/8$ which will convert horizontal polarization to diagonal $(|\psi\rangle|H\rangle \rightarrow |\psi\rangle|D\rangle)$. A polarizing beam splitter splits the beam

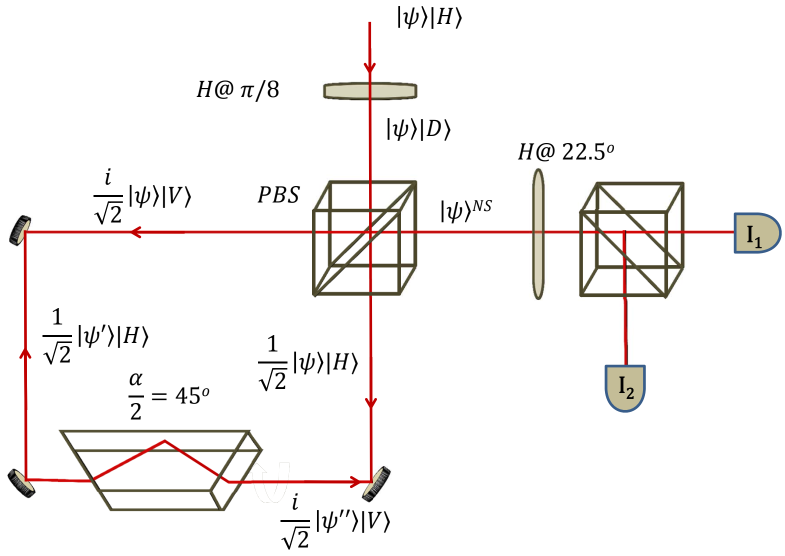

Figure 4.4: Setup for polarization assisted even/odd OAM sorter

into two paths where each of them will be orthogonally polarized. In one arm, the horizontal polarization component passes through a dove prism oriented at an angle $\pi/4$. In this case all the individual OAM states will acquire a phase of $e^{ik\pi/2}$, where k is the integer corresponding to OAM state $|m\rangle$ and the state is given as

$$|\psi'\rangle|H\rangle = \sum_k \left(e^{i2k\pi/2}c_{2k}|2k\rangle + e^{i(2k+1)\pi/2}c_{2k+1}|2k+1\rangle\right)|H\rangle \tag{4.33}$$

In the other arm with vertical polarization, on passing through the dove prism in the opposite direction, the OAM state will acquire a phase of $e^{-im\pi/2}$ and the state is denoted as

$$|\psi''\rangle|V\rangle = i\sum_k \left(e^{-i2k\pi/2}c_{2k}|2k\rangle + e^{-i(2k+1)\pi/2}c_{2k+1}|2k+1\rangle\right)|V\rangle. \tag{4.34}$$

Both the beams superpose at the same PBS and the state becomes

$$|\psi\rangle^{NS} = \frac{1}{\sqrt{2}}\left(|\psi'\rangle|H\rangle - |\psi''\rangle|V\rangle\right) \tag{4.35}$$

Writing this in diagonal basis by transforming $|H\rangle = \frac{1}{\sqrt{2}}(|D\rangle + |A\rangle)$ and $|V\rangle = \frac{1}{\sqrt{2}}(|D\rangle - |A\rangle)$, we get

$$|\psi\rangle^{NS} = \frac{1}{\sqrt{2}}\left(\frac{(|\psi'\rangle - |\psi''\rangle)}{\sqrt{2}}|D\rangle + \frac{(|\psi'\rangle + |\psi''\rangle)}{\sqrt{2}}|A\rangle\right) \tag{4.36}$$

The relative phase between even states of $|\psi'\rangle$ and $|\psi''\rangle$ is $e^{-i2k\pi} = 1$ for all integer k. Similarly the relative states between the odd states of $|\psi'\rangle$ and $|\psi''\rangle$ is $e^{-i(2k+1)\pi} = -1$. We calculate

$$\begin{aligned}
|\psi'\rangle - |\psi''\rangle &= \sum_k \left(e^{i2k\pi/2} c_{2k}|2k\rangle + e^{i(2k+1)\pi/2} c_{2k+1}|2k+1\rangle\right) - \\
&\quad \sum_k \left(e^{-i2k\pi/2} c_{2k}|2k\rangle + e^{-i(2k+1)\pi/2} c_{2k+1}|2k+1\rangle\right) \\
&= \sum_k e^{i2k\pi/2}\left(c_{2k} - e^{-i2k\pi} c_{2k})\right)|2k\rangle + \\
&\quad \sum_k e^{i(2k+1)\pi/2}\left(c_{2k+1} - e^{-i(2k+1)\pi} c_{2k+1}\right)|2k+1\rangle \\
&= 2\sum_k i^{2k+1} c_{2k+1}|2k+1\rangle. \qquad (4.37)
\end{aligned}$$

Similarly

$$|\psi'\rangle + |\psi''\rangle = 2\sum_k c_{2k}|2k\rangle. \qquad (4.38)$$

Thus

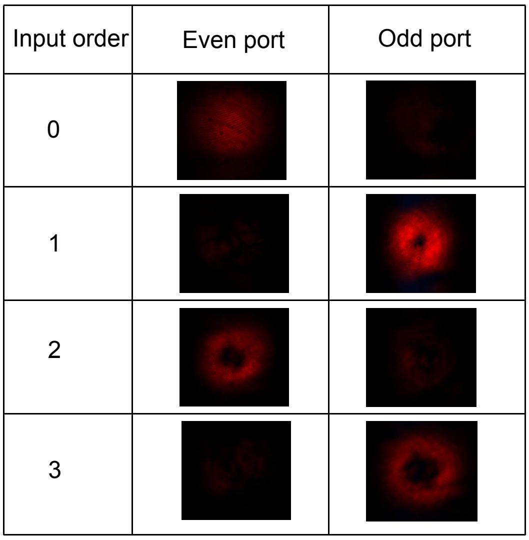

Figure 4.5: Images corresponding to the even and odd ports of the OAM sorter with the individual OAM states as input

$$|\psi\rangle^{NS} = \sum_k i^{2k+1} c_{2k+1}|2k+1\rangle|D\rangle + \sum_k c_{2k}|2k\rangle|A\rangle \qquad (4.39)$$

This is a non separable state of polarization and OAM. This state passing through a half wave plate oriented at an angle of $\pi/8$ will convert into

$$|\psi\rangle^{NS} = \sum_k i^{2k+1} c_{2k+1}|2k+1\rangle|H\rangle + \sum_k c_{2k}|2k\rangle|V\rangle \qquad (4.40)$$

This state, when passing through a PBS will decompose to the states $\sum_k c_{2k}|2k\rangle$ at one port and $\sum_k i^{2k+1} c_{2k+1}|2k+1\rangle$ on the other. We demonstrate the OAM sorting experimentally

Input Beam	Even port	Odd port
$\lvert 1\rangle + \lvert -1\rangle + \lvert 2\rangle + \lvert -2\rangle$ 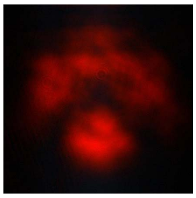	$\lvert 2\rangle + \lvert -2\rangle$ 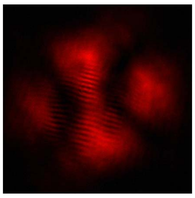	$\lvert 1\rangle + \lvert -1\rangle$ 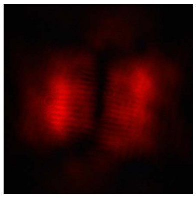
$\lvert 3\rangle + \lvert -3\rangle + \lvert 2\rangle + \lvert -2\rangle$ 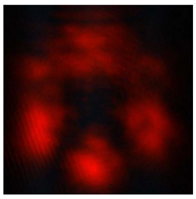	$\lvert 2\rangle + \lvert -2\rangle$ 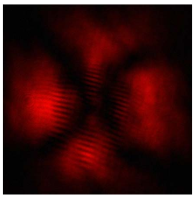	$\lvert 3\rangle + \lvert -3\rangle$ 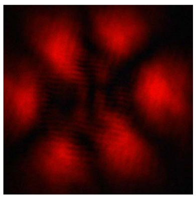

Figure 4.6: Images corresponding to the even and odd ports of the OAM sorter along with the input port images. Here input state is a superposition state of different OAM values.

with the setup given in Fig. 4.4. Separation of individual even-odd OAM states are given in Fig. 4.5. Here we have sent the different orders to the sorter and imaged the beams coming out of each ports using a CCD camera.

Now we introduce superposition states to the OAM sorter. We use the states $|1\rangle + |-1\rangle + |2\rangle + |-2\rangle$ and $|3\rangle + |-3\rangle + |2\rangle + |-2\rangle$ in the input port. The even port yield the state $|2\rangle + |-2\rangle$ in both case wile odd port gives states $|1\rangle + |-1\rangle$ and $|3\rangle + |-3\rangle$ respectively. The input and output ports' images are given in Fig. 4.6

4.4 Hyper-entanglement, hybrid entanglement and SOBA

Along with the OAM entanglement in even/odd states one can have polarization entanglement between the two photons. For this, one needs to use a cascaded type I non linear crystals with optics axis perpendicular to each other for the parametric down conversion of a light beam of azimuthal index 1. The generated state will be

$$|\psi\rangle_{12} = \frac{1}{2}\left(|H\rangle_1|H\rangle_2 + |V\rangle_1|V\rangle_2\right) \otimes \left(|E\rangle_1|O\rangle_2 + |O\rangle_1|E\rangle_2\right) \tag{4.41}$$

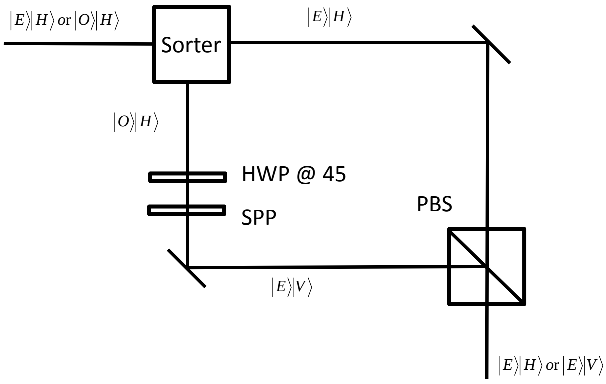

Figure 4.7: Modified OAM controlled polarization C_{NOT} gate.

This state has many applications including hyper entangled assisted Bell state analysis (HBSA) and super dense coding. Note that in hyper-entanglement, the polarization and OAM states are always separable. In other words, there is no entanglement between polarization and OAM.

Hybrid entanglement, as the name suggests, is the entanglement between two independent properties of light. The state of a single particle or two particles in two degrees of freedom are non-separable in the case of hybrid entanglement. In the biphoton systems, the polarization of one photon and orbital angular momentum of other, can be made non-separable. To generate this state, we consider two photons entangled in OAM even/odd states but separable in polarization, Eq. 4.8. We consider a modified OAM controlled polarization C_{NOT} gate (^oC_p) [137] with an extra spiral phase plate as given in Fig. 4.7. This C_{NOT} gate will do a NOT operation on both control and target. This modified ^oC_p is introduced to the first photon of the state, given in Eq. 4.5. Thus the two photon state will become

$$|\psi\rangle_{HE} = \frac{1}{\sqrt{2}} \left(|H\rangle_1|O\rangle_2 + |V\rangle_1|E\rangle_2\right)|E\rangle_1|H\rangle_2 \tag{4.42}$$

This is an interesting case, since there is no OAM-OAM entanglement or polarization polarization entanglement between the photons. However, the polarization state of photon 1 and OAM state of photon 2 are non-separable. With this state one can steer the OAM state of photon 2 by polarization measurements in photon 1.

Single photon non-separable state also considered as a hybrid entangled state is the one in which the OAM and polarization of a single photon are inseparable. However, this won't give rise to any non-local effects and hence there are objections to call such states as entangled. We consider the state given in Eq. 4.5 where state is post selected to state $|O\rangle_2|H\rangle_2$

$$|\psi\rangle_1' = |E\rangle_1|H\rangle_1. \tag{4.43}$$

Here $|\psi\rangle'$ corresponds to the state of photon 1 upon the post selection of photon 2 to the state $|O\rangle_2|H\rangle_2$. Now, we apply a Hadamard operation in polarization using a half wave plate at 22.5° and a polarization controlled OAM C_{NOT} gate ${}^pC_o$, we obtain

$$|\psi\rangle_1' = \frac{1}{\sqrt{2}}\left(|E\rangle_1|H\rangle_1 + |O\rangle_1|V\rangle_1\right). \tag{4.44}$$

Here the polarization and OAM of a single photon are non-separable. One can construct a complete Bell basis as

$$\begin{aligned}
\psi^+ &= \frac{1}{\sqrt{2}}\left(|E\rangle_1|H\rangle_1 + |O\rangle_1|V\rangle_1\right)\\
\psi^- &= \frac{1}{\sqrt{2}}\left(|E\rangle_1|H\rangle_1 - |O\rangle_1|V\rangle_1\right)\\
\phi^+ &= \frac{1}{\sqrt{2}}\left(|O\rangle_1|H\rangle_1 + |E\rangle_1|V\rangle_1\right)\\
\phi^- &= \frac{1}{\sqrt{2}}\left(|O\rangle_1|H\rangle_1 - |E\rangle_1|V\rangle_1\right)
\end{aligned} \tag{4.45}$$

A spin orbit Bell state analyser (SOBA) is a set up which distinguishes all the single photon spin orbit Bell states given above. Fig. 4.8 describes the proposed setup for the SOBA. Consider the above four Bell states as inputs of the SOBA set up. Initially an even/odd sorter sorts according to the OAM state. Lets first consider $|\psi^\pm\rangle$ as the input states. The port 1 & 2 will be

$$\text{port 1} \rightarrow \pm\frac{1}{\sqrt{2}}|O\rangle_1|V\rangle_1,\ \text{port 2} \rightarrow \frac{i}{\sqrt{2}}|E\rangle_1|H\rangle_1 \tag{4.46}$$

A half wave plate is introduced in port 2 which will convert $|H\rangle_1$ to $|V\rangle_1$ which will be the input of PBS 2. The PBS 2 will reflect the state since it is vertically polarized. In the reflected port a spiral phase plate of order 1 is introduced which will convert $|E\rangle_1$ to $|O\rangle_1$. At the same time, PBS 1 reflects the state in port 1. Thus at input ports 3 and 4 of the BS 1 we get

$$\begin{aligned}
\text{port 3} &\rightarrow \frac{i}{\sqrt{2}}|O\rangle_1|V\rangle_1\\
\text{port 4} &\rightarrow \mp\frac{1}{\sqrt{2}}|O\rangle_1|V\rangle_1
\end{aligned} \tag{4.47}$$

Two output ports of the BS 1 gives

$$\begin{aligned}
\psi_a &= -\frac{1}{2}(|O\rangle_1|V\rangle_1 \pm |O\rangle_1|V\rangle_1)\\
\psi_b &= i\frac{1}{2}(|O\rangle_1|V\rangle_1 \mp |O\rangle_1|V\rangle_1)
\end{aligned} \tag{4.48}$$

So $|\psi^+\rangle$ will go to detector D_1 and $|\psi^-\rangle$ will go to detector D_2.

Now if the input states are $|\phi^\pm\rangle$ ports 1 and 2 will have states

$$\text{port 1} \rightarrow \frac{1}{\sqrt{2}}|O\rangle_1|H\rangle_1 \text{port 2} \rightarrow \pm\frac{i}{\sqrt{2}}|E\rangle_1|V\rangle_1 \tag{4.49}$$

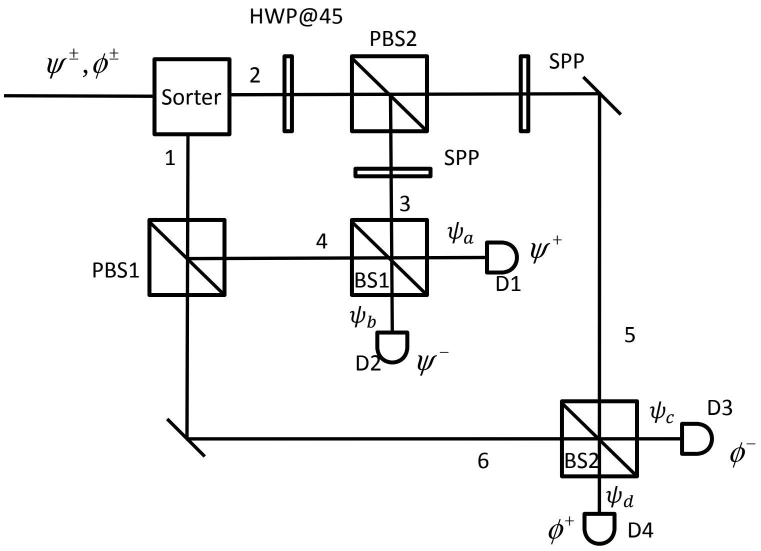

Figure 4.8: Set up for spin orbit Bell state analysis

In port 2 after the HWP the polarization will convert to $|H\rangle_1$, and in both ports the state will be transmitted by the PBS1 and PBS2. In port 2, after PBS2, a SPP is inserted. Hence at the input ports 5 and 6 of the BS 2 the states will be

$$\begin{aligned} \text{port } 5 &\rightarrow \pm\frac{i}{\sqrt{2}}|E\rangle_1|H\rangle_1 \\ \text{port } 6 &\rightarrow \frac{1}{\sqrt{2}}|E\rangle_1|H\rangle_1 \end{aligned} \tag{4.50}$$

Now two output ports of the BS 2 gives

$$\begin{aligned} \psi_c &= -\frac{1}{2}(|E\rangle_1|H\rangle_1 \mp |E\rangle_1|H\rangle_1) \\ \psi_d &= \frac{1}{2}(|E\rangle_1|H\rangle_1 \pm |E\rangle_1|H\rangle_1) \end{aligned} \tag{4.51}$$

So $|\phi^-\rangle$ will go to detector D_3 and $|\phi^+\rangle$ will go to detector D_4. Hence we can have complete deterministic unambiguous Bell state analysis.

4.5 Quantum Information Protocols Using Even/odd OAM States

Our final aim is to implement quantum information protocols using even/odd state of OAM. This could increase the efficiency of quantum communication with photons since we can have a high bright source of OAM entanglement equivalent to the polarization entanglement. We show that the even/odd entangled states violate Bell's inequality which has direct application in Ekert protocol. With hyper-entanglement we show it can be used in super densecoding.

4.5.1 Violation of Bell's Inequality and Ekert Protocol

As explained in section 4.2.4, one can do projections to general linear states. Now consider a two photon state entangled in even/odd OAM state produced by the parametric down conversion of an optical vortex of order one [138]. The state is given as

$$|\Psi\rangle_{12} = \frac{1}{\sqrt{2}} \left(|E\rangle_1 |O\rangle_2 + |O\rangle_1 |E\rangle_2 \right). \tag{4.52}$$

Consider the photon 1 with Alice and photon 2 with Bob. Alice does P_θ and $P_{\theta^\perp}$ measurements on her photon and Bob does P_χ and $P_{\chi^\perp}$ measurements on his photon. Eq. 4.24 and 4.25 describes $|\theta\rangle, |\theta^\perp\rangle$ and $|\chi\rangle, |\chi^\perp\rangle$ with replacing θ by χ. The measurement is given in section 4.2.4, θ and χ correspond to $\sin^{-1}(t)$ where t is the transmissivity of the beam splitter. In the case of polarization assisted projection as given in Fig. 4.4, θ and χ correspond to twice of the angle of the HWP . The schematic of this experiment is given in Fig. 4.9

Instead of intensity/photon counting output, which is described in 4.2.4, here we consider the coincidence between Alice's and Bob's detectors.

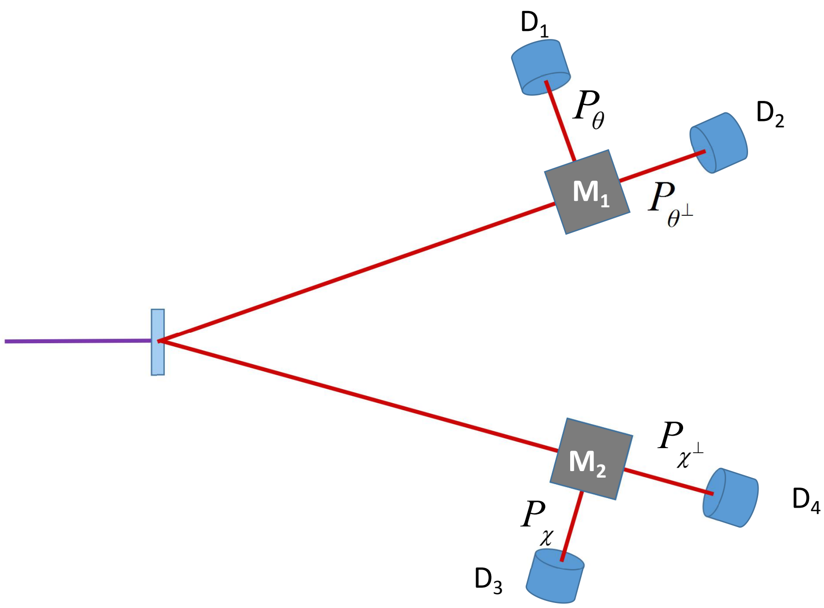

Figure 4.9: Setup for checking Bell's inequality and quantum cryptography. M1 and M2 are two measurements explained in Section 4.2.4 with angles θ and χ respectively.

Coincidence between D_1 and D_3 will give the measurement result ${}_{12}\langle\Psi|P_\theta \otimes P_\chi|\Psi\rangle_{12}$, where P_θ and P_χ are defined by Eq. 4.25 with angle θ and χ that act on photon 1 and 2 respectively.

$$D_{13} = c(\theta, \chi) = {}_{12}\langle\Psi|P_\theta \otimes P_\chi|\Psi\rangle_{12} \tag{4.53}$$

Similarly

$$D_{14} = c(\theta, \chi_\perp) = {}_{12}\langle\Psi|P_\theta \otimes P_{\chi^\perp}|\Psi\rangle_{12} \tag{4.54}$$

$$D_{23} = c(\theta_\perp, \chi) = {}_{12}\langle\Psi|P_{\theta^\perp} \otimes P_{\chi}|\Psi\rangle_{12} \tag{4.55}$$

$$D_{23} = c(\theta_\perp, \chi_\perp) = {}_{12}\langle\Psi|P_{\theta^\perp} \otimes P_{\chi^\perp}|\Psi\rangle_{12} \tag{4.56}$$

The operator is defined as

$$\begin{aligned} P_\theta \otimes P_\chi \equiv & \sum_k (\cos^2(\theta)|2k\rangle\langle 2k| + \sin(\theta)\cos(\theta)|2k\rangle\langle 1-2k| + \\ & \sin(\theta)\cos(\theta)|1-2k\rangle\langle 2k| + \sin^2(\theta)|1-2k\rangle\langle 1-2k|)\otimes \\ & \sum_l (\cos^2(\chi)|2l\rangle\langle 2l| + \sin(\chi)\cos(\chi)|2l\rangle\langle 1-2l| + \\ & \sin(\chi)\cos(\chi)|1-2l\rangle\langle 2l| + \sin^2(\chi)|1-2l\rangle\langle 1-2l|) \end{aligned} \tag{4.57}$$

Operating this on Eq. 4.6

$$\begin{aligned} {}_{12}\langle\Psi|P_\theta \otimes P_\chi|\psi\rangle_{12} = & \frac{1}{2}\left(\sum_{m=-\infty}^{+\infty} c_{2m}^*({}_1\langle 2m|_2\langle 1-2m|) + \sum_{m=-\infty}^{+\infty} c_{1-2m}^*({}_1\langle 1-2m|_2\langle 2m|)\right) \\ & P_\theta \otimes P_\chi \left(\sum_{n=-\infty}^{+\infty} c_{2n}(|2n\rangle_1|1-2n\rangle_2) + \sum_{n=-\infty}^{+\infty} c_{1-2n}(|1-2n\rangle_1|2n\rangle_2)\right) \end{aligned} \tag{4.58}$$

gives

$$\begin{aligned} C(\theta,\chi) = \sum_{m,n,k,l=-\infty}^{+\infty} \Big[& \cos^2(\theta)\sin^2(\chi)c_{2m}^*c_{1-2n}\langle 2m|2k\rangle\langle 2k|2n\rangle\langle 1-2m|1-2l\rangle \\ & \langle 1-2l|1-2n\rangle + \cos(\theta)\sin(\theta)\cos(\chi)\sin(\chi)c_{2m}^*c_{2n}\langle 2m|2k\rangle \\ & \langle 1-2k|1-2n\rangle\langle 1-2m|1-2l\rangle\langle 2l|2n\rangle + \cos(\theta)\sin(\theta) \\ & \cos(\chi)\sin(\chi)c_{1-2m}^*c_{2n}\langle 1-2m|1-2k\rangle\langle 2k|2n\rangle\langle 2m|2l\rangle \\ & \langle 1-2l|1-2n\rangle + c_{1-2m}^*c_{1-2n}\sin^2(\theta)\cos^2(\chi)\langle 1-2m|1-2k\rangle \\ & \langle 1-2k|1-2n\rangle\langle 2m|2l\rangle\langle 2l|2n\rangle \Big] \end{aligned} \tag{4.59}$$

Now using the inner product

$$\begin{aligned} C(\theta,\chi) = \sum_{k=-\infty}^{+\infty} \Big[& c_{2k}^*c_{1-2k}\cos^2(\theta)\sin^2(\chi) + \\ & \cos(\theta)\sin(\theta)\cos(\chi)\sin(\chi)(c_{2k}^*c_{2k} + c_{1-2k}^*c_{2k}) + \\ & c_{1-2k}^*c_{1-2k}\sin^2(\theta)\cos^2(\chi) \Big] \end{aligned} \tag{4.60}$$

With Eq.4.7 we can argue that $|c_{2k}| = |c_{1-2k}|$. Also we consider there is no phase between the states $|2k\rangle_1|1-2k\rangle_2$ and $|1-2k\rangle_1|2k\rangle_2$. Thus the joint probability reduces to

$$\begin{aligned} C(\theta,\chi) = &\sum_{k=-\infty}^{+\infty} |c_{2k}|^2[\cos^2(\theta)\sin^2(\chi) + 2\cos(\theta)\sin(\theta)\cos(\chi)\sin(\chi) + \sin^2(\theta)\cos^2(\chi)] \\ =&\cos^2(\theta-\chi). \end{aligned} \tag{4.61}$$

We can have a parameter

$$E(\theta,\chi) = \frac{C(\theta,\chi) + C(\theta_\perp,\chi_\perp) - C(\theta_\perp,\chi) - C(\theta,\chi_\perp)}{C(\theta,\chi) + C(\theta_\perp,\chi_\perp) + C(\theta_\perp,\chi) + C(\theta,\chi_\perp)} \tag{4.62}$$

and the Bell's inequality can be calculated as

$$B(\theta,\theta',\chi,\chi') = |E(\theta,\chi) - E(\theta,\chi') + E(\theta',\chi) + E(\theta',\chi')| \leq 2 \tag{4.63}$$

With $\theta = 0°, \chi = 22.5°$ in Eq. 4.61 give a maximum Bell's inequality violation of $2\sqrt{2}$. One can check the Bell inequality for a two photon state in even/odd OAM basis with the setup given in Fig. 4.4. Thus Ekert protocol [10] can be implemented by choosing proper measurement settings.

4.5.2 Superdense coding

In super dense coding, Alice and Bob share entangled pair of photons. Alice encodes two bits of classical information by applying unitary operation on her entangled photon changing the combined state from one Bell state to another. Thus, by acting on one particle she can encode 2 bits of information. Alice sends her entangled particle to Bob and he does a complete Bell state analysis on both the photons, which discriminate all the Bell states. But, the efficiency of the experimental Bell state analysis is very low. In polarization entanglement, all the Bell states has not been distinguished efficiently and deterministically. At the same time if we use entanglement in another degree of freedom, one can distinguish all the Bell states. This is known as hyper-entanglement assisted Bell state analysis (HBSA).

We describe hyper-entanglement assisted super dense coding protocol with even/odd OAM entanglement. Consider a two photon state which is entangled both in polarization and OAM.

$$|\Psi\rangle_{12} = |\beta^p\rangle \otimes |\Psi^o\rangle \tag{4.64}$$

where $|\beta^p\rangle$ is one of the polarization Bell states and

$$\begin{aligned} |\Psi^o\rangle = &\sum_{k=-\infty}^{+\infty} c_k(|2k\rangle_1|1-2k\rangle_2 + |2k+1\rangle_1|-2k\rangle_2) \\ \equiv&\frac{1}{\sqrt{2}}\left(|E\rangle_1|O\rangle_2 + |O\rangle_1|E\rangle_2\right) \end{aligned} \tag{4.65}$$

Alice encodes her two bits of information in the polarization Bell states. The final states will be

$$\begin{aligned}|\Psi^p\rangle^{\pm}\otimes|\Psi^o\rangle =&\frac{1}{2}\left(|H\rangle_1|V\rangle_2 \pm |V\rangle_1|H\rangle_2\right)\otimes\left(|E\rangle_1|O\rangle_2 + |O\rangle_1|E\rangle_2\right),\\ |\Phi^p\rangle^{\pm}\otimes|\Psi^o\rangle =&\frac{1}{2}\left(|H\rangle_1|H\rangle_2 \pm |V\rangle_1|V\rangle_2\right)\otimes\left(|E\rangle_1|O\rangle_2 + |O\rangle_1|E\rangle_2\right).\end{aligned} \tag{4.66}$$

Expanding

$$\begin{aligned}|\Psi^p\rangle^{\pm}\otimes|\Psi^o\rangle =& \frac{1}{2}(|H\rangle_1|E\rangle_1|V\rangle_2|O\rangle_2 + |H\rangle_1|O\rangle_1|V\rangle_2|E\rangle_2 \pm\\ & |V\rangle_1|E\rangle_1|H\rangle_2|O\rangle_2 \pm |V\rangle_1|O\rangle_1|H\rangle_2|E\rangle_2)\end{aligned} \tag{4.67}$$

$$\begin{aligned}|\Phi^p\rangle^{\pm}\otimes|\Psi^o\rangle =& \frac{1}{2}(|H\rangle_1|E\rangle_1|H\rangle_2|O\rangle_2 + |H\rangle_1|O\rangle_1|H\rangle_2|E\rangle_2 \pm\\ & |V\rangle_1|E\rangle_1|V\rangle_2|O\rangle_2 \pm |V\rangle_1|O\rangle_1|V\rangle_2|E\rangle_2)\end{aligned} \tag{4.68}$$

Single particle two qubit Bell states are defined as

$$\begin{aligned}\psi^{\pm} =&\frac{1}{\sqrt{2}}\left(|H\rangle|E\rangle \pm |V\rangle|O\rangle\right),\\ \phi^{\pm} =&\frac{1}{\sqrt{2}}\left(|H\rangle|O\rangle \pm |V\rangle|E\rangle\right).\end{aligned} \tag{4.69}$$

Using Eq.4.69 in Eq.4.67 and Eq.4.68 we get

$$\begin{aligned}|\Psi^p\rangle^{\pm}\otimes|\Psi^o\rangle =& \frac{1}{4}((\psi_1^+ + \psi_1^-)(\psi_2^+ - \psi_2^-) + (\phi_1^+ + \phi_1^-)(\phi_2^+ - \phi_2^-)\pm\\ & (\phi_1^+ - \phi_1^-)(\phi_2^+ + \phi_2^-) \pm (\psi_1^+ - \psi_1^-)(\psi_2^+ + \psi_2^-))\end{aligned} \tag{4.70}$$

$$\begin{aligned}|\Phi^p\rangle^{\pm}\otimes|\Psi^o\rangle =& \frac{1}{2}((\psi_1^+ + \psi_1^-)(\phi_2^+ + \phi_2^-) + (\phi_1^+ + \phi_1^-)(\psi_2^+ + \psi_2^-)\pm\\ & (\phi_1^+ - \phi_1^-)(\psi_2^+ - \psi_2^-) \pm (\psi_1^+ - \psi_1^-)(\phi_2^+ - \phi_2^-))\end{aligned} \tag{4.71}$$

giving

$$\begin{aligned}|\Psi^p\rangle^{+}\otimes|\Psi^o\rangle =&\frac{1}{2}(\psi_1^+\psi_2^+ - \psi_1^-\psi_2^- + \phi_1^+\phi_2^+ - \phi_1^-\phi_2^-)\\ |\Psi^p\rangle^{-}\otimes|\Psi^o\rangle =&\frac{1}{2}(\psi_1^-\psi_2^+ - \psi_1^+\psi_2^- + \phi_1^-\phi_2^+ - \phi_1^+\phi_2^-)\\ |\Phi^p\rangle^{+}\otimes|\Psi^o\rangle =&\frac{1}{2}(\psi_1^+\phi_2^+ - \psi_1^-\phi_2^- + \phi_1^+\psi_2^+ - \phi_1^-\psi_2^-)\\ |\Phi^p\rangle^{-}\otimes|\Psi^o\rangle =&\frac{1}{2}(\psi_1^-\phi_2^+ - \psi_1^+\phi_2^- + \phi_1^-\psi_2^+ - \phi_1^+\psi_2^-)\end{aligned} \tag{4.72}$$

The individual single photon spin-orbit Bell state can be distinguished using SOBA which is given in Fig. 4.8. Thus one can achieve efficient dense coding using hyper-entanglement assisted Bell state analysis. This Bell state analysis is interesting since it can be done with LOCC. A schematic for super dense coding with hyper entanglement is given in Fig. 4.10.

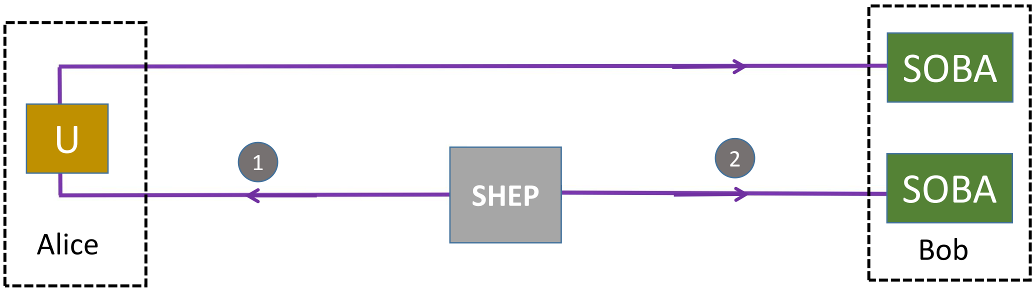

Figure 4.10: Setup for hyper entanglement assisted super sense coding. SHEP - source of hyper-entangled photons.

4.6 Conclusion

We have described the possibility of using even/odd OAM states for quantum information. We formulate appropriate measurement system for the even/odd OAM state based quantum information. Since even-odd OAM entanglement can be implemented like two qubit polarization entanglement, we describe the measurement and violation of Bell's inequality for such states. We have described hyper-entanglement and hybrid entanglement with OAM and polarization degrees of freedom. We have proposed an experimental scheme for spin orbit Bell state analysis to distinguish all the spin-orbit Bell states. This is applied in hyper entanglement assisted polarization Bell state analysis for efficient dense coding.

Chapter 5

Three Particle Hyper-Entanglement and Its Applications

In the last chapter we have seen the applicability of even/odd OAM states for quantum information. In this chapter, we describe a novel three particle hyper-entangled states which find application in telaportation and quantum cryptography.

With entanglement between two quantum bits, protocols have been demonstrated for teleporting an unknown quantum state [11], super dense coding of information [12] and secure communication [10]. An arbitrary qubit can be teleported from one particle to another with the use of an entangled pair of particles, which had been experimentally verified in different quantum systems [16, 139]. However, distinguishing all the four Bell states of the photonic qubits has remained a fundamental difficulty in achieving 100% teleportation. In the first demonstration of teleportation with photons [16], only one of the four Bell states could be distinguished from others. Thus, the efficiency of teleportation was limited to 25% only. Later on, a complete Bell state measurement was demonstrated with non-linear interaction of photons [140]. Even though they could separate all the four Bell states, the efficiency was reduced because of the non-linear process involved.

In recent years, complete Bell state analysis has been proposed with the use of hyper-entanglement [141], where the two photons are entangled in an additional degree of freedom (DOF) along with polarization. This method was utilized to increase the channel capacity of super dense coding [59]. This was done by projecting each hyper-entangled photon to four single particle two-qubit Bell states. Nevertheless, hyper-entanglement assisted Bell state analysis is not of much use in teleportation since it requires projecting the unknown state and one of the EPR particle state to any of the four Bell states. On the other hand,

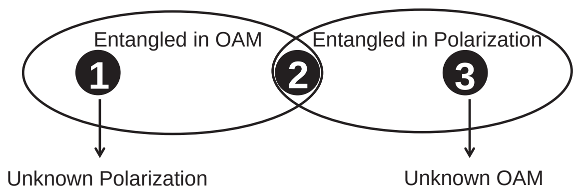

Figure 5.1: A pictorial representation of the three particle hyper-entangled state.

a hyper-entangled pair of particles can teleport a higher dimensional quantum state using hyper-entangled-Bell-state analysis which was described using Kerr non-linearity [142]. There had been a number of studies which use spin-orbit states of light for quantum information processing [85, 143–146]. Khoury and Milman [147] proposed a spin to orbit teleportation scheme with 100% efficiency that uses the OAM entanglement between the two photons and a spin-orbit Bell state analysis (SOBA).

In this article, we describe a three particle entangled state which finds applications in teleporting two qubits simultaneously and implementing an efficient key distribution protocol. In Section 5.1 we give a description of the proposed state. Along with the mathematical form of the state we give a schematic for the state preparation. The experimental procedure for the generation of the proposed state is given in Section 5.2. The state can be utilized to teleport two qubits using two SOBAs and 16 unitary transformations as given in Section 5.3. Experimental schemes for realizing the C_{NOT} gates and SOBA have also been given in Section 5.3.1. In Section 5.4 we describe a new QKD protocol using the new state, which is more efficient than the traditional Ekert protocol. Finally, we conclude in Section 5.5.

5.1 Description of the proposed state

We describe a system of particles in such a way that one particle is entangled to all other particles in different degrees of freedom. Let us consider a system consisting of three photons where photon **2** is entangled with photons **1** and **3** in different degrees of freedom namely OAM and polarization respectively. The polarization state of the photon **1** and the OAM state of the photon **3** are arbitrary or unknown. A pictorial representation of the state is given in Fig. 5.1.

Since the OAM of a photon is expressed in infinite dimensional Hilbert space, one can have higher dimensional entangled states. We take an arbitrary two dimensional subspace of the infinite dimensional OAM basis as $\{|l\rangle, |l'\rangle\}$.

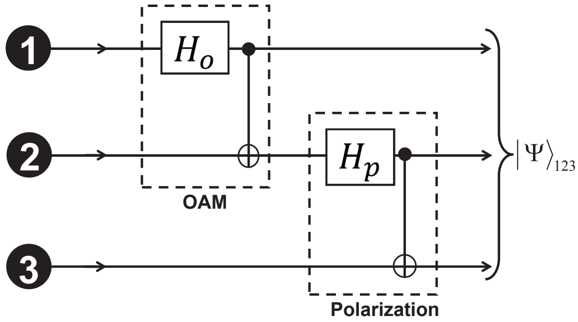

Figure 5.2: Schematic diagram for preparation of the initial state. Box named "OAM" contains a Hadamard gate (H_o) and a C_{NOT} gate acting on OAM basis and "polarization" box contains a Hadamard (H_p) and C_{NOT} gates acting on polarization basis.

The described state can be prepared using a pair of Hadamard and C_{NOT} gates in different DOFs which correspond to the polarization and the OAM. The initial states of three particles can be written as

$$|1\rangle = |\xi_p\rangle_1|l\rangle_1 \ ; \ |2\rangle = |H\rangle_2|l\rangle_2 \ ; \ |3\rangle = |H\rangle_3|\chi_o\rangle_3, \tag{5.1}$$

where $|\xi_p\rangle$ is the unknown state of polarization of the photon **1**, $|\chi_o\rangle$ is the unknown OAM state of the photon **3**, $|H\rangle$ represents horizontal and $|V\rangle$ represents vertical polarization states of a photon. The schematic diagram for preparation of the initial state is given in Fig. 5.2. To entangle photons **1** and **2** in OAM, a Hadamard gate (H_o) on photon **1** and subsequent C_{NOT} gate on photon **1** and **2** are applied. Both gates act in the OAM degree of freedom. Similarly, another Hadamard (H_p) acting on photon **2** and a C_{NOT} between photons **2** and **3** entangle them in polarization. Here, both the gates are acting on the polarization states of photons. After performing the gate operations mentioned above, the final state becomes,

$$|\Psi\rangle_{123} = |\xi_p\rangle_1 \otimes (|l, l'\rangle_{12} + |l', l\rangle_{12}) \otimes (|HV\rangle_{23} + |VH\rangle_{23})|\chi_o\rangle_3. \tag{5.2}$$

5.2 Experimental scheme for state preparation

We are proposing a method in which initially two photons are entangled in the OAM and third photon is in a pure state of OAM and polarization. By polarization gate operations on one of the entangled photons and the independent photon, one can arrive at the described state. Experimental scheme for the generation of the state is given in Fig. 5.3.

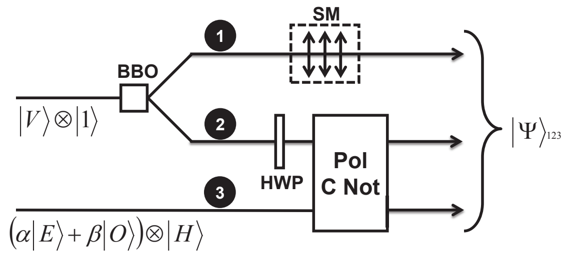

Figure 5.3: Schematic experimental set up for the state preparation. SM- Simon-Mukunda gadget, HWP- half wave plate, BBO- second order nonlinear crystal (Beta Barium Borate).

To generate the described state, we start with a Type I spontaneous parametric down conversion (SPDC) of light in a second order nonlinear crystal that gives a pair of photons entangled in the OAM [48]. A vertically polarized optical vortex beam of azimuthal index 1 has been considered as the pump. The state corresponding to the pair of photons produced by the SPDC of this beam is given by

$$|\Psi\rangle_{12} = \sum_{m=-\infty}^{+\infty} c_m |m\rangle_1 |1-m\rangle_2 \otimes |H\rangle_1 |H\rangle_2 \tag{5.3}$$

Note that the experimental realization of the quantum gates in the OAM basis $\{\, |0\rangle, \pm|1\rangle \pm |2\rangle ... \,\}$ are not straightforward. Moreover, in the teleportation, it is easier to project the state of a photon to one of its four spin-orbit Bell state if we use even/odd basis. Thus for the ease of experimental realization, we reduce the infinite dimensional entangled state to a simple two-qubit entangled state by grouping all the even and the odd OAM states and rewrite the expression for the OAM state in Eq. (5.3) as

$$\sum_{m=-\infty}^{+\infty} c_m (|m\rangle_1 |1-m\rangle_2) = \sum_{k=-\infty}^{+\infty} c_{2k}(|2k\rangle_1|1-2k\rangle_2) + \sum_{k=-\infty}^{+\infty} c_{2k+1}(|2k+1\rangle_1|-2k\rangle_2).$$

We define a transformation from the general OAM space to the even-odd OAM space as

$$g(|u\rangle_1|v\rangle_2) = f(|u\rangle_1) f(|v\rangle_2), \text{ where}$$

$$f(|x\rangle) = \begin{cases} |E\rangle, & \text{for even } x; \\ |O\rangle, & \text{for odd } x. \end{cases} \tag{5.4}$$

Applying g on the left-hand-side of Eq. (5.4) yields $\frac{1}{\sqrt{2}}(|E\rangle_1|O\rangle_2 + |O\rangle_1|E\rangle_2)$.

As explained in the previous chapter, from the conservation of OAM, we have $\sum_{k=-\infty}^{+\infty}(c_{2k})^2 = \sum_{k=-\infty}^{+\infty}(c_{2k+1})^2 = \frac{1}{2}\sum_{m=-\infty}^{+\infty}(c_m)^2 = \frac{1}{2}$.

Thus, we can rewrite Eq. (5.3) as

$$|\Psi\rangle_{12} = \frac{1}{\sqrt{2}}\left(|E\rangle_1|O\rangle_2 + |O\rangle_1|E\rangle_2\right) \otimes |H\rangle_1|H\rangle_2. \tag{5.5}$$

Note that the photons are entangled in the even/odd OAM states. Experimentally, this transformation can be implemented by post selection in the even/odd OAM basis. All the OAM operations or measurements must be performed in even/odd basis using OAM sorter [148]. This maps the general OAM state to even/odd basis which is mathematically represented by operator g. Let the photon **1** pass through a Simon-Mukunda polarization gadget which can convert its polarization to any arbitrary state [115, 116] and the photon **2** pass through a half wave plate at $\frac{\pi}{8}$. Thus polarization state of the photon **1** is encoded as the unknown state $a|H\rangle_1 + b|V\rangle_1$ and the state of the photon **2** is encoded as $\frac{1}{\sqrt{2}}(|H\rangle_2 + |V\rangle_2)$. Action of HWP on the photon **2** is a Hadamard operation. Thus, the state becomes

$$\begin{aligned} |\Psi\rangle_{12} \quad = \quad & \frac{1}{\sqrt{2}}\left(|E\rangle_1|O\rangle_2 + |O\rangle_1|E\rangle_2\right)\left(a|H\rangle_1 + b|V\rangle_1\right) \otimes \\ & \frac{1}{\sqrt{2}}(|H\rangle_2 + |V\rangle_2). \end{aligned} \tag{5.6}$$

Now, consider the photon **3** with unknown superposition state of OAM in the even/odd basis and with definite state polarization. Its state can be expressed as,

$$|\Psi\rangle_3 = (\alpha|E\rangle_3 + \beta|O\rangle_3) \otimes |V\rangle_3. \tag{5.7}$$

A polarization C_{NOT} gate is applied on photon **2** (control) and **3** (target). This operation leads to a polarization entanglement between photons **2** and **3**. Thus, the three particle state becomes

$$|\Psi\rangle_{123} = \frac{1}{2}\left(a|H\rangle_1 + b|V\rangle_1\right)\left(|E\rangle_1|O\rangle_2 + |O\rangle_1|E\rangle_2\right)\left(|HV\rangle_{23} + |VH\rangle_{23}\right)(\alpha|E\rangle_3 + \beta|O\rangle_3). \tag{5.8}$$

This is in the same form as the proposed three particle entangled state described in Section **2**, Eq. (5.2).

5.3 Simultaneous teleportation of two qubits using the new state

Teleportation of N qubits, in general, needs N pairs of entangled photons. On the other hand, teleportation of d-dimensional quantum state needs d-dimensional entanglement and one has to do a joint measurement in d^2 dimensional Bell basis [149]. However, teleportation

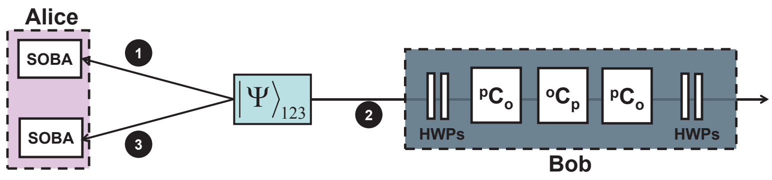

Figure 5.4: Schematic for the teleportation of spin-orbit qubits shared by photons **1** and **3**. HWPs - half wave plates.

schemes were proposed for a d dimensional OAM state using Bell filter and quantum scissors [150–152].

With the entangled state presented above, we propose an efficient scheme for teleporting a two-qubit state distributed in different DOFs. The schematic diagram is given in Fig. 5.4. The polarization state of photon **1** and the OAM state of photon **3** form a four dimensional unknown two-qubit state

$$|\Psi\rangle_u = (a|H\rangle_1 + b|V\rangle_1) \otimes (\alpha|E\rangle_3 + \beta|O\rangle_3), \tag{5.9}$$

which needs to be teleported. We can teleport the combined state to a single particle, photon **2**.

The unknown polarization (spin angular momentum) and the entangled OAM state of photon **1** and entangled polarization and the unknown OAM state of photon **3** in Eq. (5.8), can be projected to individual spin-orbit Bell states by SOBA. Alice performs the SOBA on the photons **1** and **3** and projects the state of both the particles to the corresponding spin-orbit Bell states. The SOBA, for which the OAM is in the even/odd basis, can be achieved by Mach-Zehnder interferometers involving an OAM sorter and polarizing beam splitters [147].

The states can be defined as

$$\begin{aligned} \psi^{\pm} &= \tfrac{1}{\sqrt{2}} \left(|H, E\rangle \pm |V, O\rangle\right), \\ \phi^{\pm} &= \tfrac{1}{\sqrt{2}} \left(|H, O\rangle \pm |V, E\rangle\right). \end{aligned} \tag{5.10}$$

The SOBA operation for photon **1** can be represented by a polarization controlled OAM C_{NOT} (^pC_o) gate and a polarization Hadamard (H_p) gate operation with subsequent detection. Similarly, the SOBA for photon **3** is an OAM controlled polarization C_{NOT} (^oC_p) gate and OAM Hadamard (H_o) gate operation with subsequent detection. Experimental schemes for these single particle two-qubit C_{NOT} gates and SOBA are given in Section 5.3.1.

By substituting the single particle spin-orbit Bell states into a three particle wave function in Eq. (5.8), we get

$$|\Psi\rangle_{123} = \frac{1}{4}\sum_{x,y=0}^{1}\sum_{x',y'=0}^{1} |\Phi^{xy}\rangle_1 |\Phi_q^{x'y'}\rangle_3 \otimes \Gamma_{x,y,x',y'}\left(\alpha|H\rangle_2 + \beta|V\rangle_2\right)\left(a|E\rangle_2 + b|O\rangle_2\right),$$

where $|\Phi^{xy}\rangle_1$ and $|\Phi_q^{x'y'}\rangle_3$ are single particle spin-orbit Bell states corresponding to the photons **1** & **3** respectively. $\Gamma_{x,y,x',y'}$ is a transformation matrix for the spin-orbit state of photon **2**. It has been introduced for the compact representation of the 16 states of photon **2** given in Table 5.1. After the SOBA measurements on the photons **1** and **3**, state of the photon **2** becomes

$$|\Psi(D_{|\Phi^{xy}\rangle_1|\Phi_q^{x'y'}\rangle_3})\rangle_2 = \frac{1}{4}\Gamma_{x,y,x',y'}\left(\alpha|H\rangle_2 + \beta|V\rangle_2\right)\left(a|E\rangle_2 + b|O\rangle_2\right), \tag{5.11}$$

the state corresponding to a detection of $|\Phi^{xy}\rangle_1|\Phi_q^{x'y'}\rangle_3$ in SOBAs.

The states corresponding to all possible SOBA outcomes are given in the first and the second columns of the Table 5.1. Note that the information encoded in the polarization state of the photon **1** is transferred to the OAM state of the photon **2** and the information encoded in the OAM state of the photon **3** is transferred to the polarization state of the photon **2**. So, to get the initial state, Bob has to do a swapping (U_{SWAP}) between the OAM and the polarization along with other unitary transformations which use only polarization operations. These operations can be implemented with the standard wave plates which makes the experimental realization of this method more feasible.

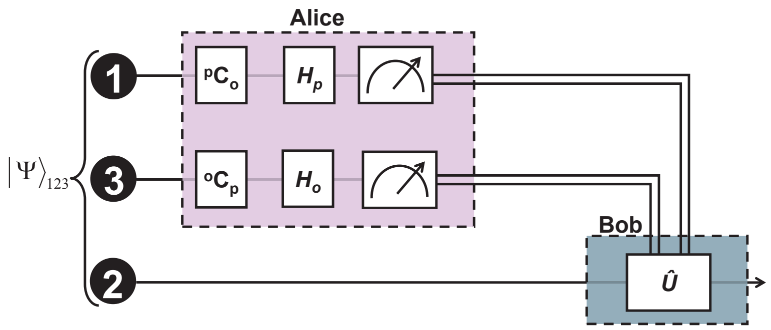

Figure 5.5: Circuit diagram for proposed teleportation scheme. Single/double lines - quantum/classical communication channels, arrow - measurement. $\hat{U}$ - unitary transformation given in Table 5.1

There are 16 possible outcomes for Alice measurements which demand 16 different unitary operations by Bob to complete the teleportation protocol. Alice communicates her measurement outcome ($|\Phi^{xy}\rangle_1|\Phi_q^{x'y'}\rangle_3$) classically to Bob. Bob does the corresponding unitary transformation $\hat{U}$ (given in the third column of Table 5.1) on state of photon **2** to

Measurement Outcome	State of Bob's Photon	Unitary Transformations ($\hat{U}$)
$\|\phi^+\phi^+\rangle$	$(\alpha\|V\rangle + \beta\|H\rangle)(a\|O\rangle + b\|E\rangle)$	$[I^o \otimes \sigma_1^p] * U_{SWAP} * [\sigma_1^p \otimes I^o]$
$\|\phi^+\phi^-\rangle$	$(\alpha\|V\rangle - \beta\|H\rangle)(a\|O\rangle + b\|E\rangle)$	$[I^o \otimes \sigma_1^p] * U_{SWAP} * [i\sigma_2^p \otimes I^o]$
$\|\phi^-\phi^+\rangle$	$(\alpha\|V\rangle + \beta\|H\rangle)(a\|O\rangle - b\|E\rangle)$	$[I^o \otimes i\sigma_2^p] * U_{SWAP} * [\sigma_1^p \otimes I^o]$
$\|\phi^-\phi^-\rangle$	$(\alpha\|V\rangle - \beta\|H\rangle)(a\|O\rangle - b\|E\rangle)$	$[I^o \otimes i\sigma_2^p] * U_{SWAP} * [i\sigma_2^p \otimes I^o]$
$\|\psi^+\psi^+\rangle$	$(\alpha\|H\rangle + \beta\|V\rangle)(a\|E\rangle + b\|O\rangle)$	$[I^o \otimes I^p] * U_{SWAP} * [I^p \otimes I^o]$
$\|\psi^+\psi^-\rangle$	$(-\alpha\|H\rangle + \beta\|V\rangle)(a\|E\rangle + b\|O\rangle)$	$[I^o \otimes I^p] * U_{SWAP} * [\sigma_3^p \otimes I^o]$
$\|\psi^-\psi^+\rangle$	$(\alpha\|H\rangle + \beta\|V\rangle)(a\|E\rangle - b\|O\rangle)$	$[I^o \otimes \sigma_3^p] * U_{SWAP} * [I^p \otimes I^o]$
$\|\psi^-\psi^-\rangle$	$(-\alpha\|H\rangle + \beta\|V\rangle)(a\|E\rangle - b\|O\rangle)$	$[I^o \otimes \sigma_3^p] * U_{SWAP} * [\sigma_3^p \otimes I^o]$
$\|\phi^+\psi^+\rangle$	$(\alpha\|H\rangle + \beta\|V\rangle)(a\|O\rangle + b\|E\rangle)$	$[I^o \otimes \sigma_1^p] * U_{SWAP} * [I^p \otimes I^o]$
$\|\phi^+\psi^-\rangle$	$(-\alpha\|H\rangle + \beta\|V\rangle)(a\|O\rangle + b\|E\rangle)$	$[I^o \otimes \sigma_1^p] * U_{SWAP} * [\sigma_3^p \otimes I^o]$
$\|\phi^-\psi^+\rangle$	$(\alpha\|H\rangle + \beta\|V\rangle)(a\|O\rangle - b\|E\rangle)$	$[I^o \otimes i\sigma_2^p] * U_{SWAP} * [I^p \otimes I^o]$
$\|\phi^-\psi^-\rangle$	$(-\alpha\|H\rangle + \beta\|V\rangle)(a\|O\rangle - b\|E\rangle)$	$[I^o \otimes i\sigma_2^p] * U_{SWAP} * [\sigma_3^p \otimes I^o]$
$\|\psi^+\phi^+\rangle$	$(\alpha\|V\rangle + \beta\|H\rangle)(a\|E\rangle + b\|O\rangle)$	$[I^o \otimes I^p] * U_{SWAP} * [\sigma_1^p \otimes I^o]$
$\|\psi^+\phi^-\rangle$	$(\alpha\|V\rangle - \beta\|H\rangle)(a\|E\rangle + b\|O\rangle)$	$[I^o \otimes I^p] * U_{SWAP} * [i\sigma_2^p \otimes I^o]$
$\|\psi^-\phi^+\rangle$	$(\alpha\|V\rangle + \beta\|H\rangle)(a\|E\rangle - b\|O\rangle)$	$[I^o \otimes I^p] * U_{SWAP} * [i\sigma_2^p \otimes I^o]$
$\|\psi^-\phi^-\rangle$	$(\alpha\|V\rangle - \beta\|H\rangle)(a\|E\rangle - b\|O\rangle)$	$[I^o \otimes \sigma_3^p] * U_{SWAP} * [i\sigma_2^p \otimes I^o]$

Table 5.1: Wave function corresponding to Bob's photon and the required unitary transformation corresponding to Alice's measurement outcome.$\sigma_1^p, \sigma_2^p, \sigma_3^p$ are Pauli matrices for polarization, I^p and I^o are identity matrices for polarization and OAM.

get

$$|\Psi\rangle_2 = (a|H\rangle_2 + b|V\rangle_2)(\alpha|E\rangle_2 + \beta|O\rangle_2). \tag{5.12}$$

which completes the teleportation of unknown state given in Eq. (5.9).

A SWAP operation is equivalent to consecutive ${}^pC_o$, ${}^oC_p$ and ${}^pC_o$ gate operations. Since the operation done in polarization will be transferred to the OAM after the SWAP operation, one can perform all the operations in polarization which are well known. Two half wave plates before and after the SWAP gate can perform 16 unitary operations which is required for the teleportation. A circuit diagram of the proposed scheme is given in Fig. 5.5.

5.3.1 Experimental realization of ${}^{p}C_{o}$, ${}^{o}C_{p}$ gates and SOBA

A Polarization controlled OAM C_{NOT} gate can be implemented using a modified Mach-Zehnder interferometer where the normal beam splitter is replaced by a polarizing beam splitter (PBS) as shown in Fig. 5.6. The arm of interferometer, through which the vertically polarized photons travel, contains a spiral phase plate (SPP) of order 1 which will convert the even OAM state to odd and vice versa. On the other arm with horizontally polarized photons, the OAM state remains unchanged. These states superpose at the second PBS and emerges as a single ${}^{p}C_{o}$ gate output. A glass block is introduced to compensate the extra phase introduced by the SPP.

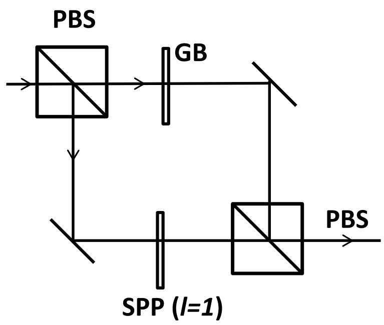

Figure 5.6: Experimental scheme for the implementation of polarization controlled OAM C_{NOT} gate (${}^{p}C_{o}$). PBS - polarizing beam splitter, SPP - spiral phase plate, GB - glass block.

We pursue a similar method to construct the OAM controlled polarization C_{NOT} gate. For that, we need to use a beam splitter which transmits the photons with even OAM state and reflects the photons with odd OAM state. This can be achieved by an OAM sorter [148]. We replace the two PBSs in the previous setup with OAM sorters and instead of the SPP we use a half wave plate at 45^0 in one arm that transforms the polarization state to its orthogonal state. The schematic of the setup is given in Fig. 5.7. The OAM sorter is another Mach-Zehnder interferometer containing dove prisms in each arm with a relative angle of 90^0.

The spin-orbit Bell state analysis with OAM in the even/odd states is explained by Khoury and Milman [147]. However, in the present protocol, the SOBA in photon **1** and photon **3** differ slightly in their implementation. As shown in the Fig. 5.8, two Mach-Zehnder interferometers with OAM sorters (OS) and polarizing beam splitters with photon detectors can implement SOBA. For the photon **1**, the block 1 the Fig. 5.8 is an OAM sorter and the

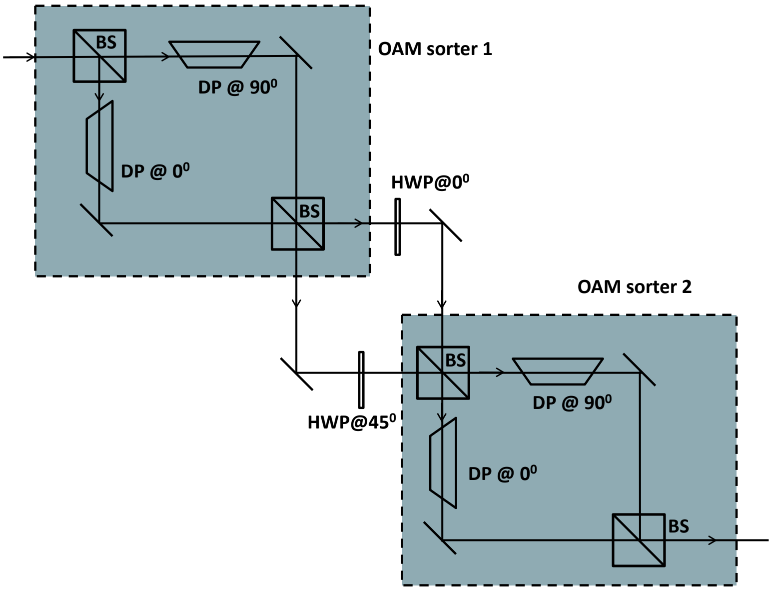

Figure 5.7: Experimental scheme for the implementation of OAM controlled polarization C_{NOT} gate (^oC_p). DP - dove prism, BS - 50:50 beam splitter, HWP - half wave plate

blocks 2 and 3 are polarizing beam splitters. For SOBA in photon **3**, the block 1 is a PBS while the blocks 2 and 3 are OAM sorters. Detection on each of the detector will indicate the corresponding spin-orbit Bell state of the photon.

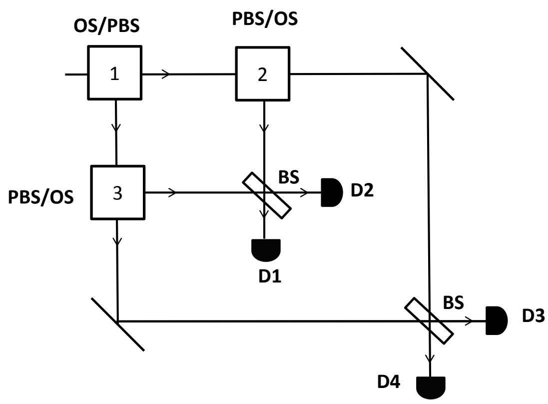

Figure 5.8: Experimental scheme for the implementation of SOBA in photon **1/3**. OS - OAM sorter, PBS - polarizing beam splitter, BS - 50:50 beam splitter

Here are the advantages of the described teleportation scheme

(i) As evident from the scheme, the number of particles required to teleport two independent qubits are reduced by 25% by taking advantage of an extra DOF per photon.

(ii) We use single particle two-qubit Bell measurement instead of two particle joint Bell measurements. Its implementation is experimentally simple and one can achieve 100% efficient Bell sate measurement and hence the teleportation.

(iii) In our scheme Bob need not to do unitary transformations on the OAM, since the same can be implemented by operations on the polarization before and after the SWAP.

(iv) The described three particle hyper-entangled states can be utilized for a multi-party teleportation scheme with two senders and a common receiver. Here Alice, and Charlie, with no entanglement channel between them, share photons **1** and **3**. The combined polarization-OAM quantum state of Alice's and Charlie's photons will be teleported to Bob who carries photon **2**.

5.4 Quantum Key Distribution

Theoretically, the entanglement based QKD protocols are equivalent to the single photon based ones (such as BB84). However, in practice, due to the strong quantum correlation and non-locality [18, 153–156], the entanglement based protocols are regarded more useful (for example, they have intrinsic randomness of the distributed key and extremely low probability of double photons). In recent years, entanglement in two degrees of freedom such as polarization and OAM has led to interesting applications in cryptography [56, 157].

Here we are proposing a QKD protocol using the entangled system described in section 5.1. We take a similar state as in Eq. (5.2) given by

$$|\Psi\rangle_{123} = |\xi_p\rangle_1 \otimes (|00\rangle_{12} + |1-1\rangle_{12} + |-11\rangle_{12}) \otimes (|HH\rangle_{23} + |VV\rangle_{23})|\chi_o\rangle_3,$$

where $|0\rangle$, $|1\rangle$ and $|-1\rangle$ are the OAM states of photons. Here we take a three dimensional subspace of infinite dimensional OAM entangled state produced by SPDC process with Gaussian beam as pump instead of even/odd entangled state.

The experimental implementation of the protocol is shown in Fig. 5.9. Alice will receive photon **2** and Bob will receive photons **1** and **3** respectively. Photon **2** is entangled with photon **3** in polarization and it is entangled with photon **1** in OAM. The photons **1** and **3** do not have any correlation. Alice will measure both OAM and Polarization states, Bob will measure polarization of photon **3** and OAM of photon **1**.

Alice and Bob randomly measure polarization states of their respective photons in the following set of basis ($\gamma_i = 0°$, $22.5°$, $45°$, $67.5°$), ($\delta_i = 22.5°$, $45°$, $67.5°$, $180°$) respectively. These measurements can be done by a half wave plate and polarizing beam splitter. Note

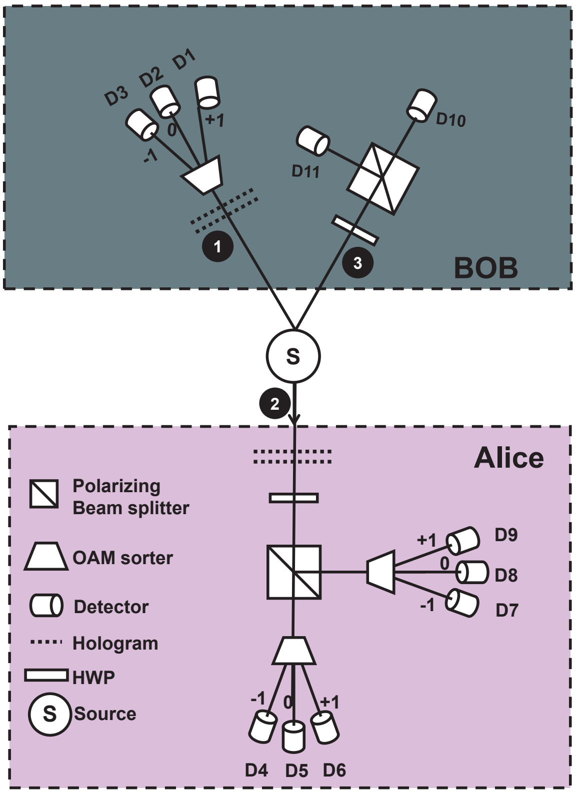

Figure 5.9: Schematic diagram for quantum key distribution between Alice and Bob. Photons 1-2 have polarization entanglement and 1-3 have OAM entanglement. D_i - detectors, HWP - half wave plate, PBS - polarizing beam splitter.

that $\gamma_i/2$ and $\delta_i/2$ are the fast axis orientation angles of the half wave plates. Each angle represents a basis which is used for measurement and corresponding to each of them, there are two measurement outcomes. The pairs of angles used by Alice and Bob for which the sum is $0°$ and $180°$ will give perfect correlation between them. The data corresponding to these correlated photons have same bits and can be used for the key. Alice and Bob will compare their polarization measurement basis for the key distribution as well as for the security of the key. After sufficient number of measurements 4/16 of the data are useful for key, two sets of 4/16 of the data are used to check CHSH inequalities (S and S$'$) and the remaining 4/16 are discarded due to unmatched bases.

For the OAM correlation of entangled photons, we follow the key sharing scheme used in [158]. In this scheme, Alice and Bob measure the OAM state of their photons in three different randomly chosen bases A_1, A_2, A_3 and B_1, B_2, B_3 respectively. This is done by a pair of shifted holograms and an OAM sorter. The set of bases (A_3 and B_3) has perfect correlation and the coincidence corresponding to it can be used to generate the key. Alice

Alice	γ_1	γ_2	γ_3	γ_4
Bob				
δ_1	S	Key	S	$\times$
δ_2	$\times$	S′	Key	S′
δ_3	S	$\times$	S	Key
δ_4	Key	S′	$\times$	S′

Table 5.2: Description of data usage corresponding to Alice's and Bob's measurement angles. Here S and S′ are used for security check through CHSH inequality and $\times$ is the discarded data.

and Bob will compare their hologram settings for QKD and security check. In total, there are 9 possible measurements. After taking sufficient number of measurements, 1/9 of the produced data can be used for the key. For Bell-type inequality check, 4/9 of the data will be used which confirms the security of the key and the remaining 4/9 of the data are redundant.

The security of the protocol is mainly checked by the violation of Bell's inequality test. All the three parties should check Bell like inequality with their data in order to check eavesdropping. If there is a violation of inequality, entanglement is preserved and there is no eavesdropping in the channel. The CHSH parameters S and S′ for photons entangled in the polarization DOF are given by [8]

$$S = E(\gamma_1, \delta_1) - E(\gamma_1, \delta_3) + E(\gamma_3, \delta_1) + E(\gamma_3, \delta_3) \tag{5.13}$$

$$S' = E(\gamma_2, \delta_2) + E(\gamma_2, \delta_4) + E(\gamma_4, \delta_2) - E(\gamma_4, \delta_4) \tag{5.14}$$

with

$$E(\gamma_i, \delta_j) = \frac{R_{12}(\gamma_i, \delta_j) + R_{1'2'}(\gamma_i, \delta_j) - R_{12'}(\gamma_i, \delta_j) - R_{1'2}(\gamma_i, \delta_j)}{R_{12}(\gamma_i, \delta_j) + R_{1'2'}(\gamma_i, \delta_j) + R_{12'}(\gamma_i, \delta_j) + R_{1'2}(\gamma_i, \delta_j)} \tag{5.15}$$

where $R_{12}, R_{1'2'}, R_{12'}$ and $R_{1'2}$ are the coincidences $P(D11, D9 + D8 + D7)$, $P(D10, D4 + D5 + D6)$, $P(D11, D4 + D5 + D6)$ and $P(D10, D9 + D8 + D7)$ respectively.

For any local realistic theory, the CHSH parameters $S, S' \leq 2$. Non-local nature of the entanglement will violate any of these inequalities and this violation can be used for checking the security of the key shared by Alice and Bob. The combination of γ and δ for Bell's inequality test and for the key distribution is given in Table 5.2.

Photons **1** and **2** have OAM correlation, so it will violate the following Bell's inequality for 3 dimensional case [158, 159]

$$\begin{aligned} S &= P(A_1 = B_1) + P(A_2 = B_1 - 1) + P(A_2 = B_2) + P(A_1 = B_2) \\ &\quad -P(A_1 = B_1 - 1) - P(A_2 = B_1) + P(A_2 = B_2 - 1) + P(A_1 = B_2 + 1) \quad (5.16) \\ &\leq 2, \quad (5.17) \end{aligned}$$

where

$$P(A_a = B_b + k) = \sum_{j=0}^{2} P(A_a = j, B_b = (j + k) Mod\ 3). \quad (5.18)$$

The shifts of holograms are chosen in such a way that they maximally violate the Bell-type inequality. j=0,1,2 corresponds to the detection of OAM states 0, 1 and -1 respectively. The coincidence measurements with the combinations of $P(D1, D6 + D9)$, $P(D1, D5 + D8)$, $P(D2, D4 + D7)$, $P(D2, D6 + D9)$, $P(D2, D5 + D8)$, $P(D2, D4 + D7)$, $P(D3, D6 + D9)$, $P(D3, D5 + D8)$ and $P(D3, D4 + D7)$ are required for the key distribution and to check the security of the key using Eq. (5.16) and (5.18).

Our protocol has three advantages compared to traditional Ekert protocol [10].

(i) If Ekert protocol is used, then around $4n$ pairs of photons, i.e., $8n$ photons (in practice, little more than $8n$) are required to establish a secret key of length n between Alice and Bob. In our approach, around $6n$ photons would be required for the same purpose. Hence, in terms of number of photons required, Ekert's protocol is 33% less efficient than ours.

(ii) On the other hand, if the same number of photons are used in Ekert and our protocol and if the target key length is also the same, then because of more entanglement resource, our protocol would have more redundancy and hence can tolerate more noise. It is easy to see that the security in each degree of freedom is equivalent to that of the Ekert protocol.

(iii) Further, this state can be used for multi-party QKD. Photons 1, 2 and 3 can be distributed amongst Alice, Bob and Charlie respectively. Now, two sets of independent keys can be generated, one for Alice-Bob and another for Alice-Charlie.

5.5 Conclusion

Possibility of a new entangled state and its application in teleporting a two-qubit OAM-polarization quantum state and in the QKD have been discussed. The new teleportation method overcomes the difficulty of measuring in two particle polarization Bell basis, by implementing independent single particle two-qubit Bell measurements. The method critically depends on the experimental realizations of polarization C_{NOT} gate as well as single particle two-qubit C_{NOT} gates. All the 16 unitary transformations which are required for this teleportation scheme can be realized with linear optical components along with a SWAP gate. Once the state given in Eq. (5.8) is achieved, one can have a 100% efficient teleportation of two simultaneous qubits. Extending this to higher dimensions is mathematically trivial though creating entanglement in different DOFs has experimental limitations. With the new QKD protocol, the sender and the receiver need to use less resource than traditional Ekert protocol to share the secret key of the same length. Multi-party schemes also can be developed for the teleportation and the QKD using the described protocols.

Chapter 6

Summary and Scope for Future Work

Entanglement is the basic resource for quantum communication and photons are the most suitable candidate for implementing them. Polarization and OAM are the two discrete degrees of freedom of photons for quantum information processing and it is important to study entanglement in such systems. In the classical systems the non-separable states which mimic the properties of entanglement are receiving much attention in the recent years. This thesis studies quantum and classical aspects of polarization and orbital angular momentum (OAM) entanglement.

In chapter 1, we have given a general introduction to entanglement and its conceptual developmental in the past 80 years. Basics of quantum information and entanglement based protocols such as superdense coding, teleportation and cryptography were briefly discussed. We have also explained briefly the elements of photonic quantum information based on discrete degrees of freedom of light i.e. polarization and OAM.In addition, we have discussed about the entanglement in polarization and OAM, its experimental implications, inter and intra system entanglement and its applications. In short, we have provided an introduction to the classical non-separable states of OAM and polarization, which mimic the entanglement and many quantum protocols, their nature and applications.

In chapter 2 and 3, we have studied the classical counterpart of hybrid entanglement between OAM and polarization. The system of interest is a laser beam for which the polarization and its spatial mode are entangled. This beam has non-uniform polarization in the transverse plane. We can implement quantum inspired measurements on this state which will lead to the violation of Bell's inequality and steering. Unlike the quantum entanglement, there is no non-locality in this case. The non-separability between two degrees of freedom, which are in general separable, makes it possible to steer the state in one DOF by performing measurement in the other.

In chapter 2 we have studied the non-separable states of OAM and polarization, its local polarization structure, its violation of Bell's inequality and its behaviour under a cyclic evolution of polarization. We have generated non-separable state of polarization and OAM using a polarizing Sagnac interferometer and studied the effect of Pancharatnam geometric phase in the non-separable state. The non-separability is confirmed by the violation of Bell-CHSH inequality. The geometric phase introduced in the polarization subsystem induces a relative phase in the Bell like state of OAM and polarization. The maximum value of the Bell parameter, B_{MAX}, maximized over the measurement angles, varies sinusoidally according to the relative phase. We obtain a constant B_{MAX} for different geometric phases by introducing a relative phase in the projected OAM state. It was also shown that the Bell CHSH inequality measurement in circular bases can remove the phase dependence of the B_{MAX} by shifting the measurement angle. We have analyzed the polarization structure of the non-separable state for different Pancharatnam phases that gives a rotation to it. This physically explains the effect of Pancharatnam phase in the joint measurement of polarization and OAM. We have also described an OAM Poincaré sphere which can represent all the OAM superposition states in $\{l, -l\}$ subspace even for $|l| \geq 1$. We also have presented an experimental method for the generation of all such states using a non-separable state of OAM and polarization. Finally, we have described the representation of OAM mixed states as non-separable states inside the Poincaré sphere.

In Chapter 3 we have studied the effect of scattering on a non-separable state. We found that the non-separability is preserved under scattering and can be retrieved using a lens. We have produced a light beam with non-separable polarization and orbital angular momentum states using a simple interferometer and experimentally verified the preservation of non-separability under scattering through a rotating ground glass. The polarization measurements and the images of the beam projected to different polarizations show the presence of non-separability for coherent and scattered light. We have also demonstrated the generation of non-maximally non-separable states of light and studied their behaviour under scattering by measuring the degree of polarization. This recovered partially coherent non-separable states can be used to generate arbitrary superposition states of OAM by polarization selection. Our results can have application in public broadcasting systems.

In chapters 4 and 5 we have conceptualised new multi-photon states of OAM and polarization, defined proper measurements with experimental schematics to used them for implementing various quantum protocols.

In chapter 4, we have described the possibility of using even/odd OAM states for quantum information. The motivation was to use OAM as a qubit like polarization without any photon loss due to the restriction of the Hilbert space. We have formulated appropriate measurement system for the even/odd OAM state based quantum information. Since even-odd OAM entanglement can be implemented like two qubit polarization entanglement, we describe the measurement and violation of Bell's inequality for such states. We have described hyper-entanglement and hybrid entanglement with OAM and polarization degrees of freedom. We have proposed an experimental scheme for spin orbit Bell state analysis to distinguish all the spin-orbit Bell states. This is applied in hyper entanglement assisted polarization Bell state analysis for efficient dense coding.

In Chapter 5 we have introduced a new three particle entangled state and their application in teleporting a two-qubit OAM-polarization quantum state and in the QKD. The new teleportation method overcomes the difficulty of measuring in two particle polarization Bell basis, by implementing independent single particle two-qubit Bell measurements. It was shown that all the 16 unitary transformations which are required for this teleportation scheme can be realized with linear optical components. With the new QKD protocol, the sender and the receiver need to use less resource than traditional Ekert protocol to share the secret key of the same length. Multi-party schemes also can be developed for the teleportation and the QKD using the described protocols.

6.1 Scope for future work

We have studied the cyclic evolution of polarization in a non-separable states and its effect on Bell's inequality. In future we intend to study the properties with non-cyclic Pancharatnam phase. In principle one can measure the Pancharatnam-Berry phase due to a non-cyclic polarization evolution using the non-separable state without any interferometric measurements. Study of scattering of non-separable states opens up many questions that need to be addressed. We intend to study the spatial and temporal correlations of the scattered non-separable light field. Here we can control the global degree of polarization by making non-maximally non-separable states and study its effect on the coherence properties of the scattered field. We also intend to do the photon statistics of the non-separable states.

We believe that the even/odd OAM states and its measurement realizations could be a whistle blower for more efficient OAM entanglement based quantum protocols. We will be experimentally verifying the even/odd entanglement and its Bell's inequality violation. The implementation of all the quantum gates mentioned will be interesting for its application to many new quantum protocols. It will be interesting to revisit Hong-Ou-Mandel experiments with photons entangled in even/odd OAM states.

The experimental realization of the three particle state could be a great step in achieving multi-party quantum communications. Simultaneous and deterministic teleportation of two qubits can be implemented for the first time using this state.

Bibliography

[1] A. Einstein, B. Podolsky, and N. Rosen, *Can quantum-mechanical description of physical reality be considered complete?* Phys. Rev. **47**, 777–780 (1935).

[2] N. Bohr, *Can quantum-mechanical description of physical reality be considered complete?* Phys. Rev. **48**, 696–702 (1935).

[3] D. Bohm, *A suggested interpretation of the quantum theory in terms of "hidden" variables. i,* Phys. Rev. **85**, 166–179 (1952).

[4] M. A. Nielsen and I. L. Chuang, *Quantum computation and quantum information* (Cambridge university press, 2010).

[5] W. K. Wootters and W. H. Zurek, *A single quantum cannot be cloned,* Nature **299**, 802–803 (1982).

[6] J. S. Bell, *On the einstein podolsky rosen paradox,* Physics **1**, 195–200 (1964).

[7] J. S. Bell, *On the problem of hidden variables in quantum mechanics,* Rev. Mod. Phys. **38**, 447–452 (1966).

[8] J. F. Clauser, M. A. Horne, A. Shimony, and R. A. Holt, *Proposed experiment to test local hidden-variable theories,* Phys. Rev. Lett. **23**, 880–884 (1969).

[9] C. E. Shannon, *A mathematical theory of communication,* Bell Syst. Tech. J. **27**, 379–423 (1948).

[10] A. K. Ekert, *Quantum cryptography based on bell's theorem,* Phys. Rev. Lett. **67**, 661–663 (1991).

[11] C. H. Bennett, G. Brassard, C. Crépeau, R. Jozsa, A. Peres, and W. K. Wootters, *Teleporting an unknown quantum state via dual classical and einstein-podolsky-rosen channels,* Phys. Rev. Lett. **70**, 1895–1899 (1993).

[12] C. H. Bennett and S. J. Wiesner, *Communication via one- and two-particle operators on einstein-podolsky-rosen states,* Phys. Rev. Lett. **69**, 2881–2884 (1992).

[13] P. Kok and B. W. Lovett, *Introduction to optical quantum information processing* (Cambridge University Press, 2010).

[14] C. V. RAMAN and S. BHAGAVANTAM, *Experimental proof of the spin of the photon.* Nature **129**, 22–23 (1932).

[15] R. A. Beth, *Mechanical detection and measurement of the angular momentum of light,* Phys. Rev. **50**, 115–125 (1936).

[16] D. Bouwmeester, J.-W. Pan, K. Mattle, M. Eibl, H. Weinfurter, and A. Zeilinger, *Experimental quantum teleportation,* Nature **390**, 575–579 (1997).

[17] K. Mattle, H. Weinfurter, P. G. Kwiat, and A. Zeilinger, *Dense coding in experimental quantum communication,* Phys. Rev. Lett. **76**, 4656–4659 (1996).

[18] T. Jennewein, C. Simon, G. Weihs, H. Weinfurter, and A. Zeilinger, *Quantum cryptography with entangled photons,* Phys. Rev. Lett. **84**, 4729–4732 (2000).

[19] L. Allen, M. W. Beijersbergen, R. Spreeuw, and J. Woerdman, *Orbital angular momentum of light and the transformation of laguerre-gaussian laser modes,* Phys. Rev. A **45**, 8185 (1992).

[20] H. He, M. E. J. Friese, N. R. Heckenberg, and H. Rubinsztein-Dunlop, *Direct observation of transfer of angular momentum to absorptive particles from a laser beam with a phase singularity,* Phys. Rev. Lett. **75**, 826–829 (1995).

[21] K. Dholakia, M. MacDonald, and G. Spalding, *Optical tweezers: the next generation,* Physics World **15**, 31 (2002).

[22] D. G. Grier, *A revolution in optical manipulation,* Nature **424**, 810–816 (2003).

[23] P. Galajda and P. Ormos, *Complex micromachines produced and driven by light,* Appl. Phys. Lett. **78** (2001).

[24] S. W. Hell, *Toward fluorescence nanoscopy,* Nat. Biotechnol. **21**, 1347–1355 (2003).

[25] L. Torner, J. P. Torres, and S. Carrasco, *Digital spiral imaging,* Opt. Express **13**, 873–881 (2005).

[26] S. Bernet, A. Jesacher, S. Fürhapter, C. Maurer, and M. Ritsch-Marte, *Quantitative imaging of complex samples by spiral phase contrast microscopy,* Opt. Express **14**, 3792–3805 (2006).

[27] J. Grover A. Swartzlander, *The optical vortex lens,* Opt. Photon. News **17**, 39–43 (2006).

[28] J. Chu, X. Li, Q. Smithwick, and D. Chu, *Coding/decoding two-dimensional images with orbital angular momentum of light,* Opt. Lett. **41**, 1490–1493 (2016).

[29] G. Gibson, J. Courtial, M. J. Padgett, M. Vasnetsov, V. Pasko, S. M. Barnett, and S. Franke-Arnold, *Free-space information transfer using light beams carrying orbital angular momentum,* Opt. Express **12**, 5448–5456 (2004).

[30] A. E. Willner, H. Huang, Y. Yan, Y. Ren, N. Ahmed, G. Xie, C. Bao, L. Li, Y. Cao, Z. Zhao, J. Wang, M. P. J. Lavery, M. Tur, S. Ramachandran, A. F. Molisch, N. Ashrafi, and S. Ashrafi, *Optical communications using orbital angular momentum beams,* Adv. Opt. Photon. **7**, 66–106 (2015).

[31] A. V. Carpentier, H. Michinel, J. R. Salgueiro, and D. Olivieri, *Making optical vortices with computer-generated holograms,* Am. J. Phys. **76**, 916–921 (2008).

[32] N. Heckenberg, R. McDuff, C. Smith, and A. White, *Generation of optical phase singularities by computer-generated holograms,* Opt. Lett. **17**, 221–223 (1992).

[33] I. M. Firth, *Holography and Computer Generated Holograms* (Mills & Boon, 1972).

[34] M. Beijersbergen, L. Allen, H. Van der Veen, and J. Woerdman, *Astigmatic laser mode converters and transfer of orbital angular momentum,* Opt. Commun. **96**, 123–132 (1993).

[35] V. V. Kotlyar, H. Elfstrom, J. Turunen, A. A. Almazov, S. N. Khonina, and V. A. Soifer, *Generation of phase singularity through diffracting a plane or gaussian beam by a spiral phase plate,* J. Opt. Soc. Am. A **22**, 849–861 (2005).

[36] J. P. Torres and L. Torner, *Twisted Photons: Applications of Light with Orbital Angular Momentum* (John Wiley & Sons, 2011).

[37] G. Gibson, J. Courtial, M. J. Padgett, M. Vasnetsov, V. Pasko, S. M. Barnett, and S. Franke-Arnold, *Free-space information transfer using light beams carrying orbital angular momentum,* Opt. Express **12**, 5448–5456 (2004).

[38] S. Grblacher, T. Jennewein, A. Vaziri, G. Weihs, and A. Zeilinger, *Experimental quantum cryptography with qutrits,* New J. Phys. **8**, 75 (2006).

[39] L. Jun-Lin and W. Chuan, *Six-state quantum key distribution using photons with orbital angular momentum,* Chin. Phys. Lett. **27**, 110303 (2010).

[40] M. Mirhosseini, O. S. Magaa-Loaiza, M. N. OSullivan, B. Rodenburg, M. Malik, M. P. J. Lavery, M. J. Padgett, D. J. Gauthier, and R. W. Boyd, *High-dimensional quantum cryptography with twisted light,* New J. Phys. **17**, 033033 (2015).

[41] K. Dholakia, N. B. Simpson, M. J. Padgett, and L. Allen, *Second-harmonic generation and the orbital angular momentum of light,* Phys. Rev. A **54**, R3742–R3745 (1996).

[42] J. Courtial, K. Dholakia, L. Allen, and M. J. Padgett, *Second-harmonic generation and the conservation of orbital angular momentum with high-order laguerre-gaussian modes,* Phys. Rev. A **56**, 4193–4196 (1997).

[43] A. Berzanskis, A. Matijosius, A. Piskarskas, V. Smilgevicius, and A. Stabinis, *Conversion of topological charge of optical vortices in a parametric frequency converter,* Opt. Commun. **140**, 273 – 276 (1997).

[44] A. Beranskis, A. Matijoius, A. Piskarskas, V. Smilgeviius, and A. Stabinis, *Sum-frequency mixing of optical vortices in nonlinear crystals,* Opt. Commun. **150**, 372 – 380 (1998).

[45] J. Arlt, K. Dholakia, L. Allen, and M. J. Padgett, *Parametric down-conversion for light beams possessing orbital angular momentum,* Phys. Rev. A **59**, 3950–3952 (1999).

[46] H. H. Arnaut and G. A. Barbosa, *Orbital and intrinsic angular momentum of single photons and entangled pairs of photons generated by parametric down-conversion,* Phys. Rev. Lett. **85**, 286–289 (2000).

[47] S. Franke-Arnold, S. M. Barnett, M. J. Padgett, and L. Allen, *Two-photon entanglement of orbital angular momentum states,* Phys. Rev. A **65**, 033823 (2002).

[48] S. P. Walborn, A. N. de Oliveira, R. S. Thebaldi, and C. H. Monken, *Entanglement and conservation of orbital angular momentum in spontaneous parametric down-conversion,* Phys. Rev. A **69**, 023811 (2004).

[49] A. Mair, A. Vaziri, G. Weihs, and A. Zeilinger, *Entanglement of the orbital angular momentum states of photons,* Nature **412**, 313–316 (2001).

[50] A. Vaziri, J.-W. Pan, T. Jennewein, G. Weihs, and A. Zeilinger, *Concentration of higher dimensional entanglement: Qutrits of photon orbital angular momentum,* Phys. Rev. Lett. **91**, 227902 (2003).

[51] A. Aiello, S. S. R. Oemrawsingh, E. R. Eliel, and J. P. Woerdman, *Nonlocality of high-dimensional two-photon orbital angular momentum states,* Phys. Rev. A **72**, 052114 (2005).

[52] A. Vaziri, G. Weihs, and A. Zeilinger, *Experimental two-photon, three-dimensional entanglement for quantum communication,* Phys. Rev. Lett. **89**, 240401 (2002).

[53] J. P. Torres, Y. Deyanova, L. Torner, and G. Molina-Terriza, *Preparation of engineered two-photon entangled states for multidimensional quantum information,* Phys. Rev. A **67**, 052313 (2003).

[54] A. C. Dada, J. Leach, G. S. Buller, M. J. Padgett, and E. Andersson, *Experimental high-dimensional two-photon entanglement and violations of generalized bell inequalities,* Nat. Phys. **7**, 677–680 (2011).

[55] M. Malik, M. Erhard, M. Huber, M. Krenn, R. Fickler, and A. Zeilinger, *Multi-photon entanglement in high dimensions,* Nat. Photon. **10**, 248–252 (2016).

[56] M. Mafu, A. Dudley, S. Goyal, D. Giovannini, M. McLaren, M. J. Padgett, T. Konrad, F. Petruccione, N. Lütkenhaus, and A. Forbes, *Higher-dimensional orbital-angular-momentum-based quantum key distribution with mutually unbiased bases,* Phys. Rev. A **88**, 032305 (2013).

[57] X.-L. Wang, X.-D. Cai, Z.-E. Su, M.-C. Chen, D. Wu, L. Li, N.-L. Liu, C.-Y. Lu, and J.-W. Pan, *Quantum teleportation of multiple degrees of freedom of a single photon,* Nature **518**, 516–519 (2015).

[58] J. T. Barreiro, N. K. Langford, N. A. Peters, and P. G. Kwiat, *Generation of hyper-entangled photon pairs,* Phys. Rev. Lett. **95**, 260501 (2005).

[59] J. T. Barreiro, T.-C. Wei, and P. G. Kwiat, *Beating the channel capacity limit for linear photonic superdense coding,* Nat. Phys. **4**, 282–286 (2008).

[60] S. P. Walborn, *Hyperentanglement: Breaking the communication barrier,* Nat. Phys. **4**, 268–269 (2008).

[61] J. T. Barreiro, T.-C. Wei, and P. G. Kwiat, *Remote preparation of single-photon "hybrid" entangled and vector-polarization states,* Phys. Rev. Lett. **105**, 030407 (2010).

[62] C. Vitelli, N. Spagnolo, L. Aparo, F. Sciarrino, E. Santamato, and L. Marrucci, *Joining the quantum state of two photons into one,* Nat. Photon. **7**, 521–526 (2013).

[63] M. M. Wilde and D. B. Uskov, *Linear-optical hyperentanglement-assisted quantum error-correcting code,* Phys. Rev. A **79**, 022305 (2009).

[64] E. Nagali and F. Sciarrino, *Generation of hybrid polarization-orbital angular momentum entangled states,* Opt. Express **18**, 18243–18248 (2010).

[65] L. Neves, G. Lima, A. Delgado, and C. Saavedra, *Hybrid photonic entanglement: Realization, characterization, and applications,* Phys. Rev. A **80**, 042322 (2009).

[66] S. P. Walborn, S. Pádua, and C. H. Monken, *Hyperentanglement-assisted bell-state analysis,* Phys. Rev. A **68**, 042313 (2003).

[67] W. A. T. Nogueira, M. Santibañez, S. Pádua, A. Delgado, C. Saavedra, L. Neves, and G. Lima, *Interference and complementarity for two-photon hybrid entangled states,* Phys. Rev. A **82**, 042104 (2010).

[68] R. Fickler, M. Krenn, R. Lapkiewicz, S. Ramelow, and A. Zeilinger, *Real-time imaging of quantum entanglement,* Sci. Rep. **3** (2013).

[69] X.-s. Ma, A. Qarry, J. Kofler, T. Jennewein, and A. Zeilinger, *Experimental violation of a bell inequality with two different degrees of freedom of entangled particle pairs,* Phys. Rev. A **79**, 042101 (2009).

[70] P. Zhang, Y. Jiang, R.-F. Liu, H. Gao, H.-R. Li, and F.-L. Li, *Implementing the deutsch's algorithm with spin-orbital angular momentum of photon without interferometer,* Opt. Commun. **285**, 838 – 841 (2012).

[71] C. Zhang, B. Guo, G. Cheng, J. Guo, and R. Fan, *Spin-orbit hybrid entanglement quantum key distribution scheme,* Sci. China. Phys. Mech. Astron. **57**, 2043–2048 (2014).

[72] S. C. Tidwell, G. H. Kim, and W. D. Kimura, *Efficient radially polarized laser beam generation with a double interferometer,* Appl. Opt. **32**, 5222–5229 (1993).

[73] R. J. C. Spreeuw, *A classical analogy of entanglement,* Found. Phys. **28**, 361–374 (1998).

[74] B. N. Simon, S. Simon, F. Gori, M. Santarsiero, R. Borghi, N. Mukunda, and R. Simon, *Nonquantum entanglement resolves a basic issue in polarization optics,* Phys. Rev. Lett. **104**, 023901 (2010).

[75] P. Ghose and A. Mukherjee, *Entanglement in classical optics,* Rev. Theor. Sci. **2**, 274–288 (2014).

[76] A. Luis, *Coherence, polarization, and entanglement for classical light fields,* Opt. Commun. **282**, 3665 – 3670 (2009).

[77] A. Aiello, F. Töppel, C. Marquardt, E. Giacobino, and G. Leuchs, *Quantumlike non-separable structures in optical beams,* New J. Phys. **17**, 043024 (2015).

[78] D. Collins and S. Popescu, *Classical analog of entanglement,* Phys. Rev. A **65**, 032321 (2002).

[79] R. J. C. Spreeuw, *Classical wave-optics analogy of quantum-information processing,* Phys. Rev. A **63**, 062302 (2001).

[80] S. J. van Enk, *Entanglement of electromagnetic fields,* Phys. Rev. A **67**, 022303 (2003).

[81] A. Luis, *Coherence, polarization, and entanglement for classical light fields,* Opt. Commun. **282**, 3665 – 3670 (2009).

[82] K. F. Lee and J. E. Thomas, *Entanglement with classical fields,* Phys. Rev. A **69**, 052311 (2004).

[83] E. Karimi and R. W. Boyd, *Classical entanglement?* Science **350**, 1172–1173 (2015).

[84] L. J. Pereira, A. Z. Khoury, and K. Dechoum, *Quantum and classical separability of spin-orbit laser modes,* Phys. Rev. A **90**, 053842 (2014).

[85] C. V. S. Borges, M. Hor-Meyll, J. A. O. Huguenin, and A. Z. Khoury, *Bell-like inequality for the spin-orbit separability of a laser beam,* Phys. Rev. A **82**, 033833 (2010).

[86] E. Karimi, J. Leach, S. Slussarenko, B. Piccirillo, L. Marrucci, L. Chen, W. She, S. Franke-Arnold, M. J. Padgett, and E. Santamato, *Spin-orbit hybrid entanglement of photons and quantum contextuality,* Phys. Rev. A **82**, 022115 (2010).

[87] M. A. Goldin, D. Francisco, and S. Ledesma, *Simulating bell inequality violations with classical optics encoded qubits,* J. Opt. Soc. Am. B **27**, 779–786 (2010).

[88] M. McLaren, T. Konrad, and A. Forbes, *Measuring the nonseparability of vector vortex beams,* Phys. Rev. A **92**, 023833 (2015).

[89] D. Francisco and S. Ledesma, *Classical optics analogy of quantum teleportation,* J. Opt. Soc. Am. B **25**, 383–390 (2008).

[90] S. M. Hashemi Rafsanjani, M. Mirhosseini, O. S. Magaña Loaiza, and R. W. Boyd, *State transfer based on classical nonseparability,* Phys. Rev. A **92**, 023827 (2015).

[91] D. Francisco, C. Iemmi, J. P. Paz, and S. Ledesma, *Simulating a quantum walk with classical optics,* Phys. Rev. A **74**, 052327 (2006).

[92] N. Bhattacharya, H. B. van Linden van den Heuvell, and R. J. C. Spreeuw, *Implementation of quantum search algorithm using classical fourier optics,* Phys. Rev. Lett. **88**, 137901 (2002).

[93] X. Song, Y. Sun, P. Li, H. Qin, and X. Zhang, *Bell's measure and implementing quantum fourier transform with orbital angular momentum of classical light,* Sci. Rep. **5**, 14113 (2015).

[94] K. H. Kagalwala, G. Di Giuseppe, A. F. Abouraddy, and B. E. Saleh, *Bell's measure in classical optical coherence,* Nat. Photon. **7**, 72–78 (2013).

[95] F. Töppel, A. Aiello, C. Marquardt, E. Giacobino, and G. Leuchs, *Classical entanglement in polarization metrology,* New J. Phys. **16**, 073019 (2014).

[96] G. Milione, T. A. Nguyen, J. Leach, D. A. Nolan, and R. R. Alfano, *Using the nonseparability of vector beams to encode information for optical communication,* Opt. Lett. **40**, 4887–4890 (2015).

[97] G. Vallone, V. D'Ambrosio, A. Sponselli, S. Slussarenko, L. Marrucci, F. Sciarrino, and P. Villoresi, *Free-space quantum key distribution by rotation-invariant twisted photons,* Phys. Rev. Lett. **113**, 060503 (2014).

[98] S. Berg-Johansen, F. Töppel, B. Stiller, P. Banzer, M. Ornigotti, E. Giacobino, G. Leuchs, A. Aiello, and C. Marquardt, *Classically entangled optical beams for high-speed kinematic sensing,* Optica **2**, 864–868 (2015).

[99] V. D'Ambrosio, N. Spagnolo, L. D. Re, S. Slussarenko, Y. Li, L. C. Kwek, L. Marrucci, S. P. Walborn, L. Aolita, and F. Sciarrino, *Photonic polarization gears for ultra-sensitive angular measurements,* Nat. Commun. **4**, 022115 (2013).

[100] M. J. Padgett and J. Courtial, *Poincaré-sphere equivalent for light beams containing orbital angular momentum,* Opt. Lett. **24**, 430–432 (1999).

[101] Q. Zhan, *Cylindrical vector beams: from mathematical concepts to applications,* Adv. Opt. Photon. **1**, 1–57 (2009).

[102] S. M. Hashemi Rafsanjani, M. Mirhosseini, O. S. Magaña Loaiza, and R. W. Boyd, *State transfer based on classical nonseparability,* Phys. Rev. A **92**, 023827 (2015).

[103] B. Perez-Garcia, M. McLaren, S. K. Goyal, R. I. Hernandez-Aranda, A. Forbes, and T. Konrad, *Quantum computation with classical light: Implementation of the deutschjozsa algorithm,* Phys. Lett. A **380**, 1925 – 1931 (2016).

[104] S. K. Goyal, F. S. Roux, A. Forbes, and T. Konrad, *Implementing quantum walks using orbital angular momentum of classical light,* Phys. Rev. Lett. **110**, 263602 (2013).

[105] P. Chowdhury, A. S. Majumdar, and G. S. Agarwal, *Nonlocal continuous-variable correlations and violation of bell's inequality for light beams with topological singularities,* Phys. Rev. A **88**, 013830 (2013).

[106] S. Prabhakar, S. G. Reddy, A. Aadhi, C. Perumangatt, G. K. Samanta, and R. P. Singh, *Violation of bell's inequality for phase-singular beams,* Phys. Rev. A **92**, 023822 (2015).

[107] S. Pancharatnam, *Generalized theory of interference and its applications,* in "Proc. Indian Acad. Sci. Sect. A," , vol. 44 (Springer, 1956), vol. 44, p. 247.

[108] M. V. Berry, *Quantal phase factors accompanying adiabatic changes,* in "Proc. R. Soc. London, Ser. A," , vol. 392 (The Royal Society, 1984), vol. 392, p. 45.

[109] C. E. R. Souza, J. A. O. Huguenin, P. Milman, and A. Z. Khoury, *Topological phase for spin-orbit transformations on a laser beam,* Phys. Rev. Lett. **99**, 160401 (2007).

[110] J. C. Loredo, M. A. Broome, D. H. Smith, and A. G. White, *Observation of entanglement-dependent two-particle holonomic phase,* Phys. Rev. Lett. **112**, 143603 (2014).

[111] R. A. Bertlmann, K. Durstberger, Y. Hasegawa, and B. C. Hiesmayr, *Berry phase in entangled systems: A proposed experiment with single neutrons,* Phys. Rev. A **69**, 032112 (2004).

[112] S. Sponar, J. Klepp, R. Loidl, S. Filipp, K. Durstberger-Rennhofer, R. A. Bertlmann, G. Badurek, H. Rauch, and Y. Hasegawa, *Geometric phase in entangled systems: A single-neutron interferometer experiment,* Phys. Rev. A **81**, 042113 (2010).

[113] G. S. Agarwal, *Su(2) structure of the poincaré sphere for light beams with orbital angular momentum,* J. Opt. Soc. Am. A **16**, 2914–2916 (1999).

[114] S. Slussarenko, V. D'Ambrosio, B. Piccirillo, L. Marrucci, and E. Santamato, *The polarizing sagnac interferometer: a tool for light orbital angular momentum sorting and spin-orbit photon processing,* Opt. Express **18**, 27205–27216 (2010).

[115] R. Simon and N. Mukunda, *Minimal three-component su(2) gadget for polarization optics,* Phys. Lett. A **143**, 165 – 169 (1990).

[116] S. G. Reddy, S. Prabhakar, A. Aadhi, A. Kumar, M. Shah, R. P. Singh, and R. Simon, *Measuring the mueller matrix of an arbitrary optical element with a universal su(2) polarization gadget,* J. Opt. Soc. Am. A **31**, 610–615 (2014).

[117] K. T. Kapale and J. P. Dowling, *Vortex phase qubit: Generating arbitrary, counterrotating, coherent superpositions in bose-einstein condensates via optical angular momentum beams,* Phys. Rev. Lett. **95**, 173601 (2005).

[118] D. Goldstein and D. H. Goldstein, *Polarized Light, Revised and Expanded*, vol. 83 (CRC Press, 2003).

[119] R. Fickler, R. Lapkiewicz, W. N. Plick, M. Krenn, C. Schaeff, S. Ramelow, and A. Zeilinger, *Quantum entanglement of high angular momenta,* Science **338**, 640–643 (2012).

[120] A. Kumar, J. Banerji, and R. Singh, *Intensity correlation properties of high-order optical vortices passing through a rotating ground-glass plate,* Opt. Lett. **35**, 3841–3843 (2010).

[121] A. Kumar, J. Banerji, and R. P. Singh, *Hanbury brown–twiss-type experiments with optical vortices and observation of modulated intensity correlation on scattering from rotating ground glass,* Phys. Rev. A **86**, 013825 (2012).

[122] A. Kumar and R. Singh, *Experimental and theoretical investigation of loss of coherence on scattering of a beam with helical wavefront,* Opt. Commun. **284**, 1510 – 1516 (2011).

[123] S. G. Reddy, S. Prabhakar, A. Kumar, J. Banerji, and R. P. Singh, *Higher order optical vortices and formation of speckles,* Opt. Lett. **39**, 4364–4367 (2014).

[124] M. P. Lavery, F. C. Speirits, S. M. Barnett, and M. J. Padgett, *Detection of a spinning object using lights orbital angular momentum,* Science **341**, 537–540 (2013).

[125] S. G. Reddy, A. Kumar, S. Prabhakar, and R. Singh, *Experimental generation of ring-shaped beams with random sources,* Opt. Lett. **38**, 4441–4444 (2013).

[126] L. Marrucci, C. Manzo, and D. Paparo, *Optical spin-to-orbital angular momentum conversion in inhomogeneous anisotropic media,* Phys. Rev. Lett. **96**, 163905 (2006).

[127] E. Karimi, S. Slussarenko, B. Piccirillo, L. Marrucci, and E. Santamato, *Polarization-controlled evolution of light transverse modes and associated pancharatnam geometric phase in orbital angular momentum,* Phys. Rev. A **81**, 053813 (2010).

[128] O. Gamel and D. F. V. James, *Measures of quantum state purity and classical degree of polarization,* Phys. Rev. A **86**, 033830 (2012).

[129] F. De Zela, *Relationship between the degree of polarization, indistinguishability, and entanglement,* Phys. Rev. A **89**, 013845 (2014).

[130] X.-F. Qian and J. H. Eberly, *Entanglement and classical polarization states,* Opt. Lett. **36**, 4110–4112 (2011).

[131] N. A. Peters, T.-C. Wei, and P. G. Kwiat, *Mixed-state sensitivity of several quantum-information benchmarks,* Phys. Rev. A **70**, 052309 (2004).

[132] Y. Yang, M. Mazilu, and K. Dholakia, *Measuring the orbital angular momentum of partially coherent optical vortices through singularities in their cross-spectral density functions,* Opt. Lett. **37**, 4949–4951 (2012).

[133] P. Ding and H. Ren, *Propagation law of partially coherent vortex beam,* Opt. Eng. **51**, 018002–1–018002–6 (2012).

[134] L. Rao and J. Pu, *Spatial correlation properties of focused partially coherent vortex beams,* J. Opt. Soc. Am. A **24**, 2242–2247 (2007).

[135] J. C. Garcia-Escartin and P. Chamorro-Posada, *Quantum computer networks with the orbital angular momentum of light,* Phys. Rev. A **86**, 032334 (2012).

[136] S. Ghosh, G. Kar, A. Roy, A. Sen(De), and U. Sen, *Distinguishability of bell states,* Phys. Rev. Lett. **87**, 277902 (2001).

[137] C. Perumangatt, A. Abdul Rahim, G. R. Salla, S. Prabhakar, G. K. Samanta, G. Paul, and R. P. Singh, *Three-particle hyper-entanglement: teleportation and quantum key distribution,* Quantum Inf. Process. **14**, 3813–3826 (2015).

[138] C. Perumangatt, G. R. Salla, A. Anwar, A. Aadhi, S. Prabhakar, and R. Singh, *Scattering of non-separable states of light,* Opt. Commun. **355**, 301 – 305 (2015).

[139] M. Riebe, H. Häffner, C. Roos, W. Hänsel, J. Benhelm, G. Lancaster, T. Körber, C. Becher, F. Schmidt-Kaler, D. James *et al.*, *Deterministic quantum teleportation with atoms,* Nature **429**, 734–737 (2004).

[140] Y.-H. Kim, S. P. Kulik, and Y. Shih, *Quantum teleportation of a polarization state with a complete bell state measurement,* Phys. Rev. Lett. **86**, 1370–1373 (2001).

[141] T.-C. Wei, J. T. Barreiro, and P. G. Kwiat, *Hyperentangled bell-state analysis,* Phys. Rev. A **75**, 060305 (2007).

[142] Y.-B. Sheng, F.-G. Deng, and G. L. Long, *Complete hyperentangled-bell-state analysis for quantum communication,* Phys. Rev. A **82**, 032318 (2010).

[143] L. Aolita and S. P. Walborn, *Quantum communication without alignment using multiple-qubit single-photon states,* Phys. Rev. Lett. **98**, 100501 (2007).

[144] C. E. R. Souza, C. V. S. Borges, A. Z. Khoury, J. A. O. Huguenin, L. Aolita, and S. P. Walborn, *Quantum key distribution without a shared reference frame,* Phys. Rev. A **77**, 032345 (2008).

[145] B. C. dos Santos, K. Dechoum, and A. Z. Khoury, *Continuous-variable hyperentanglement in a parametric oscillator with orbital angular momentum,* Phys. Rev. Lett. **103**, 230503 (2009).

[146] L. Chen and W. She, *Single-photon spin-orbit entanglement violating a bell-like inequality,* J. Opt. Soc. Am. B **27**, A7–A10 (2010).

[147] A. Z. Khoury and P. Milman, *Quantum teleportation in the spin-orbit variables of photon pairs,* Phys. Rev. A **83**, 060301 (2011).

[148] J. Leach, M. J. Padgett, S. M. Barnett, S. Franke-Arnold, and J. Courtial, *Measuring the orbital angular momentum of a single photon,* Phys. Rev. Lett. **88**, 257901 (2002).

[149] A. K. Pati and P. Agrawal, *Probabilistic teleportation of a qudit,* Phys. Lett. A **371**, 185–189 (2007).

[150] S. K. Goyal, P. E. Boukama-Dzoussi, S. Ghosh, F. S. Roux, and T. Konrad, *Qudit-teleportation for photons with linear optics,* Sci. Rep. **4** (2014).

[151] S. K. Goyal and T. Konrad, *Teleporting photonic qudits using multimode quantum scissors,* Sci. Rep. **3** (2013).

[152] S. A. Babichev, J. Ries, and A. I. Lvovsky, *Quantum scissors: Teleportation of single-mode optical states by means of a nonlocal single photon,* Europhys. Lett **64**, 1 (2003).

[153] D. Bouwmeester and A. Zeilinger, *The physics of quantum information: basic concepts,* in "The physics of quantum information," (Springer, 2000), pp. 1–14.

[154] R. Ursin, F. Tiefenbacher, T. Schmitt-Manderbach, H. Weier, T. Scheidl, M. Lindenthal, B. Blauensteiner, T. Jennewein, J. Perdigues, P. Trojek *et al.*, *Entanglement-based quantum communication over 144 km,* Nat. Phys. **3**, 481–486 (2007).

[155] N. Gisin, G. Ribordy, W. Tittel, and H. Zbinden, *Quantum cryptography,* Rev. Mod. Phys. **74**, 145–195 (2002).

[156] D. S. Naik, C. G. Peterson, A. G. White, A. J. Berglund, and P. G. Kwiat, *Entangled state quantum cryptography: Eavesdropping on the ekert protocol,* Phys. Rev. Lett. **84**, 4733–4736 (2000).

[157] V. D'Ambrosio, E. Nagali, S. P. Walborn, L. Aolita, S. Slussarenko, L. Marrucci, and F. Sciarrino, *Complete experimental toolbox for alignment-free quantum communication,* Nat. Commun. **3**, 961 (2012).

[158] S. Grblacher, T. Jennewein, A. Vaziri, G. Weihs, and A. Zeilinger, *Experimental quantum cryptography with qutrits,* New J. Phys. **8**, 75 (2006).

[159] D. Collins, N. Gisin, N. Linden, S. Massar, and S. Popescu, *Bell inequalities for arbitrarily high-dimensional systems,* Phys. Rev. Lett. **88**, 040404 (2002).

LIST OF PUBLICATIONS

Publications contributing to this thesis :

1. *Scattering of non-separable states of light*,
   Chithrabhanu Perumangatt, Salla Gangi Reddy, Ali Anwar, Aadhi A, Shashi Prabhakar, and R P Singh, Optics Communications **355**, 301-305 (2015).

2. *Three particle hyper entanglement: Teleportation and quantum key distribution*,
   Chithrabhanu Perumangatt, A. Aadhi, Salla Gangi Reddy, Shashi Prabhakar, G. K. Samanta, G. Paul, and R P Singh, Quantum Information Processing (2015), **14**, 3813-3826 (2015)

3. *Pancharatnam phase in non-separable states of light*,
   Chithrabhanu Perumangatt, Salla Gangi Reddy, Nijil Lal, Ali Anwar, R P Singh, arXiv:1605.05478 (2016) (Under revision in Journal of Optical Socity of America B).

4. *Quantum Information with Even/Odd States of Orbital Angular Momentum of Light*,
   Chithrabhanu Perumangatt, Salla Gangi Reddy, Nijil Lal, Ali Anwar, R P Singh, arXiv:1607.06422 (2016)

Other publications :

1. *Recovering the vorticity of a light beam after scattering*,
   Salla Gangi Reddy, **Chithrabhanu P**, Shashi Prabhakar, Ali Anwar, and R. P. Singh, Applied Physics Letters, **107**, 021104 (2015).

2. *Divergence of the optical vortex beams*,
   Salla Gangi Reddy, **Chithrabhanu P**, Ali Anwar, Shashi Prabhakar, J. Banerji, and R. P. Singh, Applied optics **54**, 6690-6693(2015).

3. *Non-diffracting speckles of a perfect vortex beam*,
   Salla Gangi Reddy, **Chithrabhanu P**, Aadhi A, Pravin Vaity, Shashi Prabhakar, and R. P. Singh, Journal of Optics **18** (5), 055602 (2016).

4. *Selecting the pre-detection characteristics for effective fiber coupling of entangled photon sources*,
   Ali Anwar, **Chithrabhanu P**, Salla Gangi Reddy, Nijil Lal, R. P. Singh, arXiv:1603.00554 (2016)(Accepted in Optics Communications).

5. *Non-coaxial superposition of vector vortex beams*
A Aadhi, P Vaity, **P Chithrabhanu**, S G Reddy, S Prabakar, R P Singh Applied optics **55** , 1107-1111 (2016).

6. *Spatial distribution of spontaneous parametric down-converted photons for higher order optical vortices*,
Shashi Prabhakar, Salla Gangi Reddy, A. Aadhi, Ashok Kumar, **Chithrabhanu. P**, G. K. Samanta, and R. P. Singh, Optics Communications **326**, 64-69 (2014).

7. *Violation of Bell's inequality for phase singular beams*,
Shashi Prbhakar, Salla Gangi Reddy, A. Aadhi, **Chithrabhanu. P**, and R. P. Singh, Physical Review A **92**, 023822 (2015).

8. *Two component polarization gadget*,
Salla Gangi Reddy, Shashi Prabhakar, **Chithrabhanu. P**, R. P. Singh, and R. Simon, Applied optics **55**, B14-B19 (2016).

Conference papers :

1. **Chithrabhanu P**, Aadhi A, Salla Gangi Reddy, Shashi Prabhakar, G. K. Samanta, and R. P. Singh, *A novel entangled source for higher dimensional quantum teleportation and QKD,* presented at International Conference on Optics and Optoelectronics during March 05-08, 2014 at IRDE Dehradun, India (**Best Paper Award**).

2. **Chithrabhanu. P**, Salla Gangi Reddy, Aadhi A, Shashi Prabhakar, Ali Anwar, and R. P. Singh, *Scattering of non-separable light beams,* presented at National Laser Symposium during December 03-06, 2014 at Sri Venkateswara University, Tirupathi, India.

3. A. Aadhi, **Chithrabhanu. P**, Salla Gangi Reddy, Shashi Prabhakar, Jabir MV, G. K. Samanta, and R. P. Singh, *Measurement of Berry Phase by non-interferometric method,* presented at National Laser Symposium during December 03-06, 2014 at Sri Venkateswara University, Tirupathi, India.

4. Salla Gangi Reddy, **Chithrabhanu. P**, Shashi Prabhakar, Ali Anwar, and R. P. Singh, *Revival of the vorticity in scattered optical vortices,* presented at Photonics 2014 during December 13-16, 2014 at IIT Kharagpur, India.

5. **Chithrabhanu. P**, A. Aadhi, Salla Gangi Reddy, Shashi Prabhakar, Ali Anwar, and R. P. Singh, *Construction of OAM Poincaré sphere with both coherent and partially*

coherent light beams, presented at Photonics 2014 during December 13-16, 2014 at IIT Kharagpur, India.

6. Shashi Prabhakar, Salla Gangi Reddy, **Chithrabhanu. P**, A. Aadhi, G. K. Samanta, and R. P. Singh, *Violation of Bells inequality with phase singular beams,* presented at Photonics 2014 during December 13-16, 2014 at IIT Kharagpur, India.

7. Salla Gangi Reddy, **Chithrabhanu. P**, Shashi Prabhakar, Ali Anwar, and R. P. Singh, *Divergence of the optical vortex beams with measurable parameters,* presented at International Conference on Optics and Photonics (ICOP 2015) during February 20-22, 2015 at Calcutta University, Kolkata, India.

8. **Chithrabhanu. P**, Salla Gangi Reddy, Ali Anwar, Aadhi A, Shashi Prabhakar, and R. P. Singh, *Generalized orbital angular momentum Poincaré sphere,* presented at International Conference on Optics and Photonics (ICOP 2015) during February 20-22, 2015 at Calcutta University, Kolkata, India.

9. Aadhi A, **Chithrabhanu. P**, Salla Gangi Reddy, Apurv Chaitanya, G. K. Samanta, and R. P. Singh, *Superposition of polarization singularity,* presented at International Conference on Optics and Photonics (ICOP 2015) during February 20-22, 2015 at Calcutta University, Kolkata, India.

10. **Chithrabhanu P**, Salla Gangi Reddy, Ali Anwar, Aadhi A, Shashi Prabhakar, and R. P. Singh, *Scattering of light beams with non-separable polarization and orbital angular momentum states,* presented at 3^{rd} International Conference on Optical Angular Momentum (ICOAM 2015) during August 4-7, 2015 at City College of New York, New York, USA.

11. Salla Gangi Reddy, **Chithrabhanu P**, Shashi Prabhakar, J. Banerji, and R. P. Singh, *Correlations in scattered optical vortices,* presented at Correlation Optics 2015, during September 14-18, 2015 at University of Chernivtsi, Chernivtsi, Ukraine (**Invited talk**).

12. **Chithrabhanu P**, Salla Gangi Reddy, Ali Anwar, Aadhi A, and R. P. Singh, *Pancharathnam-Berry phase in entangled systems and violation of Bell inequality* , A meeting on Quantum Information Processing and Applications (QIPA-2015) during December 07-13, 2015 at Harish-Chandra Research Institute (HRI), Allahabad, India.

Optics Communications 355 (2015) 301–305

Contents lists available at ScienceDirect

Optics Communications

journal homepage: www.elsevier.com/locate/optcom

Scattering of non-separable states of light

Chithrabhanu Perumangatt [a,*], Gangi Reddy Salla [a], Ali Anwar [a], A. Aadhi [a,b], Shashi Prabhakar [a,b], R.P. Singh [a]

[a] *Physical Research Laboratory, Navrangpura, Ahmedabad 380009, India*
[b] *IIT Gandhinagar, Chandkheda, Ahmedabad 382424, India*

ARTICLE INFO

Article history:
Received 13 April 2015
Received in revised form
23 June 2015
Accepted 28 June 2015

Keywords:
Non-separability
Orbital angular momentum
Scattering
Linear entropy

ABSTRACT

We experimentally show that the non-separability of polarization and orbital angular momentum present in a light beam remains preserved under scattering through a random medium like rotating ground glass. We verify this by measuring the degree of polarization and observing the intensity distribution of the beam when projected to different polarization states, before as well as after the scattering. We extend our study to the non-maximally non-separable states also.

1. Introduction

A combined system is said to be entangled when its state cannot be expressed as a product of states corresponding to the individual sub systems [1]. The entangled systems have interesting properties such as non-locality and contextuality which make them a great resource for various quantum protocols [2]. One generally uses the entanglement between two spatially separated particles in the same degree of freedom such as spin or polarization. However, one can also have hybrid entanglement in which two degrees of freedom of a single particle or two particles are entangled [3]. This arises due to the non-separability of two degrees of freedom. However, it is not an exclusive property of a quantum system. Similar kind of non-separability can be seen in classical optics, for example radially polarized light beams [4]. This quantum like classical entanglement has been receiving a lot of attention in recent years [5–9]. These non-separable states of light are shown to violate Bell like inequality [10,11]. Furthermore, they find applications in polarization metrology and ultra sensitive angular measurements [12,13].

Recently, it has been shown that phase singular beams or optical vortices also violate Bell's inequality for continuous variables such as position and momentum [14]. These optical vortices carry an orbital angular momentum (OAM) of $\pm l\hbar$ per photon, $\pm l$ being the azimuthal index or order of the vortex [15,16]. This OAM can be used as an additional degree of freedom along with the polarization to form a hybrid entangled state that violates Bell's inequality for discrete variables [11].

Scattering of structured light beams such as optical vortices has been studied for their coherence properties and applications [17–21]. It has been shown that one can generate partially coherent ring shaped beams from the scattering of coherent optical vortices [22]. Here, we generate light beams with non-separable OAM and polarization and verify the preservation of non-separability under scattering through a rotating ground glass (RGG). These non-separable beams can be generated using q-plates [23,24] or interferometers [10,25]. In our set up, we modify a polarizing Sagnac interferometer [25] to generate the non-separable beams by replacing dove prism with a spiral phase plate (SPP). The generated beams scatter through a RGG and the scattered light is collected by a plano-convex lens to measure their polarization and intensity distributions at the focus. We measure the degree of polarization of the beam, as a measure of non-separability [26–28], before and after scattering which should be 0 for a maximally non-separable state and 1 for a completely separable state. We also project the scattered as well as coherent light to different polarizations and record the corresponding intensity distributions which confirm the non-separability. Using the same experimental setup, we vary the degree of non-separability by controlling the intensities in the two arms of the interferometer.

In Section 2 we give a theoretical background to the OAM-polarization non-separable state and describe the methods we used to witness the non-separability. Experimental setup to generate the described states is given in Section 3. The results and discussion are given in Section 4 and finally we conclude in Section 5. For

* Corresponding author.
E-mail address: chithrabhanu@prl.res.in (C. Perumangatt).

http://dx.doi.org/10.1016/j.optcom.2015.06.066
0030-4018/

simplicity, we use the Dirac notation to describe the states even though we are using classical light beams.

2. Theoretical background

A maximally entangled/non-separable state of polarization and OAM can be written as

$$|\psi\rangle = \frac{1}{\sqrt{2}}\Big(|H\rangle|+l\rangle + |V\rangle|-l\rangle\Big) \tag{1}$$

where $|H\rangle, |V\rangle$ and $|+l\rangle, |-l\rangle$ are basis vectors of 2D complex vector spaces corresponding to the polarization and the OAM subspace respectively. We work in the paraxial domain with linear optics, where polarization and OAM are independent. Thus $\{|H\rangle, |V\rangle\}$ and $\{|+l\rangle, |-l\rangle\}$ form two mutually independent complex vector spaces. The density matrix for the non-separable state $|\psi\rangle$ is given by $\rho_{ns} = |\psi\rangle\langle\psi|$. One can obtain the reduced density matrix corresponding to the polarization ρ_p by taking a partial trace of this density matrix over OAM states,

$$\rho_p = \mathrm{Tr}_l\{\rho_{ns}\} = \sum_{i=l,-l}\langle i|\psi\rangle\langle\psi|i\rangle = \frac{I_p}{2}. \tag{2}$$

Here, I_P is a 2×2 identity matrix. For a given density matrix ρ describing a state in d dimensional Hilbert space, one can define linear entropy [29]

$$S_L = \frac{d}{d-1}(1 - \mathrm{Tr}(\rho^2)). \tag{3}$$

S_L characterizes the amount of mixedness for a given density matrix. It is known that for an entangled/non-separable state, the subsystems will be in a mixed state. Stronger the non-separability, larger the amount of mixedness present in the subsystems. Thus by measuring linear entropy S_L of the subsystem, one can measure the degree of entanglement or the non-separability. For the maximally non-separable state given in Eq. (1), one can find the linear entropy of polarization,

$$S_L = 2(1 - \mathrm{Tr}(\rho_p^2)) = 1. \tag{4}$$

This corresponds to a completely mixed polarization state in contrast to a completely polarized state with S_L=0. We know, the state of polarization represented by a Poincare sphere can be completely described by

$$\rho_p = \frac{1}{2}\sum_{i=0}^{3}\sigma_i.\, s_i \tag{5}$$

where σ_i's and s_i's are the Pauli matrices and normalized Stokes parameters respectively. The trace of square of this density matrix is given by

$$\mathrm{Tr}\{\rho_p^2\} = \tfrac{1}{2}\Big(1 + s_1^2 + s_2^2 + s_3^2\Big) = \tfrac{1}{2}(1 + DOP^2) \tag{6}$$

where DOP is the degree of polarization which is measured as the magnitude of the Stokes vector $\sqrt{s_1^2 + s_2^2 + s_3^2}$. Using Eqs. (4) and (6) one can relate DOP to the linear entropy,

$$S_L = 1 - DOP^2. \tag{7}$$

Thus for a maximally non-separable state of polarization and OAM, for which S_L=1, the degree of polarization should be zero. One can easily determine the DOP experimentally by measuring the Stokes parameters [30].

Another characteristic of the non-separable state is the contexuality. For a separable state, measurement on one degree of freedom does not affect the measurement outcome of the other. However, in the case of a non-separable state, measurement outcome in one degree of freedom will depend on the context of measurement in the other. In our experiment the OAM state of the beam varies according to the projections to different polarization states due to their non-separability. Consider a general polarization state defined as

$$|\xi\rangle = \mathrm{Cos}(\theta)|H\rangle + e^{i\phi}\mathrm{Sin}(\theta)|V\rangle \tag{8}$$

where θ and ϕ are the Euler angles corresponding to the state $|\xi\rangle$ on the Poincaré sphere. Projecting $|\psi\rangle$ given in Eq. (1) to $|\xi\rangle$, we obtain the OAM state as

$$|\psi_o\rangle_{\theta,\phi} = \langle\xi|\psi\rangle = \mathrm{Cos}(\theta)|l\rangle + e^{-i\phi}\mathrm{Sin}(\theta)|-l\rangle. \tag{9}$$

This is a pure OAM superposition state. The transverse profile of the beam will correspond to the superposition of two equal and oppositely charged vortices with different relative amplitudes and phase. Therefore, the intensity profile of the beam varies according to the polarization projections defined by θ and ϕ. For demonstration we take $(\theta, \phi) = (0, 0), (90, 0), (45, 0), (-45, 0), (45, 90)$ and $(-45, 90)$ which correspond to $|H\rangle$, $|V\rangle$, $|D\rangle = |H\rangle + |V\rangle$, $|A\rangle = |H\rangle - |V\rangle$, $|R\rangle = |H\rangle + i|V\rangle$ and $|L\rangle = |H\rangle - i|V\rangle$ polarization states.

Fig. 1 shows the theoretical intensity distributions corresponding to different polarization projections for $|l| = 2$. The projection on H (V) polarization gives a vortex of order 2(-2). The projections of the state on diagonal (D), anti-diagonal (A), left circular (L) and right circular (R) give superposition of two vortices that contain $2l$ (in our case $|l| = 2$) number of lobes with different orientations. The number of lobes confirms the order or the azimuthal index of the vortex and the change in their orientation confirms the presence of non-separability in a light beam.

3. Experiment

The experimental set up used to generate the non-separable state and to study its properties is shown in Fig. 2. We have used a diode pumped solid state green laser (Verdi 10) with vertical polarization for our study. The laser beam passes through a half wave plate, whose fast axis is oriented at −22.5° with the horizontal that

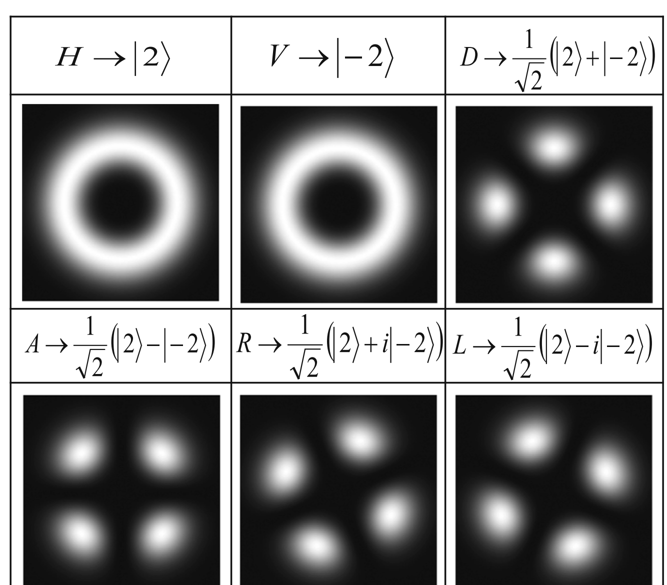

Fig. 1. Theoretical images for the transverse intensity profile of a non-separable state described by Eq. (1) with $|l| = 2$ for projections to different polarization states. H – Horizontal, V – vertical, D – diagonal, A – anit-diagonal, R – right circular, L – Left circular.

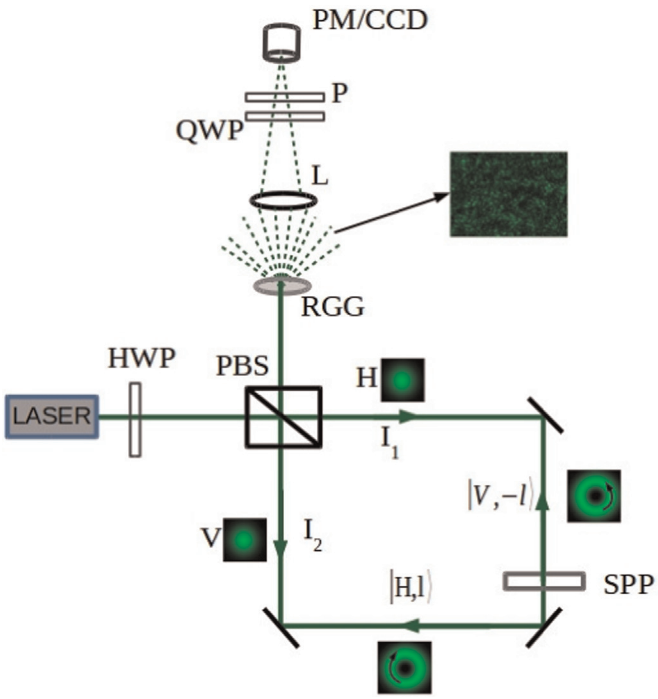

Fig. 2. Experimental setup for the generation and scattering of non-separable state of polarization and OAM. HWP – half wave plate, QWP – quarter wave plate, P – polarizer, *L* – lens with focal length 15 cm, CCD – charge coupled device (camera), PM – power meter, PBS – polarizing beam splitter.

changes beam polarization from vertical to diagonal. Then it passes through a polarizing Sagnac interferometer containing a spiral phase plate (SPP) to generate a light beam which is non-separable in polarization and OAM.

Two orthogonally polarized (H and V) counter propagating Gaussian beams are converted into optical vortices of orders l (for H) and $-l$ (for V) by the SPP designed for order $|l| = 2$. These orthogonally polarized and oppositely charged vortices superpose at the same PBS to form the described non-separable state. This non-separable state is generated only in the presence of SPP otherwise the superposition of two orthogonally polarized Gaussian beams results in a diagonally polarized Gaussian light beam. The doughnut shaped non-separable beam forms a random speckle distribution after scattering through the ground glass. A part of the scattered light collected with a lens of focal length 15 cm placed at a distance of 22 cm from the ground glass plate. The ground glass plate is rotating at ≈ 930 revolutions per minute to average out the speckles. The intensity distributions corresponding to the different polarization projections are recorded with an Evolution VF color cooled camera (pixel size 4.65 μm) kept at the focus of the lens.

The Stokes parameters are measured using a quarter wave plate and a polarizer. We project the beam to horizontal (H), vertical (V), diagonal (D), anti-diagonal (D), right circular (R) and left circular (L) polarizations and measure the intensity. The intensity measurements for determining the Stokes parameters were performed with an optical power meter (Thorlab) of sensitivity 1 nW. One can find out the Stokes parameters as

$$s_1 = \frac{I_H - I_V}{I};\quad s_2 = \frac{I_D - I_A}{I};\quad s_3 = \frac{I_R - I_L}{I} \tag{10}$$

where I is the total intensity of the beam and I_x is the intensity corresponding to x-polarization.

4. Results and discussion

We have measured the Stokes parameters (s_1, s_2, s_3) of coherent and scattered light beams for both separable (without SPP) and non-separable states (with SPP). We compare the degree of polarization of beams before and after scattering and the results are given in Table 1. From the table, it is clear that the separable light beam is completely polarized (diagonal) while the non-separable state is completely unpolarized. The deviations in degree of polarization may be due to uncertainties in the orientation of the wave plates, small misalignment of the interferometer and the measurement uncertainty of the power meter. However, our experimental findings are very close to theoretical predictions given in Section 2.

We also generate non-maximally entangled states simply by controlling intensities in the two arms of the interferometer. This can be done easily by rotating the fast axis of the HWP. Then the state becomes

$$|\psi\rangle = \frac{1}{\sqrt{I_1 + I_2}}\left(\sqrt{I_1}|H\rangle|+2\rangle + \sqrt{I_2}|V\rangle|-2\rangle\right) \tag{11}$$

By varying I_1 from 0 to I and correspondingly I_2 from I to 0, we have generated different states given in Eq. (11). Note that the total intensity, $I_1 + I_2 = I$ is always constant. For the state described in Eq. (11), we can check the mixedness of the subsystem (here polarization) by calculating S_L which also indicates the degree of non-separability. It reduces to a simple analytic expression,

$$S_L = \frac{4I_1I_2}{(I_1 + I_2)^2}. \tag{12}$$

Line curve in Fig. 3 shows the variation of linear entropy S_L of polarization with the normalized intensity in one arm of the interferometer as given in Eq. (12). The linear entropy becomes zero when $I_1 = 0$ or $I_2 = 0$, for which the state become $|H\rangle|l\rangle$ and $|V\rangle|-l\rangle$ respectively. When the two intensities are same ($I_1 = I_2$), the state becomes completely non-separable for which $S_L = 1$.

We measure the Stokes parameters and calculate the degree of polarization and linear entropy experimentally corresponding to each value of I_1 for coherent and scattered light beams. The results are shown in Fig. 3. One can clearly see that the S_L *vs.* normalized intensity curve for both the coherent and scattered light are in good agreement with the theoretical curve. The results of polarization measurements given in Table 1 and Fig. 3 which confirm the preservation of non-separability in polarization and OAM under scattering by the RGG.

Fig. 4 shows the intensity distributions for a coherent and a scattered light beam with non-separable state projected to the different polarizations. Our results show the similar behavior for both coherent and scattered light beams and are in good

Table 1
Stokes vectors and the degree of polarization corresponding to separable and non-separable states of light before and after scattering.

State	Before scattering			After scattering		
	Stokes vectors		DOP	Stoke's vectors		DOP
Separable state (without SPP)	s_1	0.044	0.957	s_1	0.056	0.924
	s_2	0.956		s_2	0.922	
	s_3	−0.02		s_3	−0.026	
Non-separable state (with SPP)	s_1	−0.03	0.001	s_1	0.01	0.001
	s_2	−0.01		s_2	−0.02	
	s_3	0.02		s_3	−0.02	

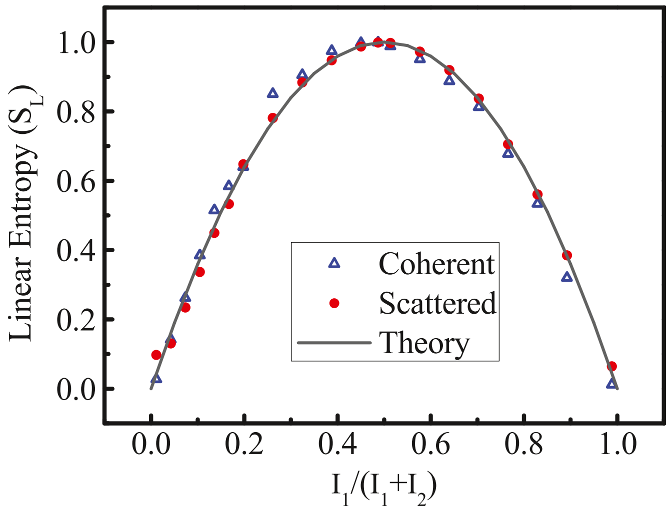

Fig. 3. Linear entropy *vs.* normalized intensity $I_1/(I_1+I_2)$ plot for coherent and scattered non-separable states of light along with theoretical curve given by Eq. (12).

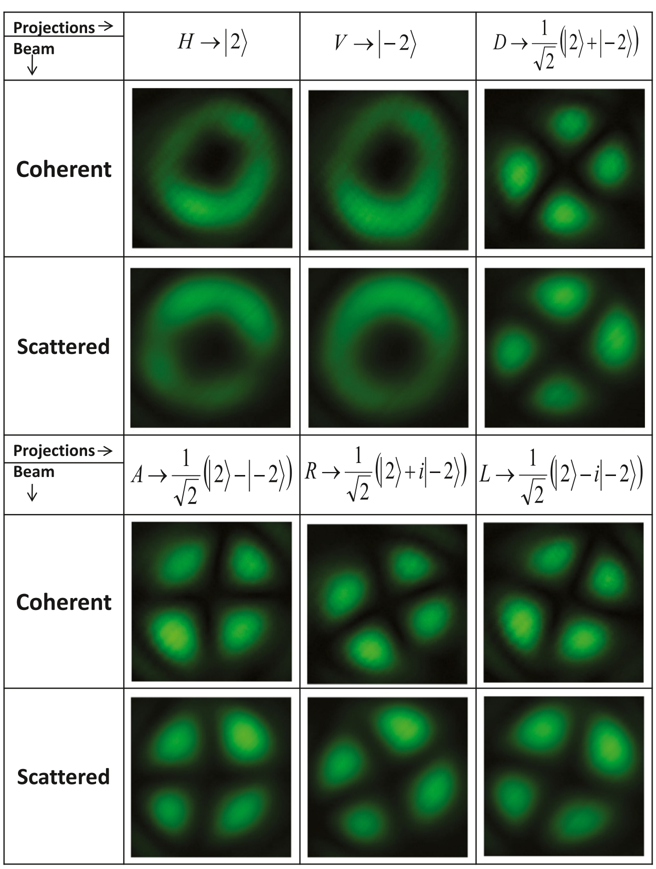

Fig. 4. Experimental images of coherent and scattered non-separable states of light with $l=2$ for different polarization projections. OAM states corresponding to each intensity distribution are also given.

agreement with the theoretical images shown in Fig. 1 that again confirm the preservation of non-separability.

We also observe that the amount of scattered light collected by the lens is irrelevant regarding the non-separable properties. In fact, one can use multiple number of lenses and collimate the scattered light again to form several copies of a partially coherent non-separable beam. This property can be used in public communication systems.

5. Conclusions

In conclusion, we have produced a light beam with non-separable polarization and orbital angular momentum states using a simple interferometer and experimentally verified the preservation of the non-separability under scattering through a rotating ground glass. The polarization measurements and the images of the beam projected to different polarizations show the presence of non-separability for coherent and scattered light. We have also demonstrated the generation of non-maximally non-separable states of light and studied their behavior under scattering by measuring the degree of polarization.

References

[1] R. Horodecki, P. Horodecki, M. Horodecki, K. Horodecki, Quantum entanglement, Rev. Mod. Phys. 81 (2009) 865–942.
[2] D. Bouwmeester, A. Ekert, A. Zeilinger, et al., The Physics of Quantum Information, Springer, Berlin, 2000.
[3] L. Neves, G. Lima, A. Delgado, C. Saavedra, Hybrid photonic entanglement: realization, characterization, and applications, Phys. Rev. A 80 (2009) 042322.
[4] Q. Zhan, Cylindrical vector beams: from mathematical concepts to applications, Adv. Opt. Photon 1 (2009) 1–57.
[5] R.J.C. Spreeuw, A classical analogy of entanglement, Found. Phys. 28 (1998) 361–374.
[6] B.N. Simon, S. Simon, F. Gori, M. Santarsiero, R. Borghi, N. Mukunda, R. Simon, Nonquantum entanglement resolves a basic issue in polarization optics, Phys. Rev. Lett. 104 (2010) 023901.
[7] B.N. Simon, S. Simon, N. Mukunda, F. Gori, M. Santarsiero, R. Borghi, N. Mukunda, R. Simon, A complete characterization of pre-Mueller and Mueller matrices in polarization optics, J. Opt. Soc. Am. A 27 (2010) 188–199.
[8] P. Ghose, A. Mukherjee, Entanglement in classical optics, Rev. Theor. Sci. 2 (2014) 274–288.
[9] A. Luis, Coherence, polarization, and entanglement for classical light fields, Opt. Commun. 282 (2009) 3665–3670.
[10] C.V.S. Borges, M. Hor-Meyll, J.A.O. Huguenin, A.Z. Khoury, Bell-like inequality for the spin–orbit separability of a laser beam, Phys. Rev. A 82 (2010) 33833.
[11] E. Karimi, J. Leach, S. Slussarenko, B. Piccirillo, L. Marrucci, L. Chen, W. She, S. Franke-Arnold, M.J. Padgett, E. Santamato, Spin–orbit hybrid entanglement of photons and quantum contextuality, Phys. Rev. A 82 (2010) 22115.
[12] F. Töppel, A. Aiello, C. Marquardt, E. Giacobino, G. Leuchs, Classical entanglement in polarization metrology, New J. Phys. 16 (2014) 73019.
[13] V. D'Ambrosio, N. Spagnolo, L. Del Re, S. Slussarenko, Y. Li, L.C. Kwek, L. Marrucci, S.P. Walborn, L. Aolita, F. Sciarrino, Photonic polarization gears for ultra-sensitive angular measurements, Nat. Commun. 4 (2013) 2432.
[14] P. Chowdhury, A.S. Majumdar, G.S. Agarwal, Nonlocal continuous-variable correlations and violation of Bell's inequality for light beams with topological singularities, Phys. Rev. A 88 (2013) 13830.
[15] L. Allen, M.W. Beijersbergen, R.J.C. Spreeuw, J.P. Woerdman, Orbital angular momentum of light and the transformation of Laguerre–Gaussian laser modes, Phys. Rev. A 45 (1992) 8185.
[16] J.P. Torres, L. Torner, Twisted Photons: Applications of Light with Orbital Angular Momentum, John Wiley & Sons, New York, 2011.
[17] A. Kumar, J. Banerji, R.P. Singh, Intensity correlation properties of high-order optical vortices passing through a rotating ground-glass plate, Opt. Lett. 35 (2010) 3841–3843.
[18] A. Kumar, J. Banerji, R.P. Singh, Hanbury Brown-Twiss-type experiments with optical vortices and observation of modulated intensity correlation on scattering from rotating ground glass, Phys. Rev. A 86 (2012) 13825.
[19] A. Kumar, R.P. Singh, Experimental and theoretical investigation of loss of coherence on scattering of a beam with helical wavefront, Opt. Commun. 284 (2011) 1510–1516.
[20] S.G. Reddy, S. Prabhakar, A. Kumar, J. Banerji, R.P. Singh, Higher order optical vortices and formation of speckles, Opt. Lett. 39 (2014) 4364–4367.
[21] M.P.J. Lavery, F.C. Speirits, S.M. Barnett, M.J. Padgett, Detection of a spinning object using light's orbital angular momentum, Science 341 (2013) 537–540.
[22] S.G. Reddy, A. Kumar, S. Prabhakar, R.P. Singh, Experimental generation of ring-shaped beams with random sources, Opt. Lett. 38 (2013) 4441–4444.
[23] L. Marrucci, C. Manzo, D. Paparo, Optical spin-to-orbital angular momentum conversion in inhomogeneous anisotropic media, Phys. Rev. Lett. 96 (2006) 163905.
[24] E. Karimi, S. Slussarenko, B. Piccirillo, L. Marrucci, E. Santamato, Polarization-controlled evolution of light transverse modes and associated Pancharatnam geometric phase in orbital angular momentum, Phys. Rev. A 81 (2010) 053813.

[25] S. Slussarenko, V. D'Ambrosio, B. Piccirillo, L. Marrucci, E. Santamato, The polarizing Sagnac interferometer: a tool for light orbital angular momentum sorting and spin–orbit photon processing, Opt. Express 18 (2010) 27205–27216.
[26] O. Gamel, D.F.V. James, Measures of quantum state purity and classical degree of polarization, Phys. Rev. A 86 (2012) 033830.
[27] F. De Zela, Relationship between the degree of polarization, indistinguishability, and entanglement, Phys. Rev. A 89 (2014) 013845.
[28] X.-F. Qian, J.H. Eberly, Entanglement and classical polarization states, Opt. Lett. 36 (2011) 4110–4112.
[29] N.A. Peters, T.-C. Wei, P.G. Kwiat, Mixed-state sensitivity of several quantum-information benchmarks, Phys. Rev. A 70 (2004) 052309.
[30] D. Goldstein, Polarized Light, Marcel Dekker, New York, 2003.

Quantum Inf Process (2015) 14:3813–3826
DOI 10.1007/s11128-015-1056-3

Three-particle hyper-entanglement: teleportation and quantum key distribution

Chithrabhanu Perumangatt[1] · Aadhi Abdul Rahim[1] · Gangi Reddy Salla[1] · Shashi Prabhakar[1] · Goutam Kumar Samanta[1] · Goutam Paul[2] · Ravindra Pratap Singh[1]

Received: 10 March 2015 / Accepted: 23 June 2015 / Published online: 16 July 2015

Abstract We present a scheme to generate three-particle hyper-entanglement utilizing polarization and orbital angular momentum (OAM) of photons. We show that the generated state can be used to teleport a two-qubit state described by the polarization and the OAM. The proposed quantum system has also been used to describe a new efficient quantum key distribution (QKD) protocol. We give a sketch of the experimental arrangement to realize the proposed teleportation and the QKD.

Keywords Teleportation · Spin–orbit Bell states · Orbital angular momentum · Hyper-entanglement · Quantum key distribution

1 Introduction

With entanglement between two quantum bits, protocols have been demonstrated for teleporting an unknown quantum state [1], super dense coding of information [2] and secure communication [3]. An arbitrary qubit can be teleported from one particle to another with the use of an entangled pair of particles, which had been experimentally verified in different quantum systems [4,5]. However, distinguishing all the four Bell states of the photonic qubits has remained a fundamental difficulty in achieving 100 % teleportation. In the first demonstration of the teleportation with photons [4], only one of the four Bell states was able to distinguish from the others. Thus, the efficiency of teleportation was limited to 25 %. Later on, a complete Bell state measurement was demonstrated with nonlinear interaction of photons[6]. Even though they could

✉ Chithrabhanu Perumangatt
chithrabhanu@prl.res.in

1 Physical Research Laboratory, Navarangpura, Ahmedabad 380009, India

2 Cryptology and Security Research Unit, R. C. Bose Centre for Cryptology and Security, Indian Statistical Institute, Kolkata 700108, India

separate all the four Bell states, the efficiency was reduced because of the nonlinear process involved.

In recent years, complete Bell state analysis has been proposed with the use of hyper-entanglement [7], where the two photons are entangled in an additional degree of freedom (DOF) along with polarization. This method was utilized to increase the channel capacity of super dense coding [8]. This was done by projecting each hyper-entangled photon to four single-particle two-qubit Bell states. Nevertheless, hyper-entanglement-assisted Bell state analysis is not of much use in teleportation since it requires projecting the unknown state and one of the EPR particle state to any of the four Bell states. On the other hand, a hyper-entangled pair of particles can teleport a higher-dimensional quantum state using hyper-entangled Bell state analysis which was described using Kerr nonlinearity [9]. There had been a number of studies which use spin–orbit states of light for quantum information processing [10–14]. Khoury and Milman [15] proposed a spin to orbit teleportation scheme with 100 % efficiency that uses the OAM entanglement between the two photons and a spin–orbit Bell state analysis (SOBA).

In this article, we describe a three-particle entangled state which finds applications in teleporting two qubits simultaneously and implementing an efficient key distribution protocol. In Sect. 2, we give a description of the proposed state. Along with the mathematical form of the state, we give a schematic for the state preparation. The experimental procedure for the generation of the proposed state is given in Sect. 3. The state can be utilized to teleport two qubits using two SOBAs and 16 unitary transformations as given in Sect. 4. Experimental schemes for realizing the C_{NOT} gates and SOBA have also been given in Sect. 4.1. In Sect. 5, we describe a new QKD protocol using the new state, which is more efficient than the traditional Ekert protocol. Finally, we conclude in Sect. 6.

2 Description of the proposed state

We describe a system of particles in such a way that one particle is entangled to all other particles in different degrees of freedom. Let us consider a system consisting of three photons where photon **2** is entangled with photons **1** and **3** in different degrees of freedom, namely OAM and polarization, respectively. The polarization state of the photon **1** and the OAM state of the photon **3** are arbitrary or unknown.

Since the OAM of a photon is expressed in infinite-dimensional Hilbert space, one can have higher-dimensional entangled states. We take an arbitrary two-dimensional subspace of the infinite-dimensional OAM basis as $\{|l\rangle, |l'\rangle\}$.

The described state can be prepared using a pair of Hadamard and C_{NOT} gates in different DOFs which correspond to the polarization and the OAM.

The initial states of three particles can be written as

$$|1\rangle = |\xi_{\mathrm{p}}\rangle_1 |l\rangle_1; \quad |2\rangle = |H\rangle_2 |l\rangle_2; \quad |3\rangle = |H\rangle_3 |\chi_o\rangle_3, \tag{1}$$

where $|\xi_{\mathrm{p}}\rangle$ is the unknown state of polarization of the photon **1**, $|\chi_o\rangle$ is the unknown OAM state of the photon **3**, $|H\rangle$ represents horizontal, and $|V\rangle$ represents vertical

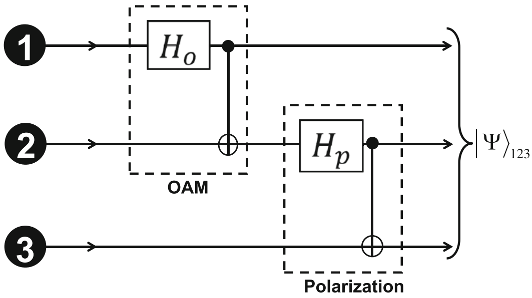

Fig. 1 Schematic diagram for preparation of the initial state. *Box* named "OAM" contains a Hadamard gate (H_O) and a C_{NOT} gate acting on OAM basis, and "polarization" *box* contains a Hadamard (H_O) and C_{NOT} gates acting on polarization basis

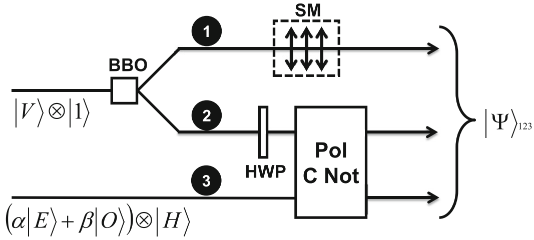

Fig. 2 Schematic experimental set up for the state preparation. *SM* Simon–Mukunda gadget, *HWP* half-wave plate, *BBO* second-order nonlinear crystal (Beta Barium Borate)

polarization states of a photon. The schematic diagram for preparation of the initial state is given in Fig. 1. To entangle photons **1** and **2** in OAM, a Hadamard gate (H_o) on photon **1** and subsequent C_{NOT} gate on photon **1** and **2** are applied. Both gates act in the OAM degree of freedom. Similarly, another Hadamard (H_o) acting on photon **2** and a C_{NOT} between photons **2** and **3** entangle them in polarization. Here, both the gates are acting on the polarization states of photons. After performing the gate operations mentioned above, the final state becomes,

$$|\Psi\rangle_{123} = |\xi_\mathrm{p}\rangle_1 \otimes (|l, l'\rangle_{12} + |l', l\rangle_{12}) \otimes (|HV\rangle_{23} + |VH\rangle_{23})|\chi_o\rangle_3. \tag{2}$$

3 Experimental scheme for state preparation

We are proposing a method in which initially two photons are entangled in the OAM and third photon is in a pure state of OAM and polarization. By polarization gate operations on one of the entangled photons and the independent photon, one can arrive at the described state. Experimental scheme for the generation of the state is given in Fig. 2.

To generate the described state, we start with a Type I spontaneous parametric down conversion (SPDC) of light in a second-order nonlinear crystal that gives a pair of photons entangled in the OAM [16]. A vertically polarized optical vortex beam of azimuthal index 1 has been considered as the pump. The state corresponding to the pair of photons produced by the SPDC of this beam is given by

$$|\Psi\rangle_{12} = \sum_{m=-\infty}^{+\infty} c_m |m\rangle_1 |1-m\rangle_2 \otimes |H\rangle_1 |H\rangle_2 \tag{3}$$

Note that the experimental realization of the quantum gates in the OAM basis $\{|0\rangle, \pm|1\rangle \pm |2\rangle ...\}$ are not straightforward. Moreover, in the teleportation, it is easier to project the state of a photon to one of its four spin–orbit Bell state if we use even/odd basis. Thus for the ease of experimental realization, we reduce the infinite-dimensional entangled state to a simple two-qubit entangled state by grouping all the even and the odd OAM states and rewrite the expression for the OAM state in Eq. (3) as

$$\sum_{m=-\infty}^{+\infty} c_m(|m\rangle_1|1-m\rangle_2) = \sum_{k=-\infty}^{+\infty} c_{2k}(|2k\rangle_1|1-2k\rangle_2) + \sum_{k=-\infty}^{+\infty} c_{2k+1}(|2k+1\rangle_1|-2k\rangle_2).$$

We define a transformation from the general OAM space to the even/odd OAM space as

$$\begin{aligned} g(|u\rangle_1|v\rangle_2) &= f(|u\rangle_1)f(|v\rangle_2), \text{ where} \\ f(|x\rangle) &= \begin{cases} |E\rangle, & \text{for even } x; \\ |O\rangle, & \text{for odd } x. \end{cases} \end{aligned} \tag{4}$$

Applying g on the left-hand side of Eq. (4) yields $\frac{1}{\sqrt{2}}(|E\rangle_1|O\rangle_2 + |O\rangle_1|E\rangle_2)$.

From the conservation of OAM, we have $\sum_{k=-\infty}^{+\infty}(c_{2k})^2 = \sum_{k=-\infty}^{+\infty}(c_{2k+1})^2 = \frac{1}{2}\sum_{m=-\infty}^{+\infty}(c_m)^2 = \frac{1}{2}$.

Thus, we can rewrite Eq. (3) as

$$|\Psi\rangle_{12} = \frac{1}{\sqrt{2}}(|E\rangle_1|O\rangle_2 + |O\rangle_1|E\rangle_2) \otimes |H\rangle_1|H\rangle_2. \tag{5}$$

Note that the photons are entangled in the even/odd OAM states. Experimentally, this transformation can be implemented by post-selection in the even/odd OAM basis. All the OAM operations or measurements must be performed in even/odd basis using OAM sorter [17]. This maps the general OAM state to even/odd basis which is mathematically represented by operator g. Let the photon **1** pass through a Simon–Mukunda polarization gadget which can convert its polarization to any arbitrary state [18,19] and the photon **2** pass through a half-wave plate at $\frac{\pi}{8}$. Thus, polarization state of the photon **1** is encoded as the unknown state $a|H\rangle_1 + b|V\rangle_1$, and the state of the photon **2** is encoded as $\frac{1}{\sqrt{2}}(|H\rangle_2 + |V\rangle_2)$. Action of HWP on the photon **2** is a Hadamard operation. Thus, the state becomes

$$\begin{aligned} |\Psi\rangle_{12} = &\frac{1}{\sqrt{2}}(|E\rangle_1|O\rangle_2 + |O\rangle_1|E\rangle_2)(a|H\rangle_1 + b|V\rangle_1) \\ &\otimes\frac{1}{\sqrt{2}}(|H\rangle_2 + |V\rangle_2). \end{aligned} \tag{6}$$

Now, consider the photon **3** with unknown superposition state of OAM in the even/odd basis and with definite state polarization. Its state can be expressed as,

$$|\Psi\rangle_3 = (\alpha|E\rangle_3 + \beta|O\rangle_3) \otimes |V\rangle_3. \tag{7}$$

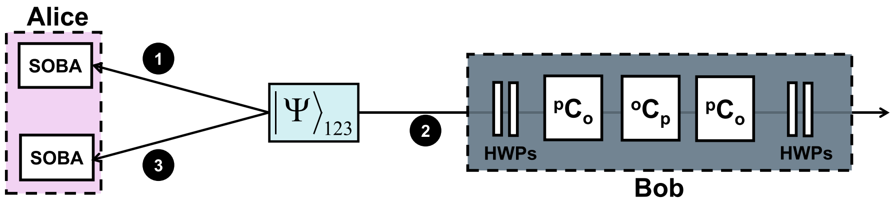

Fig. 3 Schematic for the teleportation of spin–orbit qubits shared by photons **1** and **3**. *HWPs* half-wave plates

A polarization C_{NOT} gate is applied on photon **2** (control) and **3** (target). This operation leads to a polarization entanglement between photons **2** and **3**. Thus, the three-particle state becomes

$$|\Psi\rangle_{123} = \frac{1}{2}\left(a|H\rangle_1 + b|V\rangle_1\right)\left(|E\rangle_1|O\rangle_2 + |O\rangle_1|E\rangle_2\right)\left(|HV\rangle_{23} + |VH\rangle_{23}\right)\left(\alpha|E\rangle_3 + \beta|O\rangle_3\right). \tag{8}$$

This is in the same form as the proposed three-particle entangled state described in Sect. 2, Eq. (2).

4 Simultaneous teleportation of two qubits using the new state

Teleportation of N qubits, in general, needs N pairs of entangled photons. On the other hand, teleportation of d-dimensional quantum state needs d-dimensional entanglement and one has to do a joint measurement in d^2-dimensional Bell basis [20]. However, teleportation schemes were proposed for a d-dimensional OAM state using Bell filter and quantum scissors [21–23].

With the entangled state presented above, we propose an efficient scheme for teleporting a two-qubit state distributed in different DOFs. The schematic diagram is given in Fig. 3. The polarization state of photon **1** and the OAM state of photon **3** form a four-dimensional unknown two-qubit state

$$|\Psi\rangle_u = \left(a|H\rangle_1 + b|V\rangle_1\right) \otimes \left(\alpha|E\rangle_3 + \beta|O\rangle_3\right), \tag{9}$$

which needs to be teleported. We can teleport the combined state to a single particle, photon **2**.

The unknown polarization (spin angular momentum) and the entangled OAM state of photon **1** and entangled polarization and the unknown OAM state of photon **3** in Eq. (8) can be projected to individual spin–orbit Bell states by SOBA. Alice performs the SOBA on the photons **1** and **3** and projects the state of both the particles to the corresponding spin–orbit Bell states. The SOBA, for which the OAM is in the even/odd basis, can be achieved by Mach–Zehnder interferometers involving an OAM sorter and polarizing beam splitters [15].

The states can be defined as

$$\psi^{\pm} = \frac{1}{\sqrt{2}} \left(|H, E\rangle \pm |V, O\rangle\right),$$
$$\phi^{\pm} = \frac{1}{\sqrt{2}} \left(|H, O\rangle \pm |V, E\rangle\right). \tag{10}$$

The SOBA operation for photon **1** can be represented by a polarization-controlled OAM C_{NOT} (${}^{\mathrm{p}}C_{rmo}$) gate and a polarization Hadamard (H_{o}) gate operation with subsequent detection. Similarly, the SOBA for photon **3** is an OAM-controlled polarization C_{NOT} (${}^{\mathrm{o}}C_{\mathrm{p}}$) gate and OAM Hadamard (H_{o}) gate operation with subsequent detection. Experimental schemes for these single-particle two-qubit C_{NOT} gates and SOBA are given in Sect. 4.1.

By substituting the single-particle spin–orbit Bell states into a three-particle wave function in Eq. (8), we get

$$|\Psi\rangle_{123} = \frac{1}{4} \sum_{x,y=0}^{1} \sum_{x',y'=0}^{1} |\Phi^{xy}\rangle_1 |\Phi_q^{x'y'}\rangle_3 \otimes \Gamma_{x,y,x',y'} \left(\alpha|H\rangle_2 + \beta|V\rangle_2\right) \left(a|E\rangle_2 + b|O\rangle_2\right),$$

where $|\Phi^{xy}\rangle_1$ and $|\Phi_q^{x'y'}\rangle_3$ are single-particle spin–orbit Bell states corresponding to the photons **1** & **3**, respectively. $\Gamma_{x,y,x',y'}$ is a transformation matrix for the spin–orbit state of photon **2**. It has been introduced for the compact representation of the 16 states of photon **2** given in Table 1. After the SOBA measurements on the photons **1** and **3**, state of the photon **2** becomes

$$|\Psi(D_{|\Phi^{xy}\rangle_1 |\Phi_q^{x'y'}\rangle_3})\rangle_2 = \frac{1}{4} \Gamma_{x,y,x',y'} \left(\alpha|H\rangle_2 + \beta|V\rangle_2\right) \left(a|E\rangle_2 + b|O\rangle_2\right), \tag{11}$$

the state corresponding to a detection of $|\Phi^{xy}\rangle_1 |\Phi_q^{x'y'}\rangle_3$ in SOBAs.

The states corresponding to all possible SOBA outcomes are given in the first and the second columns of Table 1. Note that the information encoded in the polarization state of the photon **1** is transferred to the OAM state of the photon **2** and the information encoded in the OAM state of the photon **3** is transferred to the polarization state of the photon **2**. So, to get the initial state, Bob has to do a swapping (U_{SWAP}) between the OAM and the polarization along with other unitary transformations which use only polarization operations. These operations can be implemented with the standard wave plates which makes the experimental realization of this method more feasible.

There are 16 possible outcomes for Alice measurements which demand 16 different unitary operations by Bob to complete the teleportation protocol. Alice communicates her measurement outcome ($|\Phi^{xy}\rangle_1 |\Phi_q^{x'y'}\rangle_3$) classically to Bob. Bob does the corresponding unitary transformation $\hat{U}$ (given in the third column of Table 1) on state of photon **2** to get

$$|\Psi\rangle_2 = \left(a|H\rangle_2 + b|V\rangle_2\right) \left(\alpha|E\rangle_2 + \beta|O\rangle_2\right). \tag{12}$$

which completes the teleportation of unknown state given in Eq. (9).

Table 1 Wave function corresponding to Bob's photon and the required unitary transformation corresponding to Alice's measurement outcome

Measurement outcome	State of Bob's photon	Unitary transformations ($\hat{U}$)
$\|\phi^+\phi^+\rangle$	$(\alpha\|V\rangle + \beta\|H\rangle)(a\|O\rangle + b\|E\rangle)$	$\left[I^{\mathrm{o}} \otimes \sigma_1^{\mathrm{p}}\right] * U_{\mathrm{SWAP}} * \left[\sigma_1^{\mathrm{p}} \otimes I^{\mathrm{o}}\right]$
$\|\phi^+\phi^-\rangle$	$(\alpha\|V\rangle - \beta\|H\rangle)(a\|O\rangle + b\|E\rangle)$	$\left[I^{\mathrm{o}} \otimes \sigma_1^{\mathrm{p}}\right] * U_{\mathrm{SWAP}} * \left[i\sigma_2^{\mathrm{p}} \otimes I^{\mathrm{o}}\right]$
$\|\phi^-\phi^+\rangle$	$(\alpha\|V\rangle + \beta\|H\rangle)(a\|O\rangle - b\|E\rangle)$	$\left[I^{\mathrm{o}} \otimes i\sigma_2^{\mathrm{p}}\right] * U_{\mathrm{SWAP}} * \left[\sigma_1^{\mathrm{p}} \otimes I^{\mathrm{o}}\right]$
$\|\phi^-\phi^-\rangle$	$(\alpha\|V\rangle - \beta\|H\rangle)(a\|O\rangle - b\|E\rangle)$	$\left[I^{\mathrm{o}} \otimes i\sigma_2^{\mathrm{p}}\right] * U_{\mathrm{SWAP}} * \left[i\sigma_2^{\mathrm{p}} \otimes I^{\mathrm{o}}\right]$
$\|\psi^+\psi^+\rangle$	$(\alpha\|H\rangle + \beta\|V\rangle)(a\|E\rangle + b\|O\rangle)$	$\left[I^{\mathrm{o}} \otimes I^{\mathrm{p}}\right] * U_{\mathrm{SWAP}} * \left[I^{\mathrm{p}} \otimes I^{\mathrm{o}}\right]$
$\|\psi^+\psi^-\rangle$	$(-\alpha\|H\rangle + \beta\|V\rangle)(a\|E\rangle + b\|O\rangle)$	$\left[I^{\mathrm{o}} \otimes I^{\mathrm{p}}\right] * U_{\mathrm{SWAP}} * \left[\sigma_3^{\mathrm{p}} \otimes I^{\mathrm{o}}\right]$
$\|\psi^-\psi^+\rangle$	$(\alpha\|H\rangle + \beta\|V\rangle)(a\|E\rangle - b\|O\rangle)$	$\left[I^{\mathrm{o}} \otimes \sigma_3^{\mathrm{p}}\right] * U_{\mathrm{SWAP}} * \left[I^{\mathrm{p}} \otimes I^{\mathrm{o}}\right]$
$\|\psi^-\psi^-\rangle$	$(-\alpha\|H\rangle + \beta\|V\rangle)(a\|E\rangle - b\|O\rangle)$	$\left[I^{\mathrm{o}} \otimes \sigma_3^{\mathrm{p}}\right] * U_{\mathrm{SWAP}} * \left[\sigma_3^{\mathrm{p}} \otimes I^{\mathrm{o}}\right]$
$\|\phi^+\psi^+\rangle$	$(\alpha\|H\rangle + \beta\|V\rangle)(a\|O\rangle + b\|E\rangle)$	$\left[I^{\mathrm{o}} \otimes \sigma_1^{\mathrm{p}}\right] * U_{\mathrm{SWAP}} * \left[I^{\mathrm{p}} \otimes I^{\mathrm{o}}\right]$
$\|\phi^+\psi^-\rangle$	$(-\alpha\|H\rangle + \beta\|V\rangle)(a\|O\rangle + b\|E\rangle)$	$\left[I^{\mathrm{o}} \otimes \sigma_1^{\mathrm{p}}\right] * U_{\mathrm{SWAP}} * \left[\sigma_3^{\mathrm{p}} \otimes I^{\mathrm{o}}\right]$
$\|\phi^-\psi^+\rangle$	$(\alpha\|H\rangle + \beta\|V\rangle)(a\|O\rangle - b\|E\rangle)$	$\left[I^{\mathrm{o}} \otimes i\sigma_2^{\mathrm{p}}\right] * U_{\mathrm{SWAP}} * \left[I^{\mathrm{p}} \otimes I^{\mathrm{o}}\right]$
$\|\phi^-\psi^-\rangle$	$(-\alpha\|H\rangle + \beta\|V\rangle)(a\|O\rangle - b\|E\rangle)$	$\left[I^{\mathrm{o}} \otimes i\sigma_2^{\mathrm{p}}\right] * U_{\mathrm{SWAP}} * \left[\sigma_3^{\mathrm{p}} \otimes I^{\mathrm{o}}\right]$
$\|\psi^+\phi^+\rangle$	$(\alpha\|V\rangle + \beta\|H\rangle)(a\|E\rangle + b\|O\rangle)$	$\left[I^{\mathrm{o}} \otimes I^{\mathrm{p}}\right] * U_{\mathrm{SWAP}} * \left[\sigma_1^{\mathrm{p}} \otimes I^{\mathrm{o}}\right]$
$\|\psi^+\phi^-\rangle$	$(\alpha\|V\rangle - \beta\|H\rangle)(a\|E\rangle + b\|O\rangle)$	$\left[I^{\mathrm{o}} \otimes I^{\mathrm{p}}\right] * U_{\mathrm{SWAP}} * \left[i\sigma_2^{\mathrm{p}} \otimes I^{\mathrm{o}}\right]$
$\|\psi^-\phi^+\rangle$	$(\alpha\|V\rangle + \beta\|H\rangle)(a\|E\rangle - b\|O\rangle)$	$\left[I^{\mathrm{o}} \otimes I^{\mathrm{p}}\right] * U_{\mathrm{SWAP}} * \left[i\sigma_2^{\mathrm{p}} \otimes I^{\mathrm{o}}\right]$
$\|\psi^-\phi^-\rangle$	$(\alpha\|V\rangle - \beta\|H\rangle)(a\|E\rangle - b\|O\rangle)$	$\left[I^{\mathrm{o}} \otimes \sigma_3^{\mathrm{p}}\right] * U_{\mathrm{SWAP}} * \left[i\sigma_2^{\mathrm{p}} \otimes I^{\mathrm{o}}\right]$

$\sigma_1^{\mathrm{p}}, \sigma_2^{\mathrm{p}}, \sigma_3^{\mathrm{p}}$ are Pauli matrices for polarization, I^{p} and I^{o} are identity matrices for polarization and OAM

A SWAP operation is equivalent to consecutive ${}^{\mathrm{p}}C_{\mathrm{o}}$, ${}^{\mathrm{o}}C_{\mathrm{p}}$ and ${}^{\mathrm{p}}C_{\mathrm{o}}$ gate operations. Since the operation done in polarization will be transferred to the OAM after the SWAP operation, one can perform all the operations in polarization which are well known. Two half-wave plates before and after the SWAP gate can perform 16 unitary operations which is required for the teleportation. A circuit diagram of the proposed scheme is given in Fig. 4.

4.1 Experimental realization of ${}^{\mathrm{p}}C_{\mathrm{o}}$, ${}^{\mathrm{o}}C_{\mathrm{p}}$ gates and SOBA

A polarization-controlled OAM C_{NOT} gate can be implemented using a modified Mach–Zehnder interferometer where the normal beam splitter is replaced by a polarizing beam splitter (PBS) as shown in Fig. 5. The reflected arm of the interferometer, through which the vertically polarized photons travel, contains a spiral phase plate (SPP) of order 1 which will convert the even OAM state to odd and vice versa. On the other arm with horizontally polarized photons, the OAM state remains unchanged.

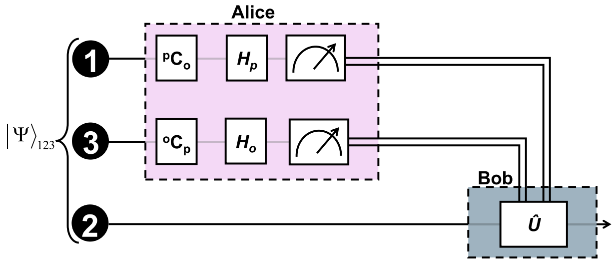

Fig. 4 Circuit diagram for proposed teleportation scheme. *Single/double lines* quantum/classical communication channels, *arrow* measurement. $\hat{U}$—unitary transformation given in Table 1

Fig. 5 Experimental scheme for the implementation of polarization-controlled OAM C_{NOT} gate (${}^{\mathrm{p}}C_{\mathrm{o}}$). *PBS* polarizing beam splitter, *SPP* spiral phase plate, *GB* glass block

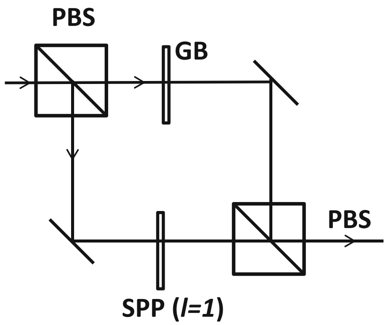

These states superpose at the second PBS and emerges as a single ${}^{\mathrm{p}}C_{\mathrm{o}}$ gate output. A glass block is introduced to compensate the extra phase introduced by the SPP.

We pursue a similar method to construct the OAM-controlled polarization C_{NOT} gate. For that, we need to use a beam splitter which transmits the photons with even OAM state and reflects the photons with odd OAM state. This can be achieved by an OAM sorter [17]. We replace the two PBSs in the previous setup with OAM sorters, and instead of the SPP, we use a half-wave plate at 45° in one arm that transforms the polarization state to its orthogonal state. The schematic of the setup is given in Fig. 6. The OAM sorter is another Mach–Zehnder interferometer containing dove prisms in each arm with a relative angle of 90°.

The spin–orbit Bell state analysis with OAM in the even/odd states is explained by Khoury and Milman [15]. However, in the present protocol, the SOBA in photon **1** and photon **3** differ slightly in their implementation. As shown in Fig. 7, two Mach–Zehnder interferometers with OAM sorters (OS) and polarizing beam splitters with photon detectors can implement SOBA. For the photon **1**, the block 1, Fig. 7, is an OAM sorter and the blocks 2 and 3 are polarizing beam splitters. For SOBA in photon **3**, the block 1 is a PBS, while the blocks 2 and 3 are OAM sorters. Detection on each of the detector will indicate the corresponding spin–orbit Bell state of the photon.

Here are the advantages of the described teleportation scheme

(i) As evident from the scheme, the number of particles required to teleport two independent qubits are reduced by 25 % by taking advantage of an extra DOF per photon.

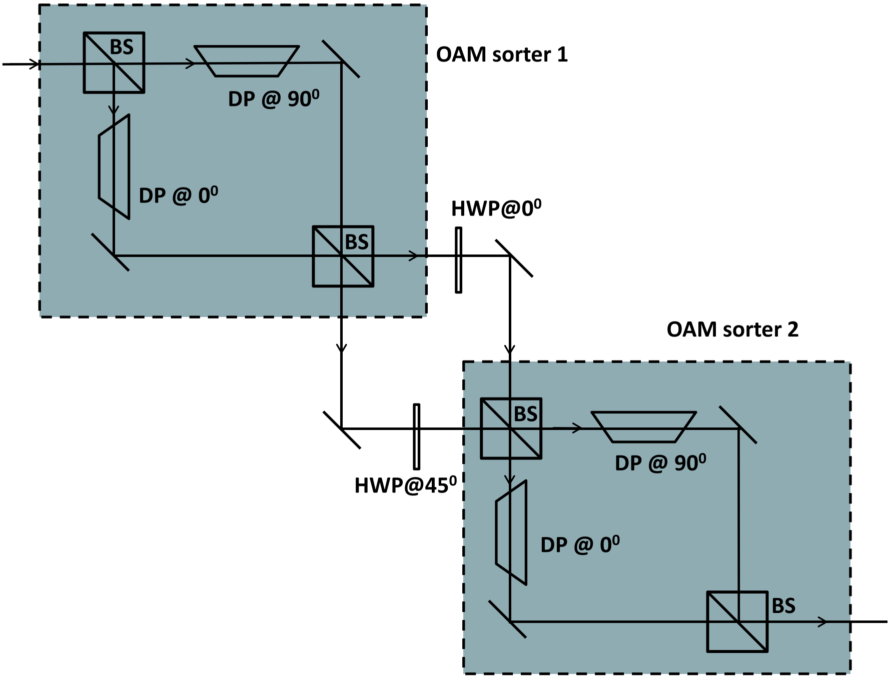

Fig. 6 Experimental scheme for the implementation of OAM-controlled polarization C_{NOT} gate ($^{\mathrm{O}}C_{\mathrm{P}}$). *DP* dove prism, *BS* 50:50 beam splitter, *HWP* half-wave plate

Fig. 7 Experimental scheme for the implementation of SOBA in photon **1/3**. *OS* OAM sorter, *PBS* polarizing beam splitter, *BS* 50:50 beam splitter

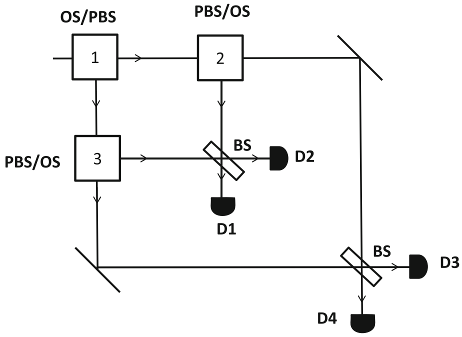

(ii) We use single-particle two-qubit Bell measurement instead of two-particle joint Bell measurements. Its implementation is experimentally simple, and one can achieve 100 % efficient Bell state measurement and hence the teleportation.

(iii) In our scheme, Bob need not to do unitary transformations on the OAM, since the same can be implemented by operations on the polarization before and after the SWAP.

(iv) The described three-particle hyper-entangled states can be utilized for a multi-party teleportation scheme with two senders and a common receiver. Here Alice and Charlie, with no entanglement channel between them, share photons **1** and **3**.

The combined polarization–OAM quantum state of Alice's and Charlie's photons will be teleported to Bob who carries photon **2**.

5 Quantum key distribution

Theoretically, the entanglement-based QKD protocols are equivalent to the non-entanglement-based ones (such as BB84). However, in practice, due to the strong quantum correlation and non-locality [24–28], the entanglement-based protocols are regarded more useful (for example, they have intrinsic randomness of the distributed key and extremely low probability of double photons). In recent years, entanglement in two degrees of freedom such as polarization and OAM has led to interesting applications in cryptography [29,30].

Here we are proposing a QKD protocol using the entangled system described in Sect. 2. We take a similar state as in Eq. (2) given by

$$|\Psi\rangle_{123} = |\xi_{\mathrm{p}}\rangle_1 \otimes (|00\rangle_{12} + |1-1\rangle_{12} + |-11\rangle_{12}) \\ \otimes (|HH\rangle_{23} + |VV\rangle_{23})\,|\chi_o\rangle_3,$$

where $|0\rangle$, $|1\rangle$ and $|-1\rangle$ are the OAM states of photons. Here we take a three-dimensional subspace of infinite-dimensional OAM entangled state produced by SPDC process with Gaussian beam as pump instead of even/odd entangled state.

The experimental implementation of the protocol is shown in Fig. 8. Alice will receive photon **2** and Bob will receive photons **1** and **3**, respectively. Photon **2** is entangled with photon **3** in polarization, and it is entangled with photon **1** in OAM. The photons **1** and **3** do not have any correlation. Alice will measure both OAM and polarization states, Bob will measure polarization of photon **3** and OAM of photon **1**.

Alice and Bob randomly measure polarization states of their respective photons in the following set of basis ($\gamma_i = 0°, 22.5°, 45°, 67.5°$), ($\delta_i = 22.5°, 45°, 67.5°, 180°$), respectively. These measurements can be done by a half-wave plate and polarizing beam splitter. Note that $\gamma_i/2$ and $\delta_i/2$ are the fast axis orientation angles of the half-wave plates. Each angle represents a basis which is used for measurement, and corresponding to each of them, there are two measurement outcomes. The pairs of angles used by Alice and Bob for which the sum is 0°, and 180° will give perfect correlation between them. The data corresponding to these correlated photons have same bits and can be used for the key. Alice and Bob will compare their polarization measurement basis for the key distribution as well as for the security of the key. After sufficient number of measurements, 4/16 of the data are useful for key, two sets of 4/16 of the data are used to check CHSH inequalities (S and S$'$), and the remaining 4/16 are discarded due to unmatched bases.

For the OAM correlation of entangled photons, we follow the key sharing scheme used in [31]. In this scheme, Alice and Bob measure the OAM state of their photons in three different randomly chosen bases A_1, A_2, A_3 and B_1, B_2, B_3, respectively. This is done by a pair of shifted holograms and an OAM sorter. The set of bases (A_3 and B_3) has perfect correlation, and the coincidence corresponding to it can be used to generate the key. Alice and Bob will compare their hologram settings for QKD and

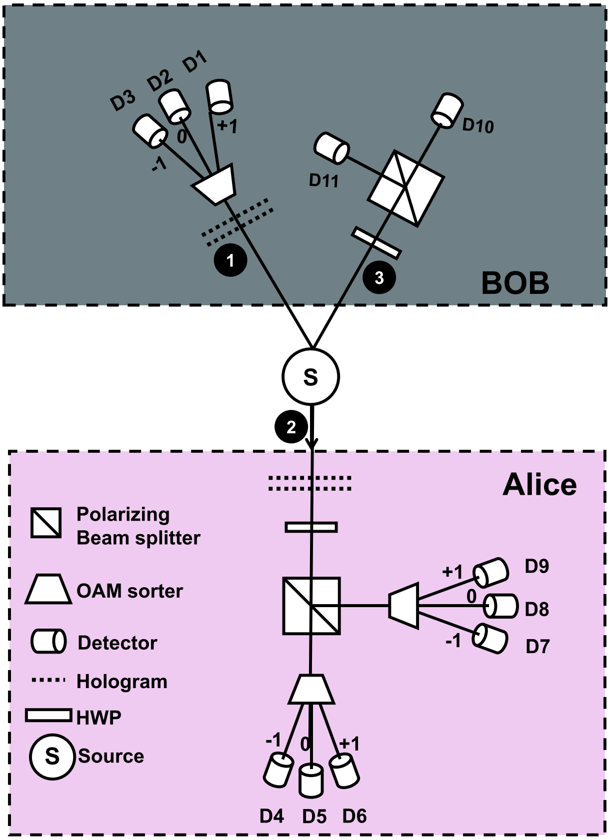

Fig. 8 Schematic diagram for quantum key distribution between Alice and Bob. Photons 1–2 have OAM entanglement, and 1–3 have polarization entanglement. D_i detectors, *HWP* half-wave plate, *PBS* polarizing beam splitter

security check. In total, there are nine possible measurements. After taking sufficient number of measurements, 1/9 of the produced data can be used for the key. For Bell-type inequality check, 4/9 of the data will be used which confirms the security of the key and the remaining 4/9 of the data are redundant.

The security of the protocol is mainly checked by the violation of Bell's inequality test. All the three parties should check Bell-like inequality with their data in order to check eavesdropping. If there is a violation of inequality, entanglement is preserved and there is no eavesdropping in the channel. The CHSH parameters S and S′ for photons entangled in the polarization DOF are given by Clauser et al. [32]

$$S = E(\gamma_1, \delta_1) - E(\gamma_1, \delta_3) + E(\gamma_3, \delta_1) + E(\gamma_3, \delta_3) \tag{13}$$

$$S' = E(\gamma_2, \delta_2) + E(\gamma_2, \delta_4) + E(\gamma_4, \delta_2) - E(\gamma_4, \delta_4) \tag{14}$$

with

Table 2 Description of data usage corresponding to Alice's and Bob's measurement angles

Alice	γ_1	γ_2	γ_3	γ_4
Bob				
δ_1	S	Key	S	$\times$
δ_2	$\times$	S′	Key	S′
δ_3	S	$\times$	S	Key
δ_4	Key	S′	$\times$	S′

Here S and S′ are used for security check through CHSH inequality, and $\times$ is the discarded data

$$E(\gamma_i,\delta_j)=\frac{R_{12}(\gamma_i,\delta_j)+R_{1'2'}(\gamma_i,\delta_j)-R_{12'}(\gamma_i,\delta_j)-R_{1'2}(\gamma_i,\delta_j)}{R_{12}(\gamma_i,\delta_j)+R_{1'2'}(\gamma_i,\delta_j)+R_{12'}(\gamma_i,\delta_j)+R_{1'2}(\gamma_i,\delta_j)} \tag{15}$$

where R_{12}, $R_{1'2'}$, $R_{12'}$ and $R_{1'2}$ are the coincidences $P(D11, D9+D8+D7)$, $P(D10, D4+D5+D6)$, $P(D11, D4+D5+D6)$ and $P(D10, D9+D8+D7)$, respectively.

For any local realistic theory, the CHSH parameters $S, S' \leq 2$. Non-local nature of the entanglement will violate any of these inequalities, and this violation can be used for checking the security of the key shared by Alice and Bob. The combination of γ and δ for Bell's inequality test and for the key distribution is given in Table 2.

Photons **1** and **2** have OAM correlation, so it will violate the following Bell's inequality for three-dimensional case [31,33]

$$\begin{aligned} S = {} & P(A_1=B_1)+P(A_2=B_1-1)+P(A_2=B_2)+P(A_1=B_2) \\ & -P(A_1=B_1-1)-P(A_2=B_1)+P(A_2=B_2-1)+P(A_1=B_2+1) \end{aligned} \tag{16}$$

$$\leq 2, \tag{17}$$

where

$$P(A_a=B_b+k)=\sum_{j=0}^{2}P(A_a=j, B_b=(j+k)Mod\ 3). \tag{18}$$

The shifts of holograms are chosen in such a way that they maximally violate the Bell-type inequality. $j=0,1,2$ corresponds to the detection of OAM states 0, 1 and -1, respectively. The coincidence measurements with the combinations of $P(D1, D6+D9)$, $P(D1, D5+D8)$, $P(D2, D4+D7)$, $P(D2, D6+D9)$, $P(D2, D5+D8)$, $P(D2, D4+D7)$, $P(D3, D6+D9)$, $P(D3, D5+D8)$ and $P(D3, D4+D7)$ are required for the key distribution and to check the security of the key using Eq. (16) and (18).

Our protocol has three advantages compared to traditional Ekert protocol [3].

(i) If Ekert protocol is used, then around $4n$ pairs of photons, i.e., $8n$ photons (in practice, little more than $8n$), are required to establish a secret key of length n between Alice and Bob. In our approach, around $6n$ photons would be required for the same purpose. Hence, in terms of number of photons required, Ekert's protocol is 33 % less efficient than ours.

(ii) On the other hand, if the same number of photons are used in Ekert and our protocol and if the target key length is also the same, then because of more entanglement resource, our protocol would have more redundancy and hence can tolerate more noise. It is easy to see that the security in each degree of freedom is equivalent to that of the Ekert protocol.

(iii) Further, this state can be used for multi-party QKD. Photons 1, 2 and 3 can be distributed among Alice, Bob and Charlie, respectively. Now, two sets of independent keys can be generated, one for Alice–Bob and another for Alice–Charlie.

6 Conclusion

Possibility of a new entangled state and its application in teleporting a two-qubit OAM–polarization quantum state and in the QKD have been discussed. The new teleportation method overcomes the difficulty of measuring in two-particle polarization Bell basis, by implementing independent single-particle two-qubit Bell measurements. The method critically depends on the experimental realizations of polarization C_{NOT} gate as well as single-particle two-qubit C_{NOT} gates. All the 16 unitary transformations which are required for this teleportation scheme can be realized with linear optical components along with a SWAP gate. Once the state given in Eq. (8) is achieved, one can have a 100 % efficient teleportation of two simultaneous qubits. Extending this to higher dimensions is mathematically trivial though creating entanglement in different DOFs has experimental limitations. With the new QKD protocol, the sender and the receiver need to use less resource than traditional Ekert protocol to share the secret key of the same length. Multi-party schemes also can be developed for the teleportation and the QKD using the described protocols.

Acknowledgments Authors wish to acknowledge Prof. Anirban Pathak, JIIT, Noida, for fruitful discussions and suggestions.

References

1. Bennett, C.H., Brassard, G., Crépeau, C., Jozsa, R., Peres, A., Wootters, W.K.: Teleporting an unknown quantum state via dual classical and Einstein–Podolsky–Rosen channels. Phys. Rev. Lett. **70**, 1895–1899 (1993)
2. Bennett, C.H., Wiesner, S.J.: Communication via one- and two-particle operators on Einstein–Podolsky–Rosen states. Phys. Rev. Lett. **69**, 2881–2884 (1992)
3. Ekert, A.K.: Quantum cryptography based on Bell's theorem. Phys. Rev. Lett. **67**, 661–663 (1991)
4. Bouwmeester, D., Pan, J.-W., Mattle, K., Eibl, M., Weinfurter, H., Zeilinger, A.: Experimental quantum teleportation. Nature **390**, 575–579 (1997)
5. Riebe, M., Häffner, H., Roos, C., Hänsel, W., Benhelm, J., Lancaster, G., Körber, T., Becher, C., Schmidt-Kaler, F., James, D., et al.: Deterministic quantum teleportation with atoms. Nature **429**, 734–737 (2004)
6. Kim, Y.-H., Kulik, S.P., Shih, Y.: Quantum teleportation of a polarization state with a complete bell state measurement. Phys. Rev. Lett. **86**, 1370–1373 (2001)
7. Wei, T.-C., Barreiro, J.T., Kwiat, P.G.: Hyperentangled bell-state analysis. Phys. Rev. A **75**, 060305 (2007)
8. Barreiro, J.T., Wei, T.-C., Kwiat, P.G.: Beating the channel capacity limit for linear photonic superdense coding. Nat. Phys. **4**, 282–286 (2008)

9. Sheng, Y.-B., Deng, F.-G., Long, G.L.: Complete hyperentangled-Bell-state analysis for quantum communication. Phys. Rev. A **82**, 032318 (2010)
10. Aolita, L., Walborn, S.P.: Quantum communication without alignment using multiple-qubit single-photon states. Phys. Rev. Lett. **98**, 100501 (2007)
11. Souza, C.E.R., Borges, C.V.S., Khoury, A.Z., Huguenin, J.A.O., Aolita, L., Walborn, S.P.: Quantum key distribution without a shared reference frame. Phys. Rev. A **77**, 032345 (2008)
12. dos Santos, B.C., Dechoum, K., Khoury, A.Z.: Continuous-variable hyperentanglement in a parametric oscillator with orbital angular momentum. Phys. Rev. Lett. **103**, 230503 (2009)
13. Borges, C.V.S., Hor-Meyll, M., Huguenin, J.A.O., Khoury, A.Z.: Bell-like inequality for the spin-orbit separability of a laser beam. Phys. Rev. A **82**, 033833 (2010)
14. Chen, L., She, W.: Single-photon spin-orbit entanglement violating a Bell-like inequality. J. Opt. Soc. Am. B **27**, A7–A10 (2010)
15. Khoury, A.Z., Milman, P.: Quantum teleportation in the spin-orbit variables of photon pairs. Phys. Rev. A **83**, 060301 (2011)
16. Walborn, S.P., de Oliveira, A.N., Thebaldi, R.S., Monken, C.H.: Entanglement and conservation of orbital angular momentum in spontaneous parametric down-conversion. Phys. Rev. A **69**, 023811 (2004)
17. Leach, J., Padgett, M.J., Barnett, S.M., Franke-Arnold, S., Courtial, J.: Measuring the orbital angular momentum of a single photon. Phys. Rev. Lett. **88**, 25901 (2002)
18. Simon, R., Mukunda, N.: Minimal three-component su (2) gadget for polarization optics. Phys. Lett. A **143**, 165–169 (1990)
19. Reddy, S.G., Prabhakar, S., Aadhi, A., Kumar, A., Shah, M., Singh, R., Simon, R.: Measuring the Mueller matrix of an arbitrary optical element with a universal SU (2) polarization gadget. J. Opt. Soc. Am. A **31**, 610–615 (2014)
20. Pati, A.K., Agrawal, P.: Probabilistic teleportation of a qudit. Phys. Lett. A **371**, 185–189 (2007)
21. Goyal, S.K., Boukama-Dzoussi, P.E., Ghosh, S., Roux, F.S., Konrad, T.: Qudit-teleportation for photons with linear optics. Sci. Rep. **4**, 4543 (2014)
22. Goyal, S.K., Konrad, T.: Teleporting photonic qudits using multimode quantum scissors. Sci. Rep. **3**, 3548 (2013)
23. Babichev, S.A., Ries, J., Lvovsky, A.I.: Quantum scissors: teleportation of single-mode optical states by means of a nonlocal single photon. Europhys. Lett. **64**, 1 (2003)
24. Jennewein, T., Simon, C., Weihs, G., Weinfurter, H., Zeilinger, A.: Quantum cryptography with entangled photons. Phys. Rev. Lett. **84**, 4729–4732 (2000)
25. Bouwmeester, D., Zeilinger, A.: The physics of quantum information: basic concepts. In: Bouwmeester, D., Ekert, A., Zeilinger, A. (eds.) The Physics of Quantum Information. Springer, Berlin, pp. 1–14 (2000)
26. Ursin, R., Tiefenbacher, F., Schmitt-Manderbach, T., Weier, H., Scheidl, T., Lindenthal, M., Blauensteiner, B., Jennewein, T., Perdigues, J., Trojek, P., et al.: Entanglement-based quantum communication over 144 km. Nat. Phys. **3**, 481–486 (2007)
27. Gisin, N., Ribordy, G., Tittel, W., Zbinden, H.: Quantum cryptography. Rev. Mod. Phys. **74**, 145–195 (2002)
28. Naik, D.S., Peterson, C.G., White, A.G., Berglund, A.J., Kwiat, P.G.: Entangled state quantum cryptography: eavesdropping on the Ekert protocol. Phys. Rev. Lett. **84**, 4733–4736 (2000)
29. Mafu, M., Dudley, A., Goyal, S., Giovannini, D., McLaren, M., Padgett, M.J., Konrad, T., Petruccione, F., Lütkenhaus, N., Forbes, A.: Higher-dimensional orbital-angular-momentum-based quantum key distribution with mutually unbiased bases. Phys. Rev. A **88**, 032305 (2013)
30. D'Ambrosio, V., Nagali, E., Walborn, S.P., Aolita, L., Slussarenko, S., Marrucci, L., Sciarrino, F.: Complete experimental toolbox for alignment-free quantum communication. Nat. Commun. **3**, 961 (2012)
31. Grblacher, S., Jennewein, T., Vaziri, A., Weihs, G., Zeilinger, A.: Experimental quantum cryptography with qutrits. New J. Phys. **8**, 75 (2006)
32. Clauser, J.F., Horne, M.A., Shimony, A., Holt, R.A.: Proposed experiment to test local hidden-variable theories. Phys. Rev. Lett. **23**, 880–884 (1969)
33. Collins, D., Gisin, N., Linden, N., Massar, S., Popescu, S.: Bell inequalities for arbitrarily high-dimensional systems. Phys. Rev. Lett. **88**, 040404 (2002)